Enhancing Graft-versus-Leukemia Responses by donor-derived CAR-modified $CD8^+$ Memory Stem T cells

Dissertation
zur Erlangung des Doktorgrades
der Biomedizinischen Wissenschaften
(Dr. rer. physiol.)

der
Fakultät für Medizin
der Universität Regensburg

vorgelegt von
Gabriele Inchingolo
aus
Regensburg, Germany

im Jahr
2026

Dekan: *Prof. Dr. Dirk Hellwig*

Betreuer/in: *Prof. Luca Gattinoni*

Tag der mündlichen Prüfung:

Table of Contents

Introductory note: The results described in the first part of present PhD thesis (**Figures 1–17, Figure 34**, **Figure 35**, **Supplementary Figures S1–S4**, and **Supplementary Tables S1–S2**), which focus on longitudinal patient immunomonitoring and the *in vivo* dynamics of CAR T_{SCM} cells, are reproduced from the manuscript entitled "*Distinct in vivo dynamics of donor-derived stem cell memory CAR T cells post-allogeneic HSCT relapse"* which was officially accepted for publication in *Cell* on 26 March 2026, https://doi.org/10.1016/j.cell.2026.03.047. In this work, I served as co–first author and was a primary contributor to the experimental design, execution, data analysis, and manuscript preparation, as detailed in the "author contributions" section of the original manuscript published in *Cell*.

The second part of the thesis (**Figures 18–33**, **Figure 36**, and **Supplementary Figures S5-6**), investigating the *in vivo* dynamics and functional fate of alloreactive CAR T cells, was entirely conceptualized, designed, and performed by me, including all experimental procedures and analyses, representing a complete dataset supporting a first-author manuscript currently in preparation. The findings of this second PhD projects were published as a peer-reviewed conference abstract in *Blood,* entitled "*In Vivo clonal dynamics of alloreactive CAR T cells reveal mechanisms limiting GvHD risk following allogeneic CAR T cell therapy*" *(Blood 146 [2025]: 105–106; Volume 146, Supplement 1, 3 November 2025; Session 702: CAR-T Cell Therapies: Basic and Translational; doi: 10.1182/blood-2025-105).*

A detailed description of my contributions, as well as those of co-authors, is provided below and further specified in Material and Methods, figure legends, and in the Supplementary material.

List of authors of the manuscript accepted in *Cell*

Luca Gattinoni[1,2,3,4,15,16,], **Gabriele Inchingolo[1,15]**, Dennis C. Harrer[5], Alberto Susana[6], Simone Puccio[6], Dragana Slavkovic-Lukic[1], Danielle A. Natrakul[8], Nicholas Strieder[9], Christoph Heuser-Loy[1], Jeremy G. Baldwin[1], Jessica Fioravanti[1,2], Yun Ji[2], Sanjivan Gautam[2], Chiara Suriano[10], Azucena Martín-Santos[1], Roland C. Schelker[1,5], Nisha Patel[11], Jennifer Mann[8], Stephanie Goff[8], Lekha Mikkilineni[12], James C. Yang[8], Mei Li M. Kwong[8], Rashmika Patel[2], Michael Rehli[5,9], Steven L. Highfill[13], David F. Stroncek[13], Steven A. Rosenberg[8], Luca Biasco[14], Enrico Lugli[6], Jennifer N. Brudno[8,15], James N. Kochenderfer[8,15,*]*

[1]Division of Functional Immune Cell Modulation, Leibniz Institute for Immunotherapy; Regensburg, Germany.

[2]Center for Cancer Research, National Cancer Institute, National Institutes of Health; Bethesda, MD, USA.

[3]University of Regensburg; Regensburg, Germany.

[4]Center for Immunomedicine in Transplantation and Oncology, University Hospital Regensburg; Regensburg, Germany.

[5]Department of Internal Medicine III, Hematology and Oncology, University Hospital Regensburg; Regensburg, Germany.

[6]IRCCS Humanitas Research Hospital; Rozzano,Italy

[7]Institute of Genetics and Biomedical Research, Milan Unit, Consiglio Nazionale delle Ricerche; Rozzano, Italy

[8]Surgery Branch, National Cancer Institute, National Institutes of Health; Bethesda, MD, USA.

[9]Next Generation Sequencing Core, Leibniz Institute for Immunotherapy; Regensburg, Germany.

[10]Epigenetic Immuno-Oncology Group, Leibniz Institute for Immunotherapy; Regensburg, Germany

[11]Hematology Section, Department of Laboratory Medicine, National Institutes of Health, Clinical Center; Bethesda, MD, USA

[12]Division of Bone and Marrow Transplantation & Cellular Therapies, Stanford University School of Medicine; Palo Alto, CA, USA.

[13]Department of Transfusion Medicine, National Institutes of Health, Clinical Center; Bethesda, MD, USA.

[14]Faculty of Population Health Science, Department of Infection Immunity and Inflammation, Zayed Centre for Research, University College of London; London, UK

[15]These authors contributed equally.

[16]Lead contact

List of Abbreviations

- **ACT:** Adoptive Cell Therapy
- **ACTB:** Actin Beta
- **ALL:** Acute Lymphoblastic Leukemia
- **APC:** Antigen Presenting Cells
- **AUC**: Area Under the Curve
- **β2M:** Beta 2-Microglobulin
- **BM:** Bone Marrow
- **CAR:** Chimeric Antigen Receptor
- **CFSE:** Carboxyfluorescein succinimidyl ester
- **CLL:** Chronic Lymphocytic Leukemia
- **CML:** Chronic Myeloid Leukemia
- **CR:** Complete Response
- **CRISPR:** Clustered Regularly Interspaced Short Palindromic Repeats
- **CRP:** C-Reactive Protein
- **CRS:** Cytokine Release Syndrome
- **CRUSTY:** *Clustering Unsupervised Methods for high dimensional Cytometry data*.
- **DLBCL:** Diffuse Large B-Cell Lymphoma
- **DLI:** Donor Lymphocyte Infusion
- **EBV:** Epstein–Barr virus
- **EFS:** Event Free Survival
- **EGA:** European Genome-phenome Archive
- **ELISA:** Enzyme-Linked Immunosorbent Assay
- **EMA:** European Medicines Agency
- **FACS:** Fluorescence-Activated Cell Sorting
- **FDA:** Food and Drug Administration
- **FL:** Follicular Lymphoma
- **G0-G4:** CRS Grade
- **GMP:** Good Manufacturing Practice
- **GvHD:** Graft-versus-host disease
- **HIV:** Human Immunodeficiency Virus
- **HLA:** Human Leukocyte Antigen
- **HSC:** Hematopoietic Stem Cell
- **HSCT:** Hematopoietic Stem Cell Transplantation

- **ICANS:** Immune Effector Cell–Associated Neurotoxicity Syndrome
- **IFN:** Interferon
- **IL:** Interleukin
- **ISA:** Integration Site Analysis
- **LTR:** Long Terminal Repeat
- **MFI:** Mean Fluorescence Intensity
- **MHC:** Major Histocompatibility Complex
- **MLR:** Mixed Lymphocyte Reaction
- **MM:** Multiple Myeloma
- **MRD:** Minimal Residual Disease
- **NHL:** Non-Hodgkin Lymphoma
- **NK:** Natural Killer
- **NY-ESO-1:** New York Esophageal Squamous Cell Carcinoma 1
- **ORR:** Overall Response Rate
- **PBMC:** Peripheral Blood Mononuclear Cells
- **PCA:** Principal Component Analysis
- **PCR:** Polymerase Chain Reaction
- **PD-1:** Programmed Cell Death Protein 1
- **PET/CT:** Positron Emission Tomography / Computed Tomography
- **PR:** Partial Response
- **R/R:** Relapsed/Refractory
- **RT:** Room Temperature
- **SD:** Stable Disease
- **T_{CM}:** Central Memory T cells
- **TCR:** T Cell Receptor
- **T_{EM}:** Effector Memory T cells
- **TGF:** Transforming Growth Factor
- **TIL:** Tumor-infiltrating lymphocytes
- **T_N:** Naïve T cells
- **TNF:** Tumor Necrosis Factor
- **T_{SCM}:** Memory stem T cells
- **T_{TE}:** Terminal Effector T cells
- **UMAP:** Uniform Manifold Approximation and Projection
- **URD:** Unrelated Donor

Detailed figure author contributions

Figure 1. Schematic overview of the modular architecture of currently FDA-approved Chimeric Antigen Receptors (CARs). *This figure was created by me with BioRender.com and was adapted from Rafiq et al., Nat Rev Clin Oncol (2020) (https://doi.org/10.1038/s41571-019-0297-y)[40]. Figure reproduced with permission from Springer Nature. License number: 6193260155172.*

Figure 2. Schematic illustrating the inverse relationship between *in vitro* effector capacity and *in vivo* anti-tumor efficacy of adoptively transferred CD8$^+$ T cell subsets. *This figure was created by me with BioRender.com and adapted from Gattinoni et al., Nat Rev Immunol (2006)[65] and Gattinoni et al., Nat Med (2017)[64]. Springer Nature. License numbers: 6193251333433 and 6193251089961.*

Figure 3. Donor-derived CAR T cell manufacturing workflow. *Figure was designed by me using BioRender.com.*

Figure 4. Standard and T_{SCM}-enriched infusion product composition. *While the experimental design, technical execution, and data analysis for **Figures 4A-C** were performed entirely by me, the graphical design was made by me under the guidance of Prof. Luca Gattinoni, co-first author of the manuscript accepted in CELL.*

Figure 5. CAR T_{SCM} products exhibit greater phenotypic uniformity than standard CAR T cells. *The experimental design, technical execution, phenograph analysis, and graphical design for **Figures 5A-C** were performed entirely by me.*

Figure 6. CAR T_{SCM} cells drive superior responses at lower doses. *The graphical design for **Figure 6A** was made by me under the guidance of Prof. Luca Gattinoni, the co-first author of the manuscript accepted in CELL. The clinical observation and graphical design shown in **Figure 6B** were made by me.*

Figure 7. CAR T_{SCM} cells show enhanced expansion and persistence. *The experimental design, technical execution, and data analysis for **Figure 7A** were performed by me and Danielle A. Natrakul, co-author of the manuscript accepted in CELL. The experimental design, coordination, execution, and analysis related to **Figures 7B-D** were performed entirely by me.*

*The graphical design for **Figures 7A-D** was made by me under the guidance of Prof. Luca Gattinoni, co-first author of the manuscript accepted in CELL.*

Figure 8. Reduced cytokine release syndrome severity following CAR T_{SCM} infusion. *The clinical observation and graphical design for **Figure 8A** were made by me. The experimental design, coordination, execution, and analysis for **Figure 8B** were performed entirely by me. The clinical correlation and graphical design for **Figure 8B** were made by me under the guidance of Prof. Luca Gattinoni, the co-first author of the manuscript accepted in CELL.*

Figure 9. Distinct cytokine kinetics differentiate standard and T_{SCM} CAR T cells. *The technical experiments conducted to generate **Figures 9A-C** were entirely and independently conceptualized, designed, and executed by me. Clinical correlation and graphical design of **Figures 9A-C** were made by me.*

Figure 10. Single-cell secretome analysis reveals a polyfunctional, IFN-γ–dominant profile in CAR T_{SCM} cells. *The technical experiments conducted to generate **Figures 10A** and **10B** were entirely and independently executed by me. The experiment related to **Figure 10A** was designed by me with the assistance of Dragana Slavkovic-Lukic, co-author of the manuscript accepted in CELL. $CD19^+$ target cells used to stimulate CAR T cells were already available at the Leibniz Institute for Immunotherapy in the laboratory of Prof. Luca Gattinoni and were originally generated at the National Institutes of Health (NIH) in the laboratory of Dr. Kochenderfer. The data analysis and graphical design for **Figures 10A** and **10B** were entirely performed by me.*

Figure 11. *In vivo* CAR T cell differentiation trajectories by high-dimensional flow cytometry. *The experimental design, technical execution, and sample analysis related to **Figures 11A-C** were performed primarily by me with the assistance of Alberto Susana, co-author of the manuscript accepted in CELL. The bioinformatic analysis used to generate **Figures 11A-C** was performed by Simone Puccio, co-author of the manuscript accepted in CELL, under my guidance and the guidance of Prof. Luca Gattinoni and Dr. Enrico Lugli, co-author of the manuscript accepted in CELL.*

Figure 12. CAR T_{SCM} cells retain the ability to reconstitute the T_{SCM} compartment. *The experimental design, technical execution, and sample analysis related to **Figures 12A**, **12B**,*

*and **12C** were performed primarily by me with the assistance of Alberto Susana, co-author of the manuscript accepted in CELL. The bioinformatic analysis used to generate **Figures 12A-C** was performed by Simone Puccio, co-author of the manuscript accepted in CELL, under my guidance and the guidance of Prof. Luca Gattinoni and Dr. Enrico Lugli, co-author of the manuscript accepted in CELL.*

Figure 13. Long-term persistence of CAR T_{SCM} cells is sustained by clonal succession. *Project planning and all the technical experiments necessary to generate **Figures 13A-G** were entirely conceived and performed by me. Protocol for Integration Site Analysis assay was developed and optimized at Leibniz Institute for Immunotherapy by me. Sequencing was performed by me and Johanna Raithel under the guidance of Michael Rheli, co-author of the manuscript accepted in CELL. Bioinformatic analyses were performed by Luca Biasco and Nicholas Strieder, both co-authors of the manuscript accepted in CELL. **Figures 13A**, **13C**, **13E**, and **13F** were generated by Luca Biasco under my guidance. **Figures 13B**, **13D**, and **13G** were generated by me under the guidance of Prof. Luca Gattinoni, co–first author of the manuscript accepted in CELL.*

Figure 14. Absence of correlation between CAR T_{SCM} expansion and clinical outcome. *The clinical correlation between treatment response and CAR T cell expansion shown in **Figure 14** was performed by me, while the graphical design was developed by me under the guidance of Prof. Luca Gattinoni, co–first author of the manuscript accepted in CELL.*

Figure 15. Leukemia progression despite CAR T_{SCM} cell expansion and preserved functionality. *The experimental design, coordination, execution, and analysis related to **Figures 15A**, **B** were performed entirely by me. The graphical design for **Figures 15A**, **B** was made by me under the guidance of Prof. Luca Gattinoni, co–first author of the manuscript accepted in CELL.*

Figure 16. IL-10–mediated immunosuppression as a potential barrier to CAR T_{SCM} expansion. *The experimental design, coordination, execution, data analysis, and graphical design related to **Figure 16A-D** were performed entirely by me.*

Figure 17. Humoral anti-CAR immunity contributes to CAR T_{SCM} treatment failure. *The experimental design, coordination, execution, and analysis related to **Figure 17A** and **17B***

*were performed entirely by me. The graphical design for **Figure 17A** was made by me, while the graphical design for **Figure 17B** was made by me under the guidance of Prof. Luca Gattinoni, co–first author of the manuscript accepted in CELL.*

Figure 18. A K562-based artificial antigen presenting cell platform to recapitulate HLA mismatch. *Experimental design, technical execution, data processing, and figure graphical design were conceived and performed exclusively by me.*

Figure 19. CD80/41BBL co-stimulation is required for efficient rHLA-dependent T cell proliferation. *Experimental design, technical execution, data processing, and figure graphical design were conceived and performed exclusively by me.*

Figure 20. Activation marker profiling identifies functional rHLA-responsive T cells. *Experimental design, technical execution, data processing, and figure graphical design were conceived and performed exclusively by me.*

Figure 21. HLA-DR$^+$CD25$^+$CD71$^+$ cells define the most functional rHLA-responsive alloreactive population. *Experimental design, technical execution, data processing, and figure graphical design were conceived and performed exclusively by me.*

Figure 22. Generation of alloreactive alloCAR T cells using the 80/BBL rHLA *e*K562 platform. *Experimental design, technical execution, data processing, and figure graphical design were conceived and performed exclusively by me. **Figure 22A** was designed on BioRender.com by me.*

Figure 23. Dual target exposure impairs TCR-mediated recognition in alloCAR T cells. *Experimental design, technical execution, data processing, and figure graphical design were conceived and performed exclusively by me.*

Figure 24. Cumulative dual antigen stimulation impairs alloCAR T cell fitness. *Experimental design, technical execution, data processing, and figure graphical design were conceived and performed exclusively by me. **Figure 24A** was designed on BioRender.com by me.*

Figure 25. AKT inhibition or BBz CAR integration enhance alloCAR T cell functionality. *Experimental design, technical execution, data processing, and figure graphical design were conceived and performed exclusively by me.* ***Figure 25A*** *was designed on BioRender.com by me.*

Figure 26. CAR signaling modulation improves alloCAR T cell persistence. *Experimental design, technical execution, data processing, and figure graphical design were conceived and performed exclusively by me.*

Figure 27. Defining the *in vivo* expansion window of allogeneic CAR T cells. *The experimental design, coordination, execution, and analysis related to* ***Figure 27A****, and* ***B*** *were performed entirely by me. Figure graphical design was performed exclusively by me.*

Figure 28. *Ex vivo* profiling of patient-derived alloCAR T cells across post-infusion time points. *The experimental design, coordination, execution, and analysis related to flow cytometry plot were performed entirely by me.* ***Figure 28*** *was designed on BioRender.com by me.*

Figure 29. Donor-derived alloCAR T cells at the expansion phase exhibit a dysfunctional signature. *Experimental design, technical execution, data processing, bioinformatic analysis, and figure graphical design were conceived and performed exclusively by me.*

Figure 30. Schematic overview of the workflow used to isolate alloT and alloCAR T from pre- and post-infusion patient PBMCs and CAR T cell products. *The experimental design, coordination, execution, and analysis related to flow cytometry plot in the figure were performed entirely by me. Figure 30 was designed on BioRender.com by me.*

Figure 31. Transcriptomic identification of proliferating alloCAR T and alloT cells. *All the technical experiments were performed by me. The graphical design and bioinformatic analysis were conceived by me and Nisha Rana, bioinformatician of Prof. Luca Gattinoni's lab.*

Figure 32. Divergent *in vivo* transcriptional profiles of alloT and alloCAR T cells. *All the technical experiments were performed by me. The FASTA data processing was performed by Nisha Rana, while bioinformatic analyses and graphical design were performed entirely by*

me.

Figure 33. Longitudinal clonal tracking of alloCAR T cells shows transient expansion and limited persistence. *All the technical experiments were performed by me. The FASTA data processing was performed by Nisha Rana, while bioinformatic analyses and graphical design were performed entirely by me.*

Figure 34. Distinct clonal dynamics of standard and CAR T_{SCM} products after transfer. *This figure was designed on BioRender.com by me.*

Figure 35. Leukemia progression in patient #23 was attributed to loss of CD19 antigen expression. ***Figures 35A*** *and* ***B*** *were generated using data from experiments conducted at the National Institutes of Health, with the permission of Dr. Jennifer Brudno and Dr. James Kochenderfer, the last authors of the manuscript accepted in CELL. The graphical design for* ***Figures 35A*** *and* ***B*** *was made by me under the guidance of Prof. Luca Gattinoni, the co-first author on the manuscript accepted in CELL.*

Figure 36. Cumulative signaling–driven dysfunction model in alloreactive CAR T cells. *This figure was designed on BioRender.com by me.*

Supplementary Tables S1 and S2 summarize patient characteristics and treatment courses. *Data from supplementary tables were collected by Dr. James Kochenderfer and Dr. Jennifer Brudno, last authors of the manuscript accepted in CELL. Table design and data organization were entirely performed by me.*

Figure S1. CAR T_{SCM} cells exhibit a delayed peak expansion relative to standard CAR T cells, related to Figure 4. *The technical experiments used to generate* ***Figure S1 (left)*** *were performed by me and Danielle A. Natrakul, the co-author of the manuscript accepted in CELL. The technical experiments used to generate* ***Figure S1 (right)*** *were conceived and performed by me. The graphical design for* ***Figure S1*** *was made by me under the guidance of Prof. Luca Gattinoni, co–first author of the manuscript accepted in CELL.*

Figure S2. Serum cytokine profiling following CAR T cell infusion, related to Figures 8 and 15. *The technical experiments used to generate **Figure S2** were conceived and performed entirely by me. The graphical design for **Figure S2** was made by me.*

Figure S3. Diversity of CAR T cell infusion products, related to Figure 13. *Project planning and all the technical experiments necessary to generate **Figure S3** were entirely conceived and performed by me. Protocol for Integration Site Analysis assay was developed and optimized at Leibniz Institute for Immunotherapy by me. Sequencing was performed by me and Johanna Raithel under the guidance of Michael Rheli, co-author of the manuscript accepted in CELL. Bioinformatic analyses were performed by Luca Biasco and Nicholas Strieder, both co-authors of the manuscript accepted in CELL. The bioinformatic analysis used for **Figure S3** was performed by Luca Biasco. The graphical design for **Figure S3** was made through my guidance and that of Luca Biasco and Prof. Luca Gattinoni, co–first author of the manuscript accepted in CELL.*

Figure S4. Enhanced humoral immunity against CARs following second CAR T cell infusion, related to Figure 17. *All the technical experiments used to generate **Figure S4** were conceived and performed by me. The graphical design for **Figure S4** was made by me under the guidance of Prof. Luca Gattinoni.*

Figure S5. Original CAR T cell products expressed high levels of CAR related to Figure 20. *All the technical experiments used to generate **Figure S5** were conceived and performed by me. The graphical design was made by me.*

Figure S6. Original CAR T cell products expressed high levels of CAR. *All the technical experiments used to generate **Figure S6** were conceived and performed by me. The graphical design for **Figure S6** was made by me.*

Figure author contribution summary

- Figures entirely conceived, designed, executed, analyzed, and graphically prepared exclusively by me:
  - **Figures: 1; 2; 3; 5A-C; 6B; 8A; 9A–C; 10A-B; 18; 19; 20; 21; 22A–B; 23; 24A–F; 25A–C; 26A–C; 27A–B; 28; 29D–H; 30; 32; 33; 34; 35; 36**
  - **Supplementary Figures: S2; S5; S6**

- Figures for which the graphical design was conceived by me under the guidance of Prof. Luca Gattinoni (while experimental work/analysis were performed by me, unless otherwise specified in captions):
  - **Figures: 4A–C; 6A; 7B–D; 8B; 11A-C; 12A-C; 13B; 13D; 13G; 14; 15A–D; 16A–D; 17A–B**
  - **Supplementary Figures: S3; S4; S1** (right panel)

- Figures generated by me with experimental planning/execution in collaboration with co-authors:
  - With Danielle A. Natrakul (National Cancer Institute): **Figures 7A; S1** (left panel)
  - With Dragana Slavkovic-Lukic: **Figure 10A** (experimental design assistance)
  - With Alberto Susana: **Figures 11A–C; 12A–C**
  - With Simone Puccio: **Figures 11A–C; 12A–C** (bioinformatic analysis, under the guidance of the author, Prof. Luca Gattinoni, and Dr. Enrico Lugli)
  - With Johanna Raithel and Michael Rheli: **Figures 13A–G; S3** (sequencing)
  - With Luca Biasco and Nicholas Strieder: **Figures 13A–G; S3** (bioinformatic analyses)
  - With Nisha Rana: **Figure 31** (bioinformatics); FASTA preprocessing for **Figure 32, Figure 33**

- Figures including externally clinical data collected from NIH generated by me under the guidance of Prof. Luca Gattinoni and Dr. James Kochenderfer:
  - **Figures: 15C–D**
  - **Tables: S1 and S2**

Abstract

CAR T cell therapy has demonstrated curative potential in advanced B-cell malignancies; however, its efficacy is limited by insufficient *in vivo* expansion, persistence, and functional heterogeneity. Although numerous retrospective studies have correlated clinical response rates with the presence of early memory T cells, particularly memory stem T cells (T_{SCM}), the frequency of these cells remains underrepresented in current approved CAR T products and their therapeutic relevance has not yet been prospectively evaluated.

The primary aim of this thesis was to link CAR T_{SCM} behavior to clinical response through in-depth longitudinal immunomonitoring of 11 patients treated with donor-derived $CD8^+$ CAR T_{SCM} cells, benchmarked against a cohort of 20 patients receiving conventional donor-derived CAR T cells. Mechanistic analyses showed that the higher complete remission rates at low doses and the improved safety profile of the T_{SCM}-treated cohort were associated with enhanced CAR T_{SCM} cell polyfunctionality, greater expansion, ability to generate both effector and self-renewing compartments through clonal succession, and a distinct cytokine profile characterized by IFNγ as the dominant inflammatory mediator versus IL-6 in the standard cohort. Importantly, treatment failure in the T_{SCM} cohort was primarily driven by tumor- and host-mediated resistance mechanisms rather than intrinsic product defects.

The secondary aim of the study was to investigate the biological mechanisms underlying the absence of graft-versus-host disease (GvHD) in both cohorts following donor-derived CAR T cell therapy. A cell-based platform was developed to expand rare, naturally occurring alloreactive T cells from the original alloHSCT donor and engineer them with a CD28-based CAR. We demonstrate that, while CAR stimulation alone was sufficient to induce severe alloreactive CAR T cell dysfunction, concomitant TCR engagement amplified activation, leading to rapid exhaustion and apoptosis. Modulation of CD28-mediated signaling (via AKT inhibition or a milder costimulatory domain such as 41BB) restored alloreactive CAR T cell functionality and persistence. Consistently, phenotypic and transcriptomic profiling along with longitudinal TCR tracking of post-infusion patient samples showed that dominant alloreactive CAR T clones displayed a dysfunctional signature at the peak of expansion, with only transient proliferation and limited persistence overtime.

Collectively, by integrating longitudinal clinical immunomonitoring with mechanistic experimental modeling, this thesis demonstrates that T_{SCM} enrichment in the infusion product improves CAR T cell efficacy and safety, and that CD28-based CAR signaling architecture constrains alloreactivity, ultimately limiting GvHD.

Introduction

Allogeneic hematopoietic stem cell transplantation

The concept that the immune system can control cancer progression was first supported in 1891 by William Coley, who observed spontaneous tumor reduction in a patient with neck sarcoma during erysipelas-associated systemic inflammation[1,2]. Based on this observation, Coley introduced a heat-inactivated bacterial preparation, also known as Coley's toxin, into clinical practice, reporting reproducible tumor regression in treated patients [3,4]. Although the underlying immunological mechanisms were not fully understood at the time, these findings provided early evidence that modulation of the immune system through appropriate molecular or biological strategies can promote tumor eradication, a principle that later became the central paradigm of modern cancer immunotherapy[5-7].

Adoptive cell therapy (ACT) represents the most direct clinical translation of this concept, involving the infusion of autologous or allogeneic immune cells into tumor-bearing patients to enhance or restore cancer immunosurveillance[8]. Steven Rosenberg, considered as the pioneer of ACT, defines it as a "living treatment" as adoptively transferred cells can proliferate *in vivo* and confer long-term protection from tumor recurrence. *Allogeneic hematopoietic stem cell transplantation* (alloHSCT) is the first example of patient-individualized ACT. Its therapeutic benefit derives from the ability of donor-derived hematopoietic stem cells (HSCs) to reconstitute normal hematopoiesis and a functional immune system capable of exerting potent antitumor activity[9]. Importantly, in this setting the choice of the donor plays a central role, as increased genetic disparity at human leukocyte antigen (HLA) loci can trigger aberrant immune responses by alloreactive T cells arising from the graft, leading to recognition of host tissues as non-self and consequent damage[10]. This side effect, described as *graft-versus-host disease* (GvHD), represents the main immune complication occurring after alloHSCT[11]. Paradoxically, the development of GvHD has also been associated with lower rates of malignant relapse and durable remission through an immune-mediated effect known as graft-versus-leukemia (GvL), whereby donor T cells recognize and eliminate residual tumor cells[12]. The GvL remains the most potent form of cellular immune therapy for hematological malignancies and some solid tumors[13]. However, although alloHSCT has been established as a

front-line therapy for high-risk patients with advanced B-cell malignancies, disease relapse remains the leading cause of mortality[14].

Balancing GvHD and GvL through lymphocyte transfer

Numerous strategies have been explored to reduce the risk of GvHD while maintaining or enhancing GvL effect. *Donor leukocyte infusion* (DLI)—the administration of unmanipulated allogeneic lymphocytes from the original transplant donor—was introduced as salvage therapy for patients with refractory or relapsed malignancies post-alloHSCT[15]. Clinical studies demonstrated that DLI alone can achieve durable complete responses in up to 80% of patients with chronic myeloid leukemia (CML) relapsing after alloHSCT[16]. However, outcomes outside of CML have been less encouraging in other progressive B-cell malignancies, showing low remission rates[17]. Additionally, the DLI is associated with a high frequency of severe GvHD, which substantially restricts its therapeutic window[18].

Building on the concept of enhancing GvL effect, researchers started exploring the possibility to transfer into the host a defined subpopulation of lymphocytes capable of eliciting an even more robust anti-tumor response. In the early 1980s, Rosenberg and colleagues discovered that the exposure of peripheral blood leukocytes derived from cancer patients to the T-cell growth factor interleukin-2 (IL-2) could induce a strong proliferation of a heterogeneous mixture of activated NK cells, NK T cells, and T cells, referred to as *lymphokine-activated killer cells* (LAKs)[19]. However, although LAKs showed potent *in vitro* cytotoxic activity, objective responses were reproducibly achieved only in renal cell carcinoma and malignant melanoma, and their administration was associated with considerable systemic toxicity[20].

In 1986, Rosenberg identified for the first time a cell population obtained from resected tumors that appears to be 50 to 100 times more potent than LAKs when used for adoptive transfer, defined as *tumor infiltrating lymphocytes* (TILs)[21]. This subpopulation of lymphocytes could be grown and expanded *in vitro* in the presence of high doses of IL-2. Although promising results were obtained in patients affected by metastatic melanoma, TILs did not often persist, resulting in non-durable anti-tumor responses[22]. Later, it was shown that administering TILs after non-myeloablative lymphodepleting chemotherapy improved persistence and efficacy by reducing immunosuppressive cells and increasing homeostatic cytokines[23]. In a landmark trial, Rosenberg's group treated 93 patients with progressive

metastatic melanoma with autologous TILs after lymphodepletion, achieving objective responses in 56% and complete responses in 22%, many of which were durable beyond three years[24]. More recently, *lifileucel*, a TIL-based product, showed higher response rates than *ipilimumab*, an anti–CTLA-4 monoclonal antibody, in patients with anti–PD-1–refractory metastatic melanoma (50% vs 20%), leading to its accelerated FDA approval in 2024 as the first cellular therapy approved for a solid tumor[25]. Nevertheless, TIL therapy encounters several manufacturing limitations. This approach requires the generation of large numbers of cells which is a complex and laborious process requiring often 3-6 weeks. In addition, patients necessitate the availability of a resectable tumor from which TILs with a tumor-specific reactivity can be isolated and expanded. Although these cells can be grown virtually from all tumors, only highly immunogenic tumors with the highest mutational burden, such as melanoma and Non-Small Cell Lung Cancer (NSCLC), give rise to an effective antitumor lymphocyte population[26].

Redirecting antitumor T cell activity via TCR gene transfer

The advent of *gene therapy* represented a major breakthrough in ACT, enabling the extension of T cell–based immunotherapies to a broader range of tumor types through targeted genetic modifications of specific genes[27]. T Cell Receptor (TCR)-gene therapy rapidly emerged as a valuable tool for ACT. In this approach, high affinity TCRs are isolated from rare tumor-reactive TILs isolated from cancer patients and subsequently introduced into viral or non-viral vectors to redirect T cell specificity toward a defined tumor antigen[28]. In 1999, Clay et al. demonstrated that retroviral transfer of a MART1-specific TCR could enable effective lysis of $MART1^{+}$ melanoma cells[29]. In 2006, Morgan and colleagues reported the first clinical trial using autologous anti-MART1 TCR–transduced T cells in metastatic melanoma, achieving complete regression in only 2 out of 15 patients[30]. Subsequent phase II studies showed modest activity, with objective responses in 6/20 patients treated with anti-MART1 TCR T cells and 3/13 patients receiving gp100-specific TCR T cells[31]. In contrast, higher response rates were observed with T cells engineered to express NY-ESO-1–specific TCRs in melanoma, metastatic sarcoma, and multiple myeloma[32,33].

However, although TCR-therapy has emerged as a promising alternative to TIL therapy and showed encouraging results in multiple early-phase trials, several challenges still limit its broader clinical application. Off-target toxicity is the first potential risk as healthy tissues may

display the same antigen targeted by TCR-engineered T cells[34]. Additionally, the introduction of an exogenous TCR poses the risk of mispairing with the endogenous TCR α- and β-chains, resulting in the formation of hybrid TCRs with unpredictable specificity[35]. Beyond toxicity-related considerations, one of the main limitations of this approach is the Major Histocompatibility Complex (MHC)-restriction since TCR-redirected T cells only recognize and bind the cognate peptides in association with specific MHC molecules. Therefore, patients selected for TCR T cell-based therapy must express not only the targeted antigen, but also the corresponding antigen-related HLA allele[34]. The HLA locus is the most polymorphic region of the human genome and identifying patients who express both biomarkers can considerably restrict the number of patients who can benefit from this therapy. Last, loss or downregulation of MHC-expression on tumor cells prevent the recognition of the target epitope by TCR-engineered T cells[36].

Chimeric Antigen Receptor T cell therapy

A framework shift in ACT involves the use of primary T cells engineered with synthetic receptors known as *chimeric antigen receptors* (CARs). CAR T cell therapy overcomes the primary limitations of TCR therapy by enabling T cells to recognize tumor cell antigens in an MHC-independent manner, greatly broadening the array of antigens that adoptively transferred T cells can recognize[38]. CAR constructs have a modular design and were developed with the intent of combining the antigen recognition capabilities of an antibody with the potent effector functions of T cells[39]. The *extracellular antigen-binding domain* of the currently approved CARs consists of the variable heavy and light chains derived from a monoclonal antibody, linked by a flexible peptide to form a single-chain variable fragment (scFv)[40]. The *intracellular signaling domain* typically comprises an activation domain and one or more co-stimulatory domains which together initiate, strengthen, and sustain the T cell response after antigen binding (**Figure 1**)[40]. CAR structure has evolved over time, mainly through modifications of the intracellular signaling domains. First-generation CARs signaled only through CD3ζ domain (signal 1), which was insufficient to induce productive T cell responses, leading to poor trafficking, limited persistence, and lack of clinical efficacy[41,42]. Second-generation CARs were developed by adding a co-stimulatory domain (signal 2), such as CD28 or 41BB, to improve T cell function, metabolism, proliferation, and persistence[43,44]. Third-generation CARs incorporate an additional co-stimulatory domain (e.g., OX40 and/or 41BB) to further enhance activation and durability[45]. Fourth-generation CARs, known as

TRUCKs, were designed to promote cytokine release upon antigen engagement, supporting CAR T cell survival and modulating the tumor microenvironment[46]. Fifth-generation CARs build on second-generation designs by integrating cytokine receptor signaling to activate JAK/STAT pathways, providing synergistic signals for full T cell activation[47].

CAR T cell therapy has demonstrated considerable results in multiple clinical trials, particularly in the treatment of advanced hematological malignancies arising along the B-cell differentiation pathway. CD19 antigen has been the most promising clinically targeted antigen due to its high expression on the surface of most malignant B cells while in normal tissues it is largely restricted to B cells, some follicular dendritic cells, and is absent on pluripotent HSCs[48]. In 2010, Kochenderfer and collaborators reported the first clinical success in a patient with advanced follicular lymphoma treated with autologous T cells engineered with a second-generation CD19 CAR fused to a CD28 costimulatory domain (FMC63-28ζ), resulting in complete eradication of blood and bone marrow (BM) malignant B cells for 39 weeks[49]. In 2011, Porter and colleagues showed results from a phase I study in a patient with TP53-deleted Chronic Lymphocytic Leukemia (CLL) treated with autologous CD19 CAR T cells incorporating a 41BB co-stimulatory domain. By day 23 post-infusion, BM evaluation showed no evidence of CLL, FISH was negative for TP53 deletion, and the patient remained in remission for up to 10 months[50]. Subsequent studies showed remarkable efficacy of anti-CD19 CAR T cells in relapsed B-acute lymphoblastic leukemia (ALL) and diffuse large B-cell lymphoma (DLBCL) after alloHSCT, with complete response rates of 57–88% and remissions lasting 3–30 months[51,52]. In 2017, the successful outcomes of these studies resulted in the FDA-approval of the first CD19-targeted CAR T cell therapy for the treatment of children and adults with B-cell ALL after two or more lines of systemic therapy following HSCT[53]. In the last decade, the remarkable success of CAR T cell-based immunotherapy encouraged numerous clinical trials, and to date seven approved CAR T cell products are available for the treatment of multiple relapsed/refractory B-cell malignancies[54].

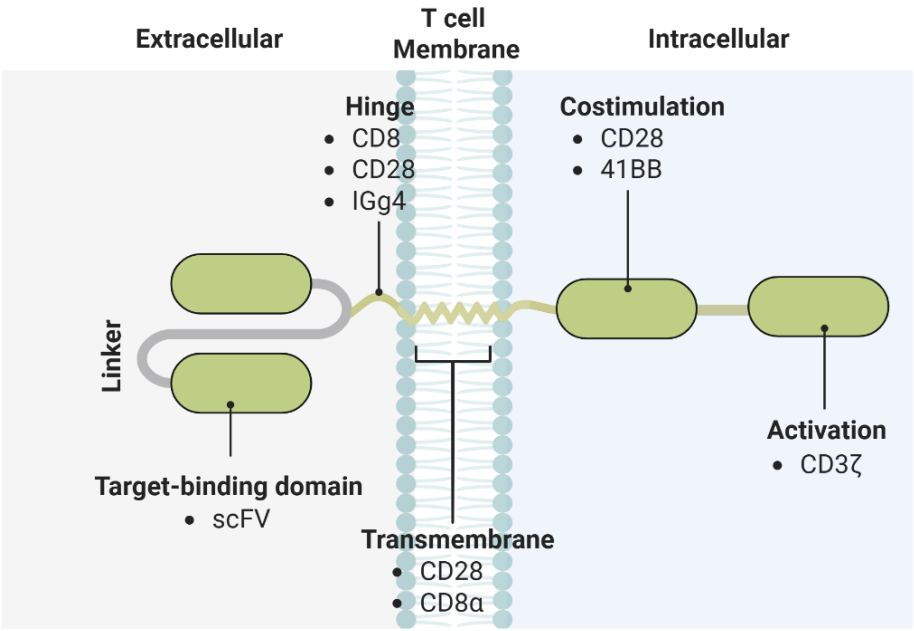

Figure 1. Schematic overview of the modular architecture of currently FDA-approved Chimeric Antigen Receptors (CARs). Chimeric antigen receptors consist of an extracellular antigen-binding domain, typically a single-chain variable fragment (scFv) derived from the murine FMC63 monoclonal antibody, a hinge or spacer region that provides conformational flexibility, and a transmembrane domain that anchors the receptor to the plasma membrane. Intracellularly, costimulatory signaling motifs coupled to the CD3ζ signaling module orchestrate T cell activation following antigen engagement. *This figure was created by me with BioRender.com and was adapted from Rafiq et al., Nat Rev Clin Oncol (2020) (https://doi.org/10.1038/s41571-019-0297-y)*[40]*. Figure reproduced with permission from Springer Nature. License number: 6193260155172.*

Limitations of CAR T Cell Therapy

Despite the outstanding clinical results achieved with CAR T cell therapy, toxicity remains a major limitation. Following infusion and upon antigen-recognition, activated CAR T cells produce a plethora of pro-inflammatory cytokines (e.g. IFN-γ and IL-6) which can aberrantly activate host immune cells, particularly macrophages[55]. This crosstalk between CAR T cells and myeloid cells amplifies cytokine production and promotes the onset of *cytokine release syndrome* (*CRS*) and *immune effector cell-associated neurotoxicity syndrome* (*ICANS*), which represent the most clinically significant adverse events associated with CAR T cell therapy[55]. This aberrant systemic inflammation results in fever, vascular leakage, hypotension, hypoxia, and organ dysfunction, and in severe cases disruption of the blood–brain barrier with accumulation of cytokines and CAR T cells in the central nervous system. A further on-target/off-tumor effect of CARs targeting B cell differentiation antigens such as CD19 is the

long-term *B cell aplasia*, which results in prolonged hypogammaglobulinemia and increased susceptibility to infections[56,57].

In addition to toxicity, durable remission remains a key challenge for CAR T cell-based therapies. Long-term follow-up of patients treated with anti-CD19 CAR T cells has shown a substantial rate of *post-treatment relapse*, with *limited in vivo expansion* and *persistence* of the infused cells[58]. Consequently, over the past two decades, increasing efforts by clinicians, scientists, and industry have focused on the identification of defined T cell subsets as optimal candidates for CAR T cell–based therapies, driven by accumulating evidence that intrinsic differences in differentiation status and metabolic fitness capacity critically influence therapeutic durability, functional persistence, and clinical outcomes.

T cell memory differentiation as a determinant of ACT efficacy

Although the ontogeny of T cells is not yet fully understood and multiple models of differentiation have been proposed, it is well established that antigen-experienced T cells progress through distinct developmental stages as they differentiate into *memory subsets*[59]. In contrast to the relative uniformity of naïve T cells (T_N), *memory T cells* do not emerge in equal fashion but instead comprise multiple subsets with distinct phenotypes, trafficking patterns, and functional properties[60]. In the early 1990s, numerous pioneering studies showed that surface markers—including adhesion molecules and chemokine receptors—can distinguish T_N from memory T cells[61,62,63]. Later, advances in polychromatic flow cytometry enabled a precise identification of distinct memory T cell subpopulations and their associated functional properties[64].

Effector memory T cells (T_{EM}), one of the first memory cells described, represent a readily available pool of more differentiated T cells, characterized by the expression of the antigen-experienced T cell marker CD45R0, the memory marker CD95, and the absence of the lymph node homing molecules CD62L and CCR7[65]. In fact, T_{EM} cells are significantly under-represented in lymph nodes and preferentially traffic to peripheral tissues due to their high expression of chemokine receptors and adhesion molecules, enabling efficient migration under inflammatory conditions and rapid effector cytokine production upon antigen recognition. However, although T_{EM} cells can provide a first line of defense by immediate cytotoxic activity, they show a low proliferative capacity and short *in vivo* persistence[66].

Concurrently with the identification of T_{EM} subset, Hamann et al. described a discrete fraction of antigen-experienced T cells within T_{EM} compartment, characterized by CD45R0 loss, CD45RA upregulation, and potent cytolytic activity with a prominent expression of perforin and Granzyme B[67]. These circulating $CD45RA^+$ tumor-reactive T cells were identified in some melanoma patients and were subsequently designated *terminal effector T cells* (T_{TE}) on the basis of their strong cytolytic potential, competence to migrate into inflamed tissues, and highly differentiated phenotype[68]. However, similarly to T_{EM} cells, T_{TE} cells lack long-term survival and shows low expansion potential, corroborating with the short telomere length and the high susceptibility to cell death[68].

During the same period, Sallusto et al. identified another memory T cell subset with high expression of the homing markers CD62L and CCR7, termed *central memory T cells* (T_{CM}) due to their lymph node–homing capacity[69]. T_{CM} cells are characterized by longer telomeres and robust IL-2 secretion with lower levels of effector cytokines in comparison to T_{EM} and T_{TE} cells. Owing to their *in vitro* and *in vivo* self-renewal capacity, robust proliferative potential, long-term persistence, and ability to rapidly differentiate into T_{EM} and T_{TE} cells upon antigen encounter, T_{CM} cells were long regarded as the least differentiated memory subset endowed with stem cell–like properties[70].

However, the evidence that memory compartment might not be confined solely to T_{EM}, T_{TE} and T_{CM}, emerged when Champagne et al. described in individuals with Human Immunodeficiency Virus (HIV) a distinct memory T cell subset with a T_N-like phenotype, that retained the ability to generate more differentiated cells[71]. In 2005, in a mouse model of human GvHD, Zhang and colleagues identified a similar memory T cell population characterized by the expression of stem cell antigen 1 (SCA1), the common IL-2 and IL-15 receptor β chain memory marker (CD122), and the anti-apoptotic molecule Bcl-2. These antigen-experienced cells were termed *memory stem T cells* (T_{SCM}) due to their ability to sustain GvHD upon serial transplantation into allogeneic hosts and reconstitute the entire spectrum of the memory while maintaining their own pool size[72].

To determine whether differentiation-associated functional and phenotypic features influence the capacity of tumor-specific T cells to mediate tumor regression, Gattinoni and collaborators used gp100-specific T cells from pmel-1 TCR transgenic mice and showed that early-

differentiated memory T cells, resembling *bona fide* T_{SCM} cells previously described by Zhang, induced greater melanoma regression than more-differentiated T cells[73]. For the first time, the same group demonstrated that priming mouse T_N cells in presence of IL-2 and 4,6-disubstituted pyrrolopyrimidine TWS119—a potent inhibitor of glycogen synthase kinase-3β (GSK-3β)—could arrest T cell differentiation and promote the generation of self-renewing, multipotent T_{SCM}-like cells[74]. TWS119-induced T_{SCM} cells rapidly produced cytokines (such as IFN-γ and IL-2) upon antigen encounter, exhibited enhanced proliferative and survival capacity, and retained the ability to self-renew and to generate more differentiated memory T cell subsets after adoptive transfer into lymphoreplete mice[74]. Building on these compelling preclinical findings, Gattinoni and colleagues subsequently identified the human counterpart of T_{SCM} cells with phenotypic and functional properties analogous to those described in mice[75]. The discovery of this early differentiated subset reshaped the hierarchy of the memory compartments, positioning T_{SCM} cells at the apex of the memory T cell differentiation tree[76]. Nevertheless, although these studies shed light on the mechanisms supporting long-lived, antigen-experienced memory T cells, the therapeutic potential of T_{SCM} cells for ACT has not been thoroughly investigated.

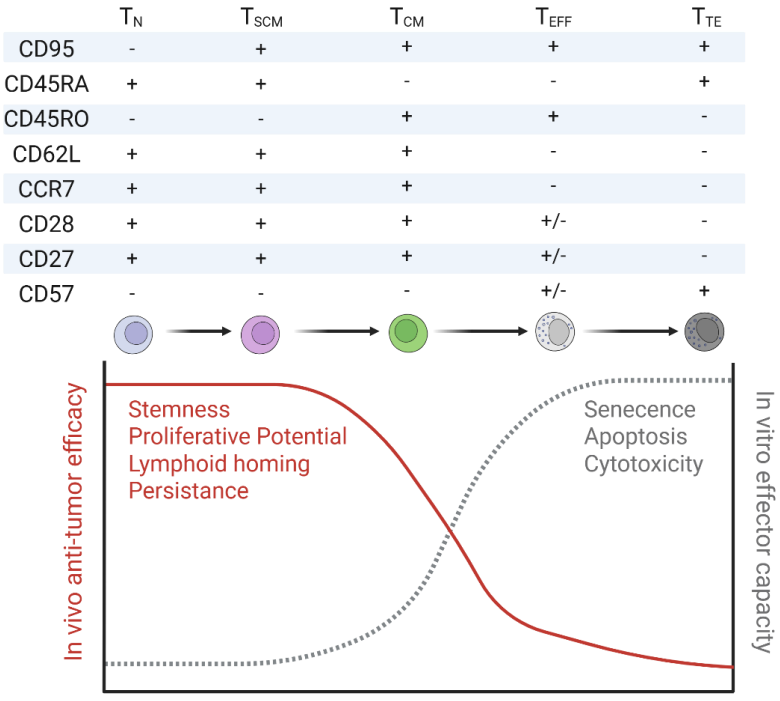

Figure 2. Schematic illustrating the inverse relationship between *in vitro* effector capacity and *in vivo* anti-tumor efficacy of adoptively transferred $CD8^+$ T cell subsets. Following a linear differentiation model, antigen stimulation drives naïve T cells (T_N) toward more differentiated states, characterized by distinct surface markers and progressive reduced proliferative capacity, persistence, and increased senescence/apoptosis. Although *in vitro* effector functions increase (dashed grey line), *in vivo* anti-tumor efficacy (red line) declines

after transfer. T_{SCM}: Memory Stem T cells; T_{CM}: Central Memory T cells; T_{EFF}: Effector Memory T cells; T_{TE}: Terminal Effector T cells. *This figure was created by me with BioRender.com and adapted from Gattinoni et al., Nat Rev Immunol (2006)[77] and Gattinoni et al., Nat Med (2017)[76]. Springer Nature. License numbers: 6193251333433 and 6193251089961.*

Aim of the Project

Gattinoni *et al.* developed a clinical-grade platform for generating CAR-modified T_{SCM} cells and provided preclinical data supporting their superior anti-leukemic activity compared to standard CD19-CAR T cell products in acute lymphoblastic leukemia xenograft[78]. To translate these findings into clinical application, a previously reported Phase I trial enrolling 20 patients with relapsed or refractory $CD19^+$ malignancies after alloHSCT treated with conventional CD19-CAR T cells (NCT01087294)[79] was amended to include a second cohort of 11 patients receiving T_{SCM}-enriched CAR T cells. Both CAR T cell products were manufactured at the National Institutes of Health (Bethesda, USA) from the original alloHSCT donor and administered to the two patient cohorts without prior chemotherapy conditioning, allowing a direct comparison without confounding effects from other treatments.

In this first-in-human study, we aim to comprehensively characterize the *in vivo* behavior of a CD19-CAR T cell product highly enriched in T_{SCM} cells and to correlate expansion, persistence, and differentiation with clinical outcomes, in order to assess whether CAR T_{SCM} cells provide a superior therapeutic platform compared with conventional CAR T cells. Single-cell functional profiling and multiplex cytokine assays were performed to evaluate CAR T cell activity and safety. In addition, high-resolution flow cytometry and longitudinal *in vivo* tracking through retroviral integration site analysis were performed to reconstruct the *in vivo* differentiation trajectories and clonal dynamics of both T_{SCM} and standard CAR T cells following infusion. Finally, mechanistic analyses were performed to investigate tumor- and

host-derived factors contributing to treatment failure and disease relapse in nonresponding patients.

The second aim of this thesis is to investigate the absence of GvHD following allogeneic CAR T cell therapy and to define the potential of alloreactive CAR T cells to trigger alloresponses. To address this, a cell-based platform was developed to enable precise identification and characterization of rare donor-derived alloreactive T cells engineered with a CD28-based CAR. In parallel, phenotypic and transcriptompic profiling along with longitudinal TCR clonal tracking were performed in two selected patients receiving allogeneic CAR T cells from HLA-mismatched donors to define the *in vivo* dynamics of alloreactive CAR T cells.

Material and Methods

Preliminary note: *The clinical trial protocol was approved by the National Institutes of Health (NIH) Institutional Review Board (**IRB**; **NIH protocol #10-C-0054**, approval date: March 13, 2010). An investigational new drug (**IND 14172**) application for anti-CD19 CAR T_{SCM} cells was cleared by the U.S. Food and Drug Administration. Written informed consent for protocol interventions and for the collection of blood and tissue samples was obtained from all patients. The trial was registered at ClinicalTrials.gov (**NCT01087294**). All patients and matched donors provided informed consent in compliance with the Declaration of Helsinki.*

For each method described below, the author's direct technical execution—whether performed independently or with the assistance of a co-author of the project—is explicitly indicated at the end of each paragraph.

Trial design, patient cohort, and toxicity

The study was designed as a single-center, phase 1 dose-escalation clinical trial of donor-derived anti-CD19 CAR T cells in patients with relapsed or refractory B-cell malignancies following ≥9/10 human leukocyte antigen (HLA)-matched sibling or unrelated donor alloHSCT, as previously reported (NCT01087294)[79]. Patients received a single infusion of

CAR T cells with no preconditioning chemotherapy. Second infusions were allowed for patients with a partial response (PR), stable disease (SD), or relapse after complete response (CR) and continued uniform expression of CD19 on the malignancy. After the initial 20 patients were treated with the conventional cell culture process (hereinafter standard cohort), the trial protocol was amended to allow treatment of a second cohort of 11 patients, who received CAR $CD8^+$ T_{SCM}-enriched cells on a separate dose-escalation. The characteristics and clinical course of the patients who received standard CAR T cells and CAR T_{SCM} cells are summarized in the **Supplementary Tables S1** and **S2**, respectively. Minimal acute GvHD was defined as grade 0-I[80], and minimal chronic GvHD was defined as chronic GvHD with no organ site with a score exceeding 1, except for the skin, for which a score of 1 or 2 was allowed[81]. Malignancy responses were assessed with published criteria for non-Hodgkin lymphoma[82,83] and chronic lymphocytic leukemia[84]. Criteria for CR of B-cell acute lymphoblastic leukemia were as previously described[85]. Cytokine release syndrome was graded per the American Society for Transplantation and Cellular Therapy criteria[85].

Note: *All the clinical procedures described above, including patient enrollment, patient treatment, imaging, toxicity evaluation, and collection of biological samples were not performed by me but were carried out at the National Institutes of Health (US) under the direction of Dr. Jennifer Brudno and Dr. James N. Kochenderfer, last authors of the manuscript accepted in CELL.*

Donor-derived CAR T cell manufacturing

As previously reported[79], standard CAR-modified T cells were generated from patient peripheral blood mononuclear cells (PBMCs) cultured in complete AIMV medium with 5% human AB serum and 300 IU/mL IL-2. T cell proliferation was initiated with 50 ng/mL anti-CD3 antibody (OKT3). Two days after activation, 2×10^6 PBMCs were added to six-well plates pre-coated with Retronectin and anti-CD19 CAR gammaretroviral vector. After overnight incubation, cells were then transferred to fresh complete AIMV medium supplemented with 300 IU/mL IL-2 for further expansion. On day 8, standard CAR T cells were infused into 20 patients. A clinical-grade platform for the generation of CD19 CAR-modified T_{SCM} cells was previously developed[78]. Briefly, CAR-modified $CD8^+$ T_{SCM}-enriched cells were prepared from PBMCs obtained from each patient's transplant donor leukapheresis. $CD8^+CD62L^+CD45RA^+$ T cells were serially enriched using Fab-Streptamer™ technology and stimulated with CD3/CD28 microbeads in media supplemented with IL-7, IL-21, and the glycogen synthase 3β inhibitor TWS119. T cells were subsequently transduced with anti-

CD19 CAR gammaretroviral vector and freshly infused into patients after 7 days of culture. Both infused T cell products were transduced using the same MSGV-FMC63-28 anti-CD19 CAR retroviral vector.

Note: *CD19 CAR T cells were manufactured at the National Institutes of Health Clinical Center Cell Processing Facility. David F. Stroncek and Steven L. Highfill, both co-authors of the manuscript accepted in CELL, performed process development for cellular manufacturing and supervised cellular manufacturing.*

Real-time qPCR for measuring blood CAR T cell absolute levels

Similar to an approach used previously by other investigators[79], circulating CAR T cells were quantified up to 36 days post-infusion using a qPCR assay targeting the integrated FMC63 CAR transgene sequence. Genomic DNA (gDNA) from pre- and post-CAR T cell infusion samples were extracted with the QIAGEN DNeasy Blood and Tissue Kit and subsequently amplified in duplicate with CAR-specific primers and TaqMan probes (Applied Biosystems). Patient-standard curves were generated by performing qPCR on 5-fold serial dilutions of infusion product gDNA into pre-CAR T cell infusion gDNA of the same patient. The percentage of CAR^+ T cells in the infused products was determined by flow cytometry using an anti-FMC63 antibody (Acro Biosystem). To calculate the percentage of CAR T cells at each post-infusion time point, qPCR results from gDNA post-infusion samples were compared to the patient-specific standard curve. All samples were normalized to the patient β-actin gene, using a β-actin standard curve generated by qPCR on a pCMV6-AC β-actin plasmid with the PrimePCR™ Probe Assay for ACTB (Bio-Rad). The absolute circulating CAR T cell number was calculated by multiplying the percentage of CAR^+ T cells by the sum of the absolute number of blood lymphocytes and monocytes, expressed as CAR^+ T cells per μL of peripheral blood. All results were normalized to the total infused CAR T cell doses. The R^2 value for all qPCR assays was ≥ 0.99.

Note: *Real-time qPCR protocol was developed by me with the assistance of Danielle A. Natrakul, co-author of the manuscript accepted in CELL. Technical execution and data analysis were performed entirely by me.*

Assessment of serum cytokine concentration

Serum samples collected before and after CAR T cell infusion were cryopreserved in liquid nitrogen, thawed, and analyzed for cytokine levels. Cytokine measurement was performed using the MILLIPLEX Human High Sensitivity T Cell Magnetic Bead Panel (GM-CSF, IFN-

γ, TNF-α, IL-1β, IL-2, IL-4, IL-5, IL-6, IL-7, IL-8, IL-10, IL-12, IL-13) and the MILLIPLEX Human Cytokine/Chemokine/Growth Factor Panel (IL-1RA, IL-35, TGF-β1, TGF-β2, TGF-β3) kits, following the manufacturer's protocols. Cytokines were detected using the Luminex MAGPIX system with xPONENT 4.2 software. Median Fluorescent Intensity (MFI) values were processed using the 5-parameter logistic regression method in Belysa software version 1.0.19 to calculate analyte concentrations. All standard curves exhibited R^2 values ≥ 0.99.

Note: *All experimental procedures and associated data analyses described above were performed exclusively by me.*

CAR T cell functionality evaluation by single-cell multiplex cytokine profiling

Cryopreserved CAR T cell infusion products were thawed and cultured overnight in AIMV complete medium (Thermo Fisher Scientific) supplemented with 5% FBS (Cytiva), 100 U/mL penicillin, 100 µg/mL streptomycin, 2 mM Glutamax, and 10 mM HEPES (Thermo Fisher Scientific). Cytokine supplementation included either IL-2 (250 IU/mL) for standard CAR T cells or a combination of IL-7 (5 ng/mL) and IL-21 (30 ng/mL) for CAR-modified T_{SCM}-$CD8^+$-enriched cells. After overnight recovery, CAR T cells were stained with Pacific Blue anti-CD8, APC anti-CD19 CAR antibodies, and 7-AAD to exclude dead cells. Viable $CD8^+CAR^+$ T cells were isolated by fluorescence-activated cell sorting and subsequently co-cultured with K562 cell lines engineered to express CD19 antigen at an effector to target ratio 1:1. $CD19^+$ target cells used to stimulate CAR T cells were already available at the Leibniz Institute for Immunotherapy in the laboratory of Prof. Luca Gattinoni and were originally generated at the National Institutes of Health (NIH) in the laboratory of Dr. Kochenderfer. Following 16h of antigen stimulation, $CD19^+$ K562 cells were depleted using CD235a-specific magnetic microbeads (Miltenyi Biotec) according to the manufacturer's instructions. Negatively selected $CD8^+CAR^+$ T cells were stained with stain-cell membrane 405 and AF647 anti-CD8, then resuspended in cytokine-free AIMV complete medium at a density of 1×10^6/mL. For single-cell secretomic analysis, 30,000 CAR T cells were loaded onto a single-cell barcode microchip (IsoPlexis). A 32-cytokine panel was used for assessing the following secreted analytes: CCL11, GM-CSF, GZMB, IFN-γ, IL-10, IL-12, IL-13, IL-15, IL-17A, IL-17F, IL-1β, IL-2, IL-21, IL-22, IL-4, IL-5, IL-6, IL-7, IL-8, IL-9, IP-10, CCL2, CCL13, CCL3, CCL4, Perforin, CCL5, s41BB, sCD40, TGF-β1, TNF-α, and TNF-β. Raw data from IsoLight were processed and analyzed using IsoSpeak software, and high-dimensional single-cell data were further analyzed with the unsupervised VIA clustering algorithm implemented in the CRUSTY web tool (https://crusty.humanitas.it/)[86], with parameter K set to 100.

Note: *The IsoPlexis assay was designed by me with the assistance of Dragana Slavkovic-Lukic, co-author of the manuscript accepted in CELL. The technical execution, including CAR T cell processing, co-culture, chip loading, and data analysis were entirely performed by me. Sample and instrument preparation for cell sorting was entirely performed by me. Cell sorting was performed by the sorting facility at the Leibniz Institute for Immunotherapy.*

Polychromatic flow cytometry

A 23-color flow cytometry panel was devised to broadly characterize T cell differentiation, activation, and exhaustion markers involved with immunotherapy response, including CD28, CD38, CD29, CD57, OX40, CD45R0, PD1, CD8, CD95, HLA-DR, CD4, CD25, TIGIT, CD127, CCR7, CD45RA, CD3, T-bet, Ki67, Granzyme (GZM) B, and GZMK. This panel was used to assess the status of CAR T cells from the day of infusion through up to one-year post-transfer. Cryopreserved PBMCs were thawed in RPMI medium supplemented with 10% fetal bovine serum (FBS), 100 U/mL penicillin, 100 µg/mL streptomycin, 2 mM L-glutamine, and 20 mM HEPES. Cells were washed in phosphate-buffered saline without calcium and magnesium (PBS) and stained immediately with Zombie Aqua Fixable Viability Dye (ThermoFisher) for 15 minutes at room temperature. After washing, cells were stained in a 1:1 mix of FACS buffer (PBS, 2% FBS) and BD Horizon™ Brilliant Stain Buffer (BD Biosciences) using monoclonal antibodies (mAbs). PE CAR (FMC63) was from AcroBiosystem, BV786 CD28 (CD28.2); BV711 CD38 (HIT2), APC-Cy7 CD29 (TS2/16), CD45R0 (UCHL1) were from BioLegend; BV605 CD57 (NK-1), BV650 OX40 (ACT35), BV570, BV480 PD1 (EH12.1), BUV805 CD8 (HIT8a), BUV737 CD95 (DX2), BUV661 HLA-DR (G46-6), BUV615 CD4 (SK3), BUV563 CD25 (2A3), PE-CF594 CCR7 (150503), BUV395 CD45RA (5H9), BUV496 CD3 (UCHT1), FITC Ki67 (B56), AF700 Granzyme (GZM) B (GB11) were from BD Biosciences; PerCP-eF710 TIGIT (MBSA43), Pe-Cy5 CD127 (eBioRDR5), PeCy5.5 T-bet (eBio4B10), were from eBioscience and AF647 GZMK (GM6C3) was from Santa Cruz. Chemokine receptors were stained in medium for 20 minutes at 37°C, while other surface markers were stained at room temperature for 20 minutes. Intracellular staining for Ki67, T-bet, GZMB, and GZMK was performed using the FoxP3 transcription factor staining buffer set (eBioscience/Thermo Fisher) per the manufacturer's protocol, followed by incubation with specific mAbs for 30 minutes at 4°C. Samples were acquired using a FACS Symphony A5 flow cytometer (BD Biosciences). Flow cytometry data were compensated in FlowJo software version 10 using single-stained controls prepared with BD CompBeads incubated with the respective fluorochrome-conjugated antibodies.

To assess CAR T cell phenotype in both standard and T_{SCM} infusion products, a 10-color flow cytometry panel using PE CAR, BV786 CD28, BV570 CD45R0, BUV805 CD8, BUV737 CD95, BUV615 CD4, AF700 CD27, PE-CF594 CCR7, BUV395 CD45RA, and BUV496 CD3 was optimized. PBMCs were thawed and processed as described above. For cluster analysis of infusion products, dead cells and aggregates were excluded, and $CD3^+CAR^+$ T cells were gated. From each patient sample, 3,000 events were biexponentially transformed and exported using FlowJo. Data were analyzed with the Phenograph algorithm, implemented in the CRUSTY web tool (https://crusty.humanitas.it/)[86], using parameter K = 100, Resolution = 0.9. Bioinformatic analyses for **Figure 6A-F** were performed as follows. Slingshot was used to infer continuous, branching lineage structures in low-dimensional data. After performing dimensionality reduction and clustering, Slingshot modeled developmental trajectories to delineate lineage relationships within the dataset. Wishbone was utilized to improve the resolution of cell-state transitions[87]. Derivative analysis was employed to time key events along the inferred trajectory computed with Slingshot, refining the temporal ordering of cellular differentiation. PCA plots and Balloon plots were generated using custom Python scripts utilizing the Matplotlib and Seaborn libraries.

Note: *The experimental design, technical execution, and sample analysis of Flow Cytometry data were performed primarily by me with the assistance of Alberto Susana, co-author of the manuscript accepted in CELL. The bioinformatic analysis (Slingshot, Wishbone, and PCA) were performed by Simone Puccio, co-author of the manuscript accepted in CELL, under my guidance and that of Prof. Luca Gattinoni and Dr. Enrico Lugli, co-author of the manuscript accepted in CELL.*

CAR T cell longitudinal tracking via integration site analysis

The frequency and genomic loci of retroviral CAR integration sites were assessed for each T cell memory subset obtained from infusion CAR T cell product and post-infusion samples. Cryopreserved samples were thawed in RPMI medium supplemented with 10% FBS, 100 U/mL penicillin, 100 µg/mL streptomycin, and 2 mM L-glutamine. After washing with PBS, cells were stained with Zombie Aqua Fixable Viability Dye for 15 minutes at room temperature. Chemokine receptors CD95 and CCR7 were stained for 20 minutes at 37°C, while CD3, CD8, CD45RA, and CD45R0 were stained for 20 minutes at room temperature. $CD3^+CD8^+$ T cell memory subsets were sorted by FACS as follows: T_{SCM} cells ($CCR7^+CD45RA^+CD45R0^-CD95^+$), T_{CM} cells ($CCR7^+CD45RA^-$), T_{EM} cells ($CCR7^-CD45RA^-$), and T_{TE} cells ($CCR7^-CD45RA^+$). From each sorted memory subset,

gDNA was extracted using the Qiagen QIAamp DNA Blood Mini Kit, followed by whole-genome amplification with the Qiagen Repli-G Mini Kit per manufacturer's instructions. Integration site analysis (ISA) was performed using a previously described non-restrictive vector-genome Junction amplification method combined with high-throughput sequencing[88]. Briefly, amplified gDNA was fragmented by sonication to generate ~1000 bp fragments and ligated to a linker cassette (LC) with a known sequence. Two rounds of exponential PCRs (35 cycles each) were conducted using primers specific to the vector long terminal repeats (LTRs) and the LCs. A final PCR step introduced Illumina adapter sequences and a unique index for each sample, enabling multiplexing for next-generation sequencing on the Illumina NextSeq 2000. A set of 24 fusion PCR primers was designed to bind the vector LTR, and a set of 24 fusion PCR primers designed to bind the LC (all primers were purchased from Integrated DNA Technology). Fusion PCR products were purified, quantified, and pooled in an equimolar fashion. Prepared pooled libraries were quantified and loaded onto the Illumina NextSeq 2000. Sequencing reads were demultiplexed based on the sample-specific indices and analysis of sequencing reads including mapping and annotation to the human genome (hg18 version) was performed using the IS-Seq bioinformatic pipeline[88].

Note*: Project planning and all the technical experiments described here were entirely conceived and conceived by me. Protocol for Integration Site Analysis assay was developed and optimized at Leibniz Institute for Immunotherapy entirely by me. Sequencing was performed by me and Johanna Raithel under the guidance of Michael Rheli, co-author of the manuscript accepted in CELL. Bioinformatic analyses were performed by Luca Biasco and Nicholas Strieder, both co-authors of the manuscript accepted in CELL. Sample and instrument preparation for cell sorting was entirely performed by me. Cell sorting was performed by the sorting facility at the Leibniz Institute for Immunotherapy.*

Anti-CAR immune responses

Serum samples were collected from patients before and after CAR T cell infusion to assess humoral immunogenicity against the mouse FMC63. Anti-mouse CD19 CAR (mCD19 CAR) antibodies were quantified using an anti-CD19 (FMC63) CAR immunogenicity ELISA kit (Acro Biosystems) per manufacturer's instructions. Absorbance was measured at 450 nm and 630 nm using a Spark 10M multimode microplate reader (TECAN). To reduce background noise, the OD630 nm value was subtracted from the OD450 nm reading. A standard curve was generated using SparkControl software V2.3 with a four-parameter logistic model, and anti-mCD19 CAR antibody concentrations were calculated accordingly.

Note: *All experimental procedures and associated data analyses described above were performed exclusively by me.*

Lentiviral and Gamma-Retroviral vector production

Coding sequences for CD80, 41BBL, CD74, and HLA-DMαβ were obtained from the VectorBuilder database and cloned into the customizable pLV lentiviral vector backbone (VectorBuilder) under the EF1α promoter. Patient- and donor-specific HLA variants were identified by a 2-digit resolution HLA-typing of genomic DNA (gDNA) extracted from pre-infusion recipient and original donor apheresis PBMCs using HLA Fusion v4.6.0.13925 (One Lambda) at Universitätsklinikum Regensburg. The QIAGEN DNeasy Blood and Tissue Kit was used for gDNA extraction. Based on the typing results, the mismatched-HLA alleles identified for patient 11 were HLA-DRα*01:01 and HLA-DRβ1*13:05, while the mismatched-HLA alleles for patient 20 were HLA-DQα*02:01 and HLA-DQβ1*03:01. The corresponding HLA sequences were retrieved from the NCBI database and cloned into the pLV backbone (VectorBuilder) under the EF1α promoter.

Second-generation lentiviral vectors were produced by transient transfection of Lenti-X HEK-293T cells (Takara) with the pMD2.g envelope plasmid, the psPAX2 (GenScript) packaging plasmid, and the respective transgene plasmids using Lipofectamine 3000 (Thermo Fisher Scientific). The medium was replaced 6h post-transfection, and supernatants were harvested after 24h and 48h. Lentiviral supernatants were pooled, filtered through a 0.22 µm Stericup filter (Millipore), and concentrated by centrifugation at 20,000 rpm for 2h at 20°C with Optima Ultracentrifuge (Beckman coulter). Pellets were resuspended in PBS to achieve a 1000x concentration.

The gamma-retroviral construct encoding the anti-CD19 CAR with a 41BBz costimulatory domain (BBz CAR) was kindly provided by Dr. James Kochenderfer (National Cancer Institute). The BBz CAR consisted of anti-CD19 scFv FMC63, a CD8 hinge and transmembrane region, and 41BB and CD3-ζ cytoplasmic regions. Gamma-retrovirus was generated by transfecting HEK-293Tgp (gag-pol) packaging cell lines with RD114 envelope plasmid and the BBz CAR construct using Lipofectamine 2000 (Thermo Fisher Scientific). The medium was replaced after 6h from transfection, then the viral supernatants collected at 24h and 48h were pooled, filtered, and concentrated as described above.

The anti-CD19 CAR incorporating a CD28 costimulatory domain (28z CAR) was generated from PG13-CD19-CAR-H3 producer cell lines, kindly provided by Dr. Steven Rosenberg (National Cancer Institute). The 28z CAR consisted of anti-CD19 scFv FMC63, a CD8 hinge

region, CD28 transmembrane and cytoplasmic regions, and a CD3-ζ cytoplasmic region12,49. Briefly, cryopreserved PG13-CD19-CAR-H3 cells were thawed and cultured in RPMI 1640 medium (Gibco) supplemented with 10% fetal bovine serum (FBS; Cytiva), 100 U/mL penicillin, and 100 μg/mL streptomycin for 4 days, with passaging every 2 days. The day prior to supernatant collection, the culture medium was replaced with complete RPMI 1640 medium, and viral supernatant was harvested after 24h, filtered and concentrated as described above.

Note: *All experimental procedures and associated data analyses described above were performed exclusively by me.*

Generation of K562-based antigen presenting cells

K562 cells were kindly provided by Wolfgang Herr's lab and maintained in RPMI 1640 medium (Gibco), supplemented with 5% FBS (Cytiva), 100 U/mL penicillin, and 100 μg/mL streptomycin. To induce HLA molecule upregulation, K562 cells were stimulated with 20 ng/mL interferon (IFN)-γ (PeproTech) for 16h. HLA-Class I and Class II expression on K562 cells was assessed with either APC anti-human HLA-A,B,C antibody (Biolegend, clone W6/32) or APC anti-human HLA-DR, DP, DQ antibody (Biolegend, clone Tu39) on BD Symphony A5 flow cytometer. Following IFNγ-stimulation, cells were electroporated with TrueCut Cas9 Protein v2 (ThermoFisher) and pre-assembled single guide RNA (sgRNA) (IDT) targeting the β2-microglobulin (B2M) gene (AAGTCAACTTCAATGTCGGA) in P4 buffer (Lonza) with a 4D Nucleofector X unit (Lonza). Cells were rested in the incubator at 37°C for 10 min, then resuspended in complete RPMI 1640 medium. After 6 days from electroporation, cells were restimulated with 20 ng/mL IFN-γ for 16h and stained with APC-conjugated anti-HLA-A, B, C antibody. HLA class I-negative cells were isolated by fluorescence-activated cell sorting on a BD Aria Fusion and transduced with a lentivirus encoding CD74 (invariant chain). As CD74 is an intracellular protein, B2M-knockout (KO) K562 cells were single-cell sorted into a 96 well plate and expanded. Individual clones were fixed and permeabilized using the Intracellular Fixation and Permeabilization kit (eBioscience) according to the manufacturer's instructions and stained with APC anti-human CD74 antibody (BioLegend, LN2). The clone exhibiting the highest expression of CD74 was selected and sequentially transduced with three separate lentiviruses encoding CD80, 41BBL and HLA-DMαβ. After 6 days post-transduction, B2M KO/CD74+ K562 cells were stained with FITC anti-CD80 (BioLegend, 2D10), PE/Cyanine7 anti-41BBL (BioLegend, 5F4), and PE anti-HLA-DM (BioLegend, MaP.DM1) antibodies, and then viable $CD80^{+}$/$41BBL^{+}$/HLA-

DM^+ cells were sorted. Zombie Violet Fixable Viability Kit (BioLegend) was used to exclude dead cells. Finally, to generate a K562-based platform capable of presenting the relevant mismatched-HLA molecules, engineered K562 cells (eK562) were sequentially transduced with HLA-DRα*01:01 followed by HLA-DRβ1*13:05 chains for generating the HLA of patient 11 or with HLA-DQα*02:01 and HLA-DQβ1*03:01 chains for reconstructing the HLA of patient 20. Transduced cells were subsequently stained and sorted using APC-conjugated anti-human HLA-DR antibody (BioLegend, clone L243) or APC-conjugated anti-human HLA-DQ antibody (Thermo Fisher Scientific, clone SK10), respectively.

Note: *All experimental procedures and associated data analyses described above were performed exclusively by me. Sample and instrument preparation for cell sorting was entirely performed by me. Cell sorting was performed by the sorting facility at the Leibniz Institute for Immunotherapy.*

Characterization of proliferating T cells

Cryopreserved PBMCs from original donor apheresis samples and from healthy individuals carrying the same HLA loci of the donors (purchased from Cellular Technology Limited) were thawed in AIM-V medium (Thermo Fisher Scientific) supplemented with 10% fetal bovine serum (FBS; Cytiva), 100 U/mL penicillin, 100 µg/mL streptomycin, 2 mM GlutaMAX, and 10 mM HEPES. After overnight recovery, PBMCs were labelled with 2.5 µM CellTrace CFSE dye (Invitrogen) and stimulated in a mixed lymphocyte reaction (MLR) with irradiated HLA-mismatched eK562 cells (90 Gy) at a 2:1 T cell-to-*e*K562 ratio in complete AIM-V medium in the absence of cytokines. Control conditions included CFSE-labelled donor PBMCs either left unstimulated or stimulated with *e*K562 cells lacking HLA expression. To evaluate activation of proliferating (CFSE-) T cells, cells were harvested 6 days post-MLR and stained with the following anti-human antibodies: BUV496 anti-CD3, BUV805 anti-CD8, BUV615 anti-CD4, BV421 anti-CD40L, PerCP-Cy5.5 anti-CD69, Alexa Fluor 700 anti-CD71, BUV563 anti-CD25, and BUV661 anti-HLA-DR. Dead cells were excluded using Zombie NIR Fixable Viability Dye (BioLegend). Samples were acquired on a FACS Symphony A5 flow cytometer (BD Biosciences). Compensation was performed in FlowJo software version 10 using single-stained BD CompBeads incubated with the corresponding fluorochrome-conjugated antibodies.

Note: *All experimental procedures and associated data analyses described above were performed exclusively by me.*

Generation of alloreactive T cell and transduction

MLR assay with cryopreserved PBMCs from donor original apheresis samples and from healthy individuals carrying the same HLA loci of the donors was performed as described above. After 6 days of stimulation, cells were stained with the following antibodies: BV786 anti-CD3, APC anti-CD8, BV605 anti-CD4, BUV737 anti-HLA-DR, Alexa Fluor 700 anti-CD71, PE-Cy7 anti-CD25, and Zombie Violet dye. Viable $CFSE^+$ or $CFSE^-$ $CD3^+CD8^+CD4^+$ T cells—either expressing or lacking HLA-DR, CD25, and CD71—were isolated by fluorescence-activated cell sorting and resuspended in complete AIM-V medium supplemented with recombinant human interleukin-2 (600 IU/mL).

To generate alloreactive CAR T cells, sorted $HLA\text{-}DR^+CD25^+CD71^+$ T cells were immediately transduced with either BBz CAR or 28z CAR using retronectin-coated plates preloaded with the respective gamma-retroviral vector. Transduced cells were expanded for 6 days in complete AIM-V medium supplemented with rhIL-2 (500 IU/mL). For iAKT-28z CAR T cells, alloreactive T cells sorted from the MLR were transduced with a 28z CAR in presence of 5µM AKT inhibitor (Merck) and maintained in culture for 6 days in complete AIM-V medium supplemented with rhIL-2 (500 IU/mL). Prior to downstream functional assays transduced alloreactive CAR T cells were sorted for CAR expression using BD FACSAria™ Fusion Flow Cytometer.

Note: *All experimental procedures and associated data analyses described above were performed exclusively by me. Sample and instrument preparation for cell sorting was entirely performed by me. Cell sorting was performed by the sorting facility at the Leibniz Institute for Immunotherapy.*

IFN-γ ELISpot assay

To evaluate the alloreactive potential of each sorted T cell subset, 4×103 $CFSE^+$ or $CFSE^-$ T cells—either expressing or lacking HLA-DR, CD25, and CD71—were seeded into a MultiScreen HTS 96-well filtration plate (Millipore) pre-coated with 10 µg/mL anti-human IFN-γ capture antibody (Mabtech, clone 1-D1K). Subsequently, 2 × 104 HLA-mismatched eK562 cells were used as stimulator cells at a final 1:5 E:T ratio and incubated for 24 hours at 37 °C. Controls consisted of sorted T cells alone or stimulated with eK562 cells lacking HLA expression. After incubation, plates were washed with PBS-Tween and incubated with 2 µg/mL biotinylated anti-IFN-γ antibody (Mabtech, clone 7-B6-1) for 2 h at 37°C. Streptavidin-Peroxidase ABC complex (Vector Laboratories) was added and further incubated for 1h at room temperature (RT). Following three additional PBS-Tween washes, 3-

amino-9-ethylcarbazole (AEC) substrate solution (Sigma), freshly supplemented with H2O2 (Sigma), was added and incubated for additional 10 minutes at RT. The reaction was stopped by rinsing the plate with tap water. IFN-γ-spots were counted using an ImmunoSpot S6 reader (Cellular Technology Limited) and analyzed with ImmunoSpot Capture v5.0 software using default parameters.

Note: *All experimental procedures and associated data analyses described above were performed exclusively by me.*

In vitro co-culture assays

For intracellular cytokine staining, alloreactive CAR T cells were pre-incubated with GolgiStop™ (BD Biosciences) and co-cultured with the respective target cells at a 1:5 E:T ratio in a 96-well round bottom plate. Following 12 hours of incubation, cells were stained with Zombie NIR Fixable Viability Dye for 10 minutes at RT. After washing, surface markers were stained with the following antibodies: PE CAR (Acrobiosystem, FMC63), Alexa Fluor 700 anti-CD30, BUV805 anti-CD8, and BUV496 anti-CD4. After 20 min of incubation, cells were washed and subsequently fixed and permeabilized using the Intracellular Fixation and Permeabilization Kit according to the manufacturer's instructions, followed by the staining with the respective monoclonal antibodies: PE CAR (Acrobiosystem, FMC63), BV421 anti-Granzyme B, BB700 anti-IFN-γ, APC anti-IL-2, BV711 anti-CD107a, and BUV496 anti-TNFα. Stained cells were incubated for 30 min at 4 °C, washed and immediately acquired.

For co-culture experiments, alloreactive CAR T cells were co-cultured with the respective target cells at the E:T ratios of 2:1, 1:2, and 1:5. Targets included CFSE-labelled HLA-mismatched eK562 cells, CellTrace™ Violet-labelled $CD19^+$ eK562 cells (ThermoFisher Scientific), or a combination of both. After 3 days, cells were stained with Zombie NIR Fixable Viability Dye for 10 min at RT, following incubation with PE CAR, PerCP-eF710 anti-TIGIT, BV421 anti-PD1, BV650 anti-TIM3, and Alexa Fluor 700 anti-CD3, anti-CD8, and anti-CD4. After washing, TrueCount™ Beads (BD Bioscience) were added to each well and absolute numbers of alloreactive CAR T cells and targets were assessed by flow cytometry. Target elimination efficiency was calculated as follows: [1 − (number of residual target cells in presence of alloreactive CAR T cells)/(number of residual target cells alone)] × 100.

Note: *All experimental procedures and associated data analyses described above were performed exclusively by me.*

Polychromatic Flow Cytometry and Phosflow

A 13-color flow cytometry panel was devised to assess the activation and exhaustion status of alloreactive CAR T cells and their non-CAR alloreactive counterparts from the original donor apheresis and post-infusion samples. Cryopreserved PBMCs were thawed in complete AIM-V media and labelled with 2.5 μM CellTrace CFSE dye. MLR was carried out using irradiated HLA-mismatched eK562 cells, as described above. Following 6 days of stimulation, cells from MLR were collected, washed in PBS and stained with Zombie NIR Fixable Viability Dye for 10 min at RT. After washing, cells were stained in a 1:1 mix of FACS buffer (PBS, 2% FBS) and BD Horizon™ Brilliant Stain Buffer (BD Biosciences) using the following monoclonal antibodies: PE anti-CD19 CAR (AcroBiosystem, FMC63), BV650 anti-TIM3, PerCP-eF710 anti-TIGIT, BV421 anti-LAG3, BV480 anti-PD1, BUV805 anti-CD8, Alexa Fluor 700 anti-CD71, BUV615 anti-CD4, BUV661 anti-HLA-DR, BUV563 anti-CD25, and BUV496 anti-CD3. To detect molecules potentially downregulated upon activation, intracellular staining for CAR, CD3, CD8, and CD4 was performed using the Intracellular Fixation and Permeabilization Kit, followed by incubation with the respective monoclonal antibodies for 30 min at 4 °C. Stained cells were washed and immediately acquired on a BD FACS Symphony A5 flow cytometer. From each patient or donor apheresis sample, dead cells and aggregates were excluded, then proliferating T cells ($CFSE^{-}CD3^{+}CD8^{+}CD4^{+}$) were first separated based on CAR expression. Both CAR^{+} and CAR^{-} proliferating T cells co-expressing HLA-DR, CD25, and CD71 were individually gated. For clustering downstream analysis, 1,000 events from each sample were biexponentially transformed and exported from FlowJo. High-dimensional single-cell data were subsequently analyzed with the Phenograph algorithm, implemented in the CRUSTY web tool, using parameter K = 400 and Resolution = 0.5. After performing dimensionality reduction and clustering, balloon plot and Uniform Manifold Approximation and Projection (UMAP) were generated using custom Python scripts.

Phosphorylation status of alloreactive CAR T cells was assessed following 6 day post-MLR as described above. Cells were collected, washed, and stained with Zombie NIR Fixable Viability Dye for 10 min at RT. Then, cells were washed and stained with PE CAR, BV786 CD3, BUV496 CD4, BUV737 HLA-DR, AF700 CD71, BV605 CD25, and BUV805 CD8. After surface marker stain, cells were washed, fixed with BD Phosflow™ Fix Buffer I (BD Bioscience) and permeabilized with BD Phosflow™ Perm Buffer III (BD Bioscience) according to the manufacturer's instructions. Intracellular staining was performed using PE CAR, PerCP-Cy5.5 anti-pSTAT3, APC anti-pSTAT5, BV421 anti-pAKT. Samples were

washed three times with PBS-2% FBS and immediately acquired on a BD FACS Symphony A5 flow cytometer.

Note: *All experimental procedures and associated data analyses described above were performed exclusively by me.*

Gene expression and single cell TCR sequencing

Cryopreserved patient PBMCs collected at multiple time points (pre-infusion to 3 months post-CAR T cell infusion) were thawed in complete AIM-V medium and labeled with 2.5 µM CellTrace CFSE dye. Mixed lymphocyte reactions (MLR) were performed using irradiated HLA-mismatched *e*K562 stimulator cells, as previously described. After 6 days of co-culture, viable T cells ($CFSE^+$ $CAR^+CD3^+CD4^+CD8^+$ and $CFSE^+$ $CAR^-CD3^+CD4^+CD8^+$) were sorted by flow cytometry and subsequently stained with TotalSeq™-A anti-human Hashtag antibodies and a panel of TotalSeq™-A CITE-seq antibodies (BioLegend).

Cells from all samples were pooled and processed using the Chromium GEM-X Single Cell 5' Kit v3 with Cell Surface Protein and V(D)J Enrichment (10x Genomics, PN-1000505), according to the manufacturer's instructions. Following gel bead-in-emulsion (GEM) generation, reverse transcription and cDNA amplification were performed, and libraries for gene expression, T cell receptor (TCR) V(D)J, and feature barcoding (CITE-seq and HTO) were generated. Libraries were sequenced on an Illumina NovaSeq 6000 system using paired-end reads.

Note: *All the technical experiments including sample preparation for sequencing were entirely performed by me. Sample and instrument preparation for cell sorting was entirely performed by me. Cell sorting was performed by the sorting facility at the Leibniz Institute for Immunotherapy. Sequencing was performed by me and Johanna Raithel under the guidance of Michael Rheli, co-author of the project. Bioinformatic analyses were performed by Nisha Rana and Nicholas Strieder, co-author of the manuscript accepted in CELL.*

Statistical analysis

Statistical analyses were conducted using Prism software v10.2.3 (GraphPad Software, La Jolla, California, USA). Comparisons between standard and T_{SCM}-enriched CAR T cells were conducted using the Mann-Whitney test. For comparisons involving three or more independent groups, one-way ANOVA or Kruskal-Wallis test (as appropriate), two-way ANOVA or multiple *t*-test with Holm–Šídák correction were used as appropriate. The Wilcoxon test was employed for paired analysis. The Chi-square test was applied to compare

the rate of CRs. EFS curves were compared using the log-rank (Mantel-Cox) test. Pearson correlation was used to generate the correlation plot. Statistical significance was indicated as follows: *$p < 0.05$, **$p < 0.01$, ***$p < 0.001$, ****$p < 0.0001$.

Note: *Statistical analysis was performed by me under the guidance of Prof. Luca Gattinoni and Dr. James Kochenderfer, last author of the manuscript accepted in CELL.*

Data availability

The fastq files relative to the sequencing of IS amplicons generated for this study are being deposited at EGA under StudyID: EGAS00001008119 and DatasetID: EGAD00001015540. All other data supporting the findings of this study are available from the corresponding author on reasonable request.

Note: *Sequencing data were deposited on EGA by Nicholas Strieder, co-author of the manuscript accepted in CELL.*

Results

Standard and T_{SCM}-enriched infusion product compositions

To enable a rigorous interpretation of the clinical outcomes and biological findings, the manufacturing procedure and phenotypic composition of the two CAR T cell products were first compared (**Figure 3**). Briefly, standard CAR T cells were generated by activating peripheral blood mononuclear cells (PBMCs) collected from the original alloHSCT donor following a protocol analogous to that used for axicabtagene ciloleucel[89] and administered to a cohort of 20 patients[79]. CAR T_{SCM} cells were manufactured from enriched naïve $CD8^+$ T cells isolated from the respective transplant donors as previously reported[78]. More specifically, the protocol employed IL-7, which provides essential instructive signals for T_{SCM} cell differentiation, and IL-21, which exerts strong inhibitory effects on effector T cell differentiation[78]. The glycogen synthase kinase 3 beta (GSK-3β) inhibitor TWS119 was further included into the cytokine cocktail to stabilize β-catenin and enhance WNT signaling, promoting maximal induction of Transcription Factor 7 (*TCF7*) and Lymphoid Enhancer Binding Factor 1 (*LEF1*), key transcription factors governing stemness[75,78].

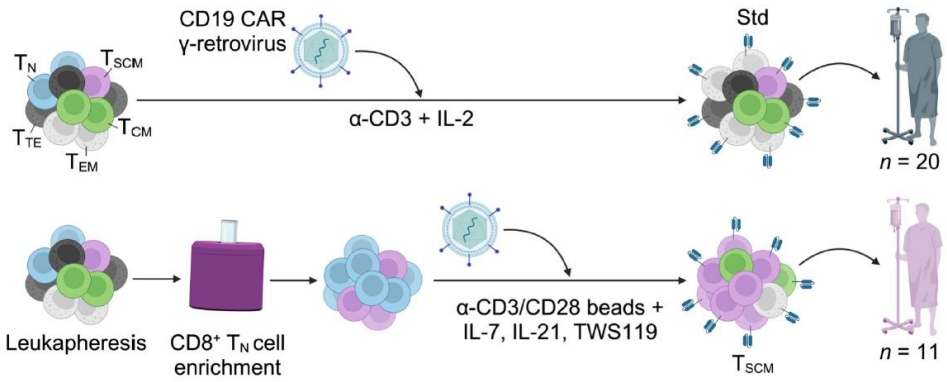

Figure 3. Donor-derived CAR T cell manufacturing workflow. Schematic representation of the manufacturing processes for generating standard (top) and T_{SCM} CAR products (bottom). A more detailed description of the manufacturing procedure is provided in the "*Materials and Methods*" section. T_N, naïve T cells, T_{SCM}, memory stem T cells, T_{CM}, central memory T cells, T_{EM} effector memory T cells, T_{TE}, terminal effector T cells. ***Figure 3*** *was designed by me using BioRender.com*.

High resolution, multi-parametric flow cytometry analysis was performed to define the compositions of both products (**Figure 4A**). CAR T_{SCM} cells were predominantly composed of CD8 T cells (mean ± SD: 98.7% ± 1.1%). In contrast, conventional CAR T cells showed a more balanced CD8 and CD4 distribution (mean ± SD: 54.7% ± 17.3% and 41.4% ± 17.1%, respectively) (**Figure 4B**). CAR T_{SCM} products displayed a markedly higher proportion of T_{SCM} cells (median: 78.4% vs. 8.4%), while standard CAR T cell products exhibited greater heterogeneity, predominantly enriched in T_{EM} and T_{TE} subsets (median: 34.2% and 21%, respectively) (**Figure 4C**).

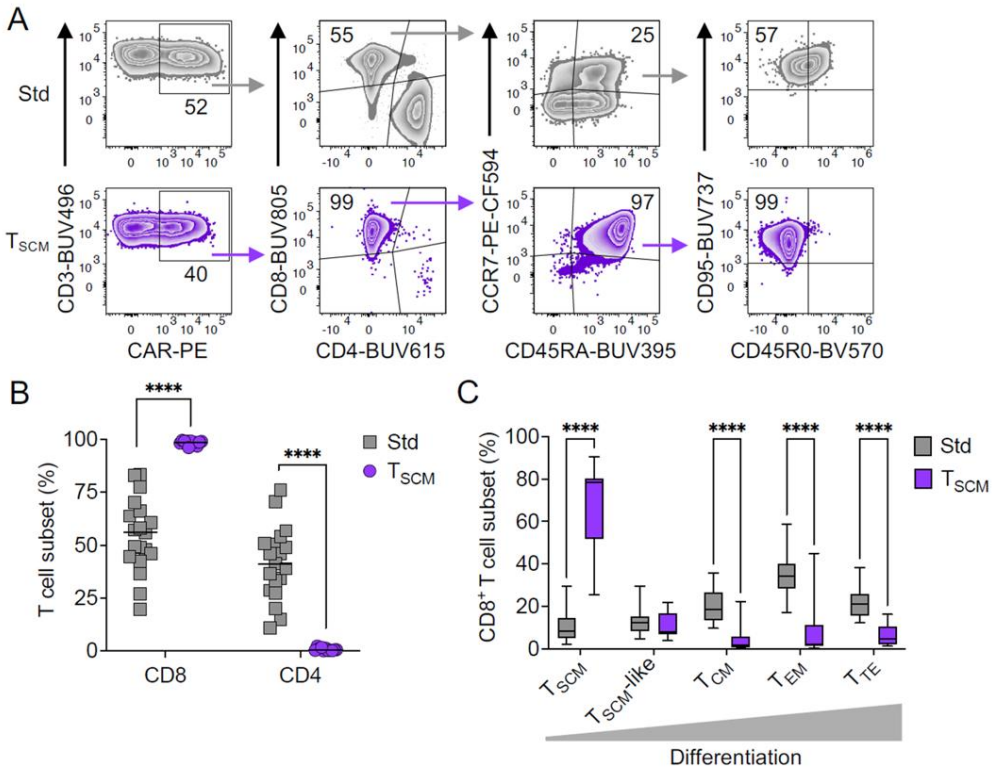

Figure 4. Standard and T_{SCM}-enriched infusion product phenotypic analysis. (**A**) Flow cytometry gating strategy used to characterize the composition of standard and T_{SCM} CAR products. T_{SCM} were defined as $CCR7^+CD45RA^+CD45R0^-CD95^+$ cells; T_{CM} as $CCR7^+CD45RA^-$; T_{EM} as $CCR7^-CD45RA^-$; T_{TE} as $CCR7^-CD45RA^+$; T_{SCM}-like cells as $CCR7^+CD45RA^+$ not displaying the full T_{SCM} phenotype. Numbers indicate the percentage of cells in each quadrant. (**B**) Percentage of $CD8^+$, $CD4^+$ T cells (**C**) and distribution of indicated subsets within standard and CAR T_{SCM} products. Data are shown after gating on live $CD3^+CAR^+$ cells. Results from standard (n = 19) and T_{SCM}-enriched (n = 11) CAR T cell products are shown as box-and-whisker plots. Box plot shows the median, interquartile range and whiskers extending up to 1.5 times the interquartile range (****p <0.0001; multiple t-test, Holm-Šídák correction for multiple comparisons). *The experimental design, technical execution, and data analysis of the respective **Figures 4A-C** were performed entirely by me. The graphical design for **Figures 4A-C** was made by me under the guidance of Prof. Luca Gattinoni, co-first author of the manuscript accepted in CELL.*

Phenograph analysis of both products identified 10 clusters with distinct marker expression and distribution (**Figures 5A**–**C**). Strikingly, CAR T_{SCM} cells were homogenously localized to clusters 4, 6, 8, and 9, which shared specific T_{SCM} features with only minor expression differences. Conversely, conventional CAR T cells showed a diverse phenotype and were largely restricted to clusters 2, 3, and 5, which carried T_{EM}-like characteristics (**Figures 5A**–**C**). Collectively, these results demonstrate that T_{SCM}-specific culture conditions produce a relatively uniform CAR T_{SCM} product, whereas the standard approach yields a more heterogeneous population enriched for T_{EM} and T_{TE} cells.

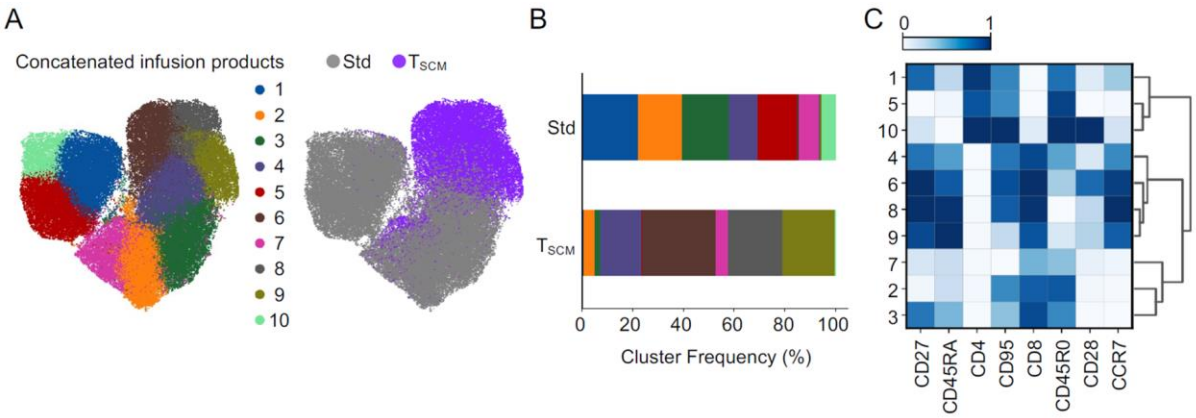

Figure 5. CAR T_{SCM} products exhibit greater phenotypic uniformity than standard CAR T cells. (**A**) UMAP plots of concatenated CAR T cell products showing cluster (left) and treatment distribution (right). Data on UMAP are shown after gating on live $CD3^+CAR^+$ cells. (**B**) Stacked bar graph showing the percentage of each cluster in standard and T_{SCM}-enriched CAR T cell products. (**C**) Heatmap of the relative expression (*z*-score) of memory markers in each cluster. Hierarchical clustering (dendrogram) highlights similarities and differences between clusters. *The experimental design, technical execution, phenograph CRUSTY analysis, and graphical design for* ***Figures 5A-C*** *were performed entirely by me.*

Superior CAR T_{SCM} expansion yields complete responses at low doses

Having established the key manufacturing and phenotypic features of the two donor-derived CAR T cell products, the next step was to determine whether these product characteristics translated into differences in *in vivo* clinical activity. Importantly, patients in the standard cohort received considerably higher numbers of CAR T cells compared to the T_{SCM} cohort (median: 290 million vs. 66 million, respectively) (**Figure 6A**, **Tables S1** and **S2**). However, despite the reduced dose in the T_{SCM} arm, overall response rates (ORR) were comparable, reaching 45% in the standard group and 55% in the T_{SCM} group (**Figure 6B**, left). Notably, at equivalent infusion levels ($< 3 \times 10^8$ CAR T cells), T_{SCM}-treated patients achieved more frequent complete remissions: 5 of 11 (45%) compared with 1 of 10 (10%) in the standard group (**Figure 6B**, right).

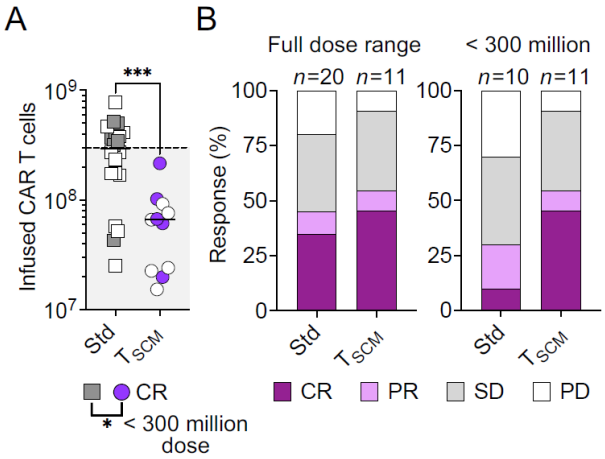

Figure 6. CAR T_{SCM} cells drive superior responses at lower doses. (**A**) Total dose range of infused CAR T cells in standard ($0.4–8.2 \times 10^6$ kg^{-1}, $n = 20$) and T_{SCM} ($0.25–2 \times 10^6$ kg^{-1}, $n = 11$) cohorts for first cell infusions. Doses below the black dashed line in the grey box correspond to dose values $< 3 \times 10^8$ infused CAR T cells. Empty and filled symbols represent non-complete and complete responders, respectively. Data are shown as individual values while horizontal black bars represent median values (*$p < 0.05$, one-tailed chi-square test [proportion of CRs for $< 3 \times 10^8$ infused CAR T cells]; *** $p < 0.001$, two-tailed Mann-Whitney test [comparison of CAR T infusion doses]). (**B**) Best response rates (%) to first infusion in standard and T_{SCM} recipients, shown for the full dose range (left) and doses $< 3 \times 10^8$ (right) infused CAR T cells. CR: complete response; PR: partial response; SD: stable disease; PD: progressive disease. *The graphical design for **Figure 6A** was made by me under the guidance of Prof. Luca Gattinoni, the co-first author of the manuscript accepted in CELL. The clinical observation and graphical design shown in **Figure 6B** were made by me.*

Expansion kinetics and overall exposure—quantified as peak levels and area under the curve (AUC), respectively—have been consistently correlated to the therapeutic activity of CAR T cells across multiple studies[90-92]. To determine whether the enhanced responses at lower doses observed with CAR T_{SCM} products were related to superior expansion, circulating CAR T cells were quantified by qPCR over the first 36 days post-infusion (**Figure 7A**). T_{SCM} cells exhibited a delayed expansion peak, occurring during the second week after infusion, whereas standard CAR T cells peaked in the first week (**Figure 7A**; **Figure S1**). Furthermore, T_{SCM} recipients reached a higher per-cell peak concentration (median: 30.4 vs. 6.7 CAR T cells/µL) and a greater per-cell $AUC_{d0–36}$ (median: 185.8 vs. 27.5 CAR T cells/µL) compared with patients receiving standard CAR T cells (**Figures 7A**, **B**). Consistently, flow cytometry analysis validated these qPCR findings, confirming both the delayed expansion (**Figure S1**) and the superior peak levels of CAR T_{SCM} cells (median: 7.3% vs. 1%) (**Figures 7C**, **D**). Collectively, these observations indicate that the improved efficacy of CAR T_{SCM} cells at reduced doses is driven by their enhanced expansion and persistence.

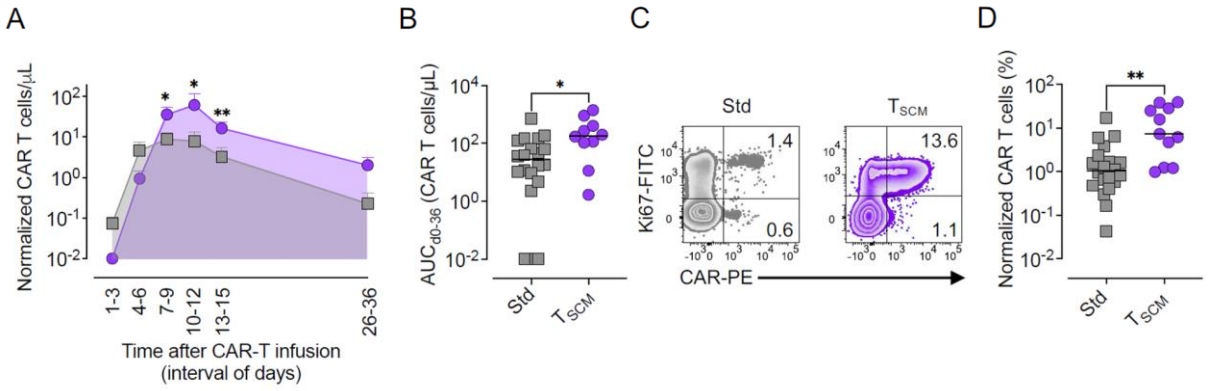

Figure 7. CAR T_{SCM} cells show enhanced expansion and persistence. (**A**) Absolute circulating CAR^+ T cell numbers per microliter of blood assessed by qPCR. Cells are normalized to the total infused dose (per 10^8 infused cells). Data are grouped into 3-day intervals (*$p < 0.05$; **$p < 0.01$, two-tailed Mann-Whitney test). (**B**) Area under the curve (AUC) from day 0 to day 36 post-infusion (*$p < 0.01$, two-tailed Mann-Whitney test). (**C**) Flow cytometry plot showing the frequency of proliferating CAR T cells at the peak of expansion as assessed by Ki67 staining in patients #14 (standard) and #27 (T_{SCM}). Numbers indicate the percentage of cells in each quadrant. (**D**) Frequency of CAR T cells in peripheral blood at the peak of expansion in standard and T_{SCM} recipients. Cells are normalized to the total infused dose (per 10^8 infused cells); (** $p < 0.01$, two-tailed Mann-Whitney test). *The experimental design, technical execution, and data analysis for **Figure 7A** were performed by me and Danielle A. Natrakul (National Cancer Institute), co-author of the manuscript accepted in CELL. The experimental design, coordination, execution, and analysis related to **Figures 7B**, **7C**, and **7D** were performed entirely by me. The graphical design for **Figures 7A-D** was made by me under the guidance of Prof. Luca Gattinoni, the co-first author of the manuscript accepted in CELL.*

CAR T_{SCM} cells exhibit a favorable safety profile

The infusion of donor-derived CAR T_{SCM} cells was generally well tolerated, with no evidence of GvHD and low incidence of cytokine release syndrome (CRS) or other serious adverse events (**Tables S1**). Notably, no grade 4 (G4) CRS occurred in the T_{SCM} group. Only a single patient, characterized by 40–50% ALL blast involvement in the bone marrow (BM), experienced grade 3 (G3) CRS. In contrast, 28.6% of individuals treated with conventional CAR T cells developed grade 3–4 CRS (**Figure 8A**, left). This difference was also evident among patients receiving standard CAR T cells at doses equivalent to those given in the T_{SCM} arm (**Figure 8A**, right). In the standard patients with G3–4 events showed higher peak expansion compared with those with milder (G1–2) toxicities (**Figure 8B**). Strikingly, T_{SCM} recipients reached peak expansion levels similar to those associated with G3–4 CRS in the standard cohort but experienced only G1–2 toxicities (**Figure 8B**).

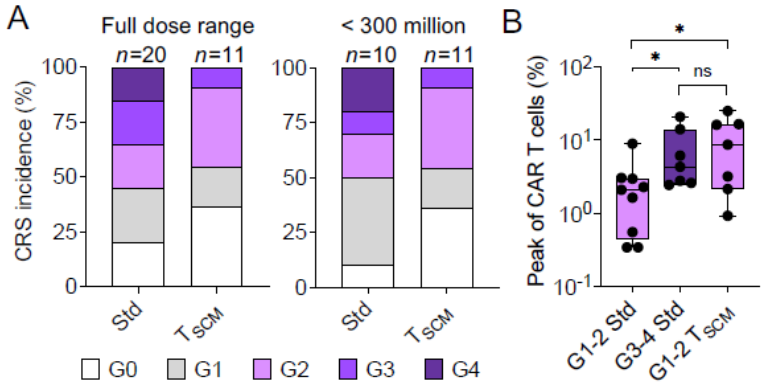

Figure 8. Reduced cytokine release syndrome severity following CAR T_{SCM} infusion. (**A**) Incidence of cytokine release syndrome (CRS) in standard vs. T_{SCM} recipients. Stacked bar graphs show CRS severity grades (G0-G4, by ASTCT criteria) after first cell infusions displayed for the full dose range (left) and doses < 3×10^8 infused CAR T cells (right). (**B**) Correlation between the percentage of CAR T cells at the peak of expansion (measured by flow cytometry) and CRS severity (*$p < 0.05$, one-way ANOVA, Kruskal-Wallis test). *The clinical observation and graphical design for **Figure 8A** were made by me. The experimental design, coordination, execution, and analysis for **Figure 8B** were performed entirely by me. The clinical correlation and graphical design for **Figure 8B** were made by me under the guidance of Prof. Luca Gattinoni, the co-first author of the manuscript accepted in CELL.*

To investigate whether these differences reflected distinct cytokine dynamics, multiplex bead-based cytokine analysis was performed on serum patients post-CAR T cell therapy. Standard CAR T cell recipients exhibited an early IL-6 peak immediately after infusion (**Figure 9A**). Conversely, T_{SCM} administration was associated with a delayed increase in IFN-γ during the second week, mirroring their expansion profile (**Figure 9A**). Other cytokines showed no clear differential behavior (**Figure S2**). Interestingly, IL-6 correlated with CRS severity only in the standard cohort, whereas IFN-γ appeared to be the main mediator of toxicity in the T_{SCM} group (**Figure 9B**, **C**).

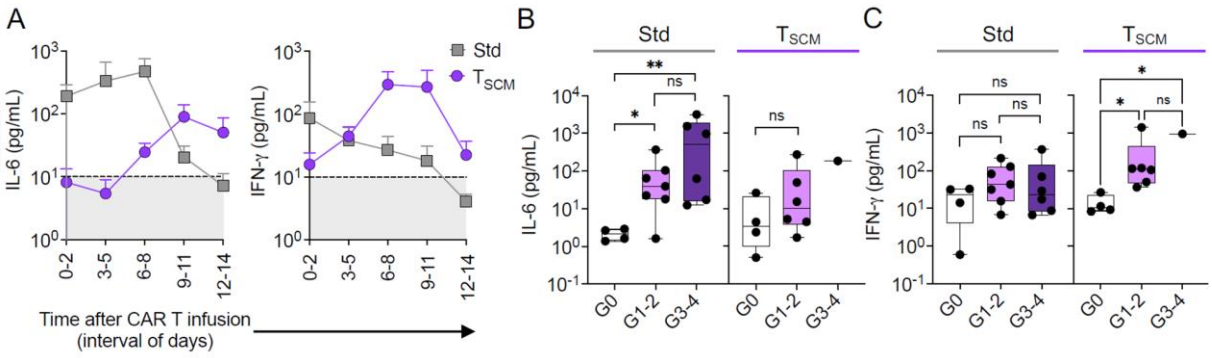

Figure 9. Distinct cytokine kinetics differentiate standard and T_{SCM} CAR T cells. (**A**) Serum levels of IL-6 (left) and IFN-γ (right) in responder patients over two weeks after infusion of standard or T_{SCM}-enriched CAR T

cells. Time post-infusion is represented in day intervals. The grey box, outlined by a black dashed line, indicates the physiological reference levels of each cytokine. (standard $n = 7$; T_{SCM} $n = 6$). (**B**, **C**) Serum peak levels of IL-6 (**B**) and IFN-γ (**C**) in standard ($n = 17$) and T_{SCM}-enriched ($n = 11$) CAR T cell recipients stratified according to CRS grade (*p <0.05; **p <0.01, one-way ANOVA, Kruskal-Wallis test). *The technical experiments conducted to generate **Figures 9A-C** were entirely and independently conceptualized, designed, and executed by me. Clinical correlation and graphical design of **Figures 9A-C** were made by me.*

To further explore the role of $CD8^+$ T cells in triggering CRS, we isolated $CD8^+CAR^+$ T cells from both CAR T cell infusion products and conducted single-cell secretome profiling after stimulation with $CD19^+$ target cells. Unsupervised clustering revealed 14 groups based on cytokine/chemokine secretion signatures (**Figure 10A**). Consistent with the multiplex data, clusters enriched for IL-6 production (clusters 1 and 2) were more frequent in the standard product, whereas clusters 11 and 14—defined by robust IFN-γ secretion—were dominant in the T_{SCM} population (**Figure 10B**). Moreover, CAR T_{SCM} products showed a higher proportion of the highly polyfunctional cluster 3 (**Figure 10B**). Together, these findings suggest that the reduced toxicity observed with CAR T_{SCM} therapy is shaped by its unique cytokine dynamics and profile.

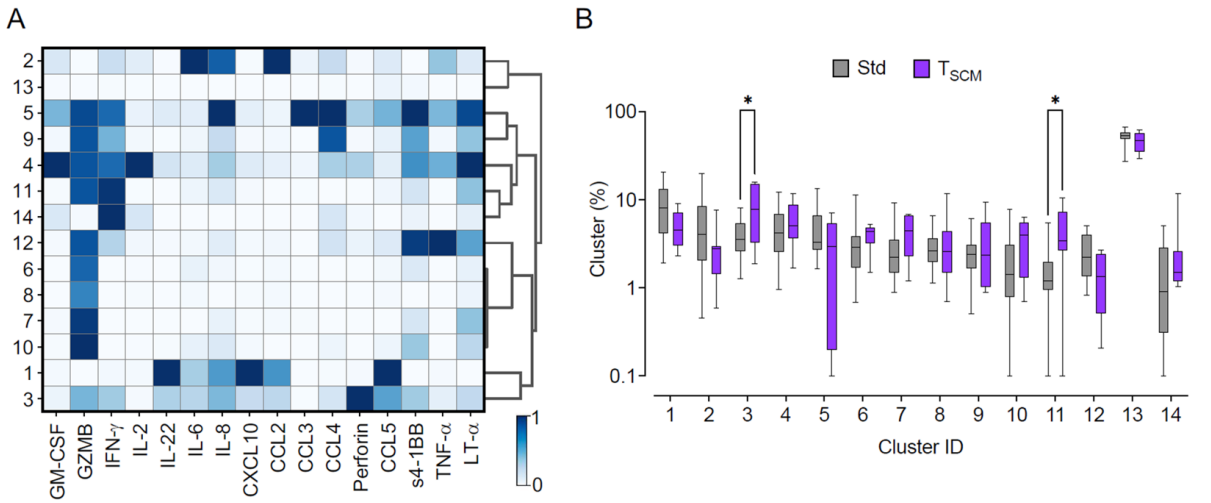

Figure 10. Single-cell secretome analysis reveals a polyfunctional, IFN-γ–dominant profile in CAR T_{SCM} cells. (**A**) Heatmap showing the relative expression (z-score) of single-cell secreted cytokines by sorted CAR^+CD8^+ T cells from standard ($n = 20$) and T_{SCM}-enriched ($n = 8$) CAR T cell products after stimulation with $CD19^+$ K562. Clusters were identified using VIA algorithm. (**B**) Relative contribution of each cluster within standard and T_{SCM} $CD8^+$ products. Cluster percentage was normalized to the total number of clusters per patient (*$p < 0.05$; **$p <$ 0.01, multiple t-test, Holm-Šídák correction for multiple comparisons). *The technical experiments conducted to generate **Figures 10A** and **10B** were entirely and independently executed by me. The experiment related to **Figure 10A** was designed by me with the assistance of Dragana Slavkovic-Lukic, co-*

*author of the manuscript accepted in CELL. CD19⁺ target cells used to stimulate CAR T cells were already available at the Leibniz Institute for Immunotherapy in the laboratory of Prof. Luca Gattinoni and were originally generated at the National Institutes of Health (NIH) in the laboratory of Dr. Kochenderfer. The data analysis from IsoPlexis for **Figures 10A** and **10B** was entirely performed by me. Unsupervised clustering analysis to generate **Figure 10A** was performed entirely by me using the CRUSTY tool. The graphical design for **Figures 10A** and **10B** was made by me.*

CAR T_{SCM} cells exhibit distinct *in vivo* fates

To characterize the *in vivo* differentiation trajectories of standard and T_{SCM}-enriched CAR T cells, we performed high-dimensional flow cytometry on post-infusion samples using a 23-color panel including canonical activation, differentiation, and exhaustion markers. Unsupervised clustering identified 17 phenotypically distinct T cell clusters across the two cohorts (**Figure 11A**). Differentiation trajectories were reconstructed using Slingshot analysis, aligning clusters along a pseudotime axis according to marker expression patterns. Cluster 15, representing *bona fide* T_N cells, was selected as the starting point for trajectory inference. A primary T cell differentiation path (white line) was identified which progressed sequentially from T_N cells (clusters 15, 4) to T_{SCM} cells (cluster 8), then transitioned into T_{CM} cells (cluster 9), proliferating effectors (Prol. T_{EFF}; clusters 13, 6, 5, 11, 10), and ultimately resting T_{EFF} and T_{TE} subsets (clusters 17, 2, 12, 1) (**Figure 11B**). Wishbone analysis further confirmed the temporal ordering of early, activation, and late differentiation markers, producing patterns consistent with the pseudotime-based differentiation model shown in **Figure 11B** (**Figure 11C**).

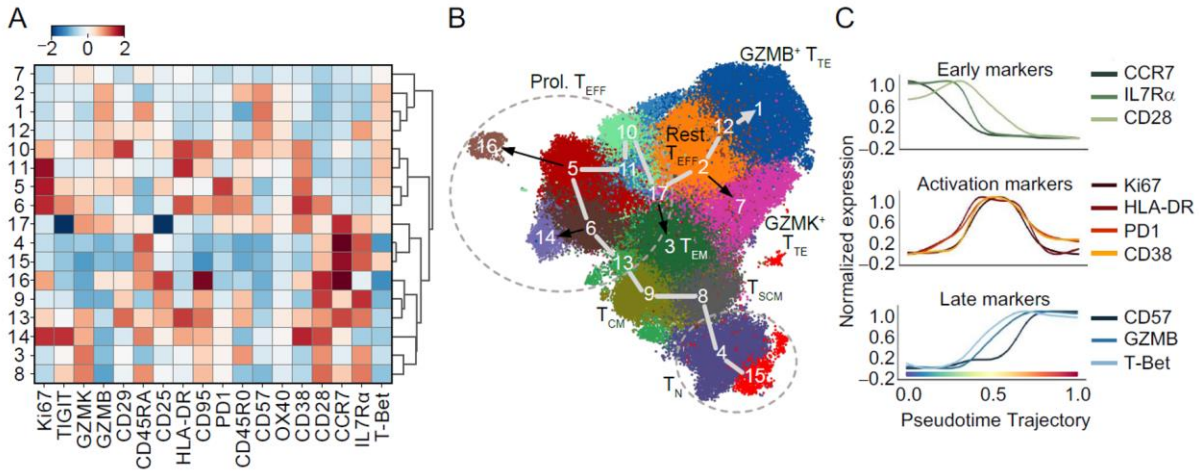

Figure 11. *In vivo* CAR T cell differentiation trajectories by high-dimensional flow cytometry. (**A**) Heatmap showing the relative expression (*z*-score) of differentiation and activation markers in post-CAR T cell infusion samples from standard (n = 20) and T_{SCM}-enriched (n = 11) CAR T cell recipients. Clusters were

identified using VIA algorithm. (**B**) Pseudotime trajectory reconstitution of $CD8^+$ T cell differentiation along the UMAP generated using post-infusion samples from standard and T_{SCM} recipients. A main inferred trajectory (white line) diverges into four minor differentiation branches (black arrows). Trajectories and branches were generated using the Slingshot package, assuming the T_N cluster (C_{15}) as the root. (**C**) Normalized expression of early memory, activation, and late differentiation markers along the main pseudotime trajectory. *The experimental design, technical execution, and sample analysis related to* ***Figures 11A-C*** *were performed primarily by me with the assistance of Alberto Susana, co-author of the manuscript accepted in CELL. The bioinformatic analysis used to generate* ***Figures 11A-C*** *was performed by Simone Puccio, co-author of the manuscript accepted in CELL, under my guidance and the guidance of Prof. Luca Gattinoni and Dr. Enrico Lugli, co-author of the manuscript accepted in CELL.*

Additionally, we performed principal component analysis (PCA) to further delineate specific T cell trajectories within the two cohorts at different time points following CAR T cell therapy and define the cluster contribution over time (**Figure 12A**). T cells at early time points (d5-8) markedly differed between the T_{SCM} and standard cohorts. During the second week (d9-11 and 12-14), the T_{SCM} trajectory gradually shifted toward the phenotypic state observed in the standard cohort on d5-8 (**Figure 12A**). This observation aligns with the distinct expansion kinetics of the two products, with peak expansion occurring during the first week for standard CAR T cells and the second week for CAR T_{SCM} cells (**Figure 12A**). Notably, the two trajectories further diverged along the PCA2 axis as cells transitioned to the memory phase (days 28–35) (**Figure 12A**). CAR T_{SCM} cells exhibited a delayed progression into proliferating intermediate T_{EFF} cells, peaking at days 12–14, compared to standard CAR T cells, which reached this stage as early as days 5–8 (**Figures 12B**, and **C**). By days 28–35, while standard CAR T cells were enriched in proliferating and resting late effector subsets, CAR T_{SCM} cells robustly repopulated the T_{SCM} compartment and maintained a pool of very early proliferating T_{EFF} cells (**Figures 12B**, and **C**). These findings highlight a distinct differentiation program in CAR T_{SCM} cells, characterized by delayed effector differentiation and sustained regeneration of stem-like and early memory subsets.

A B

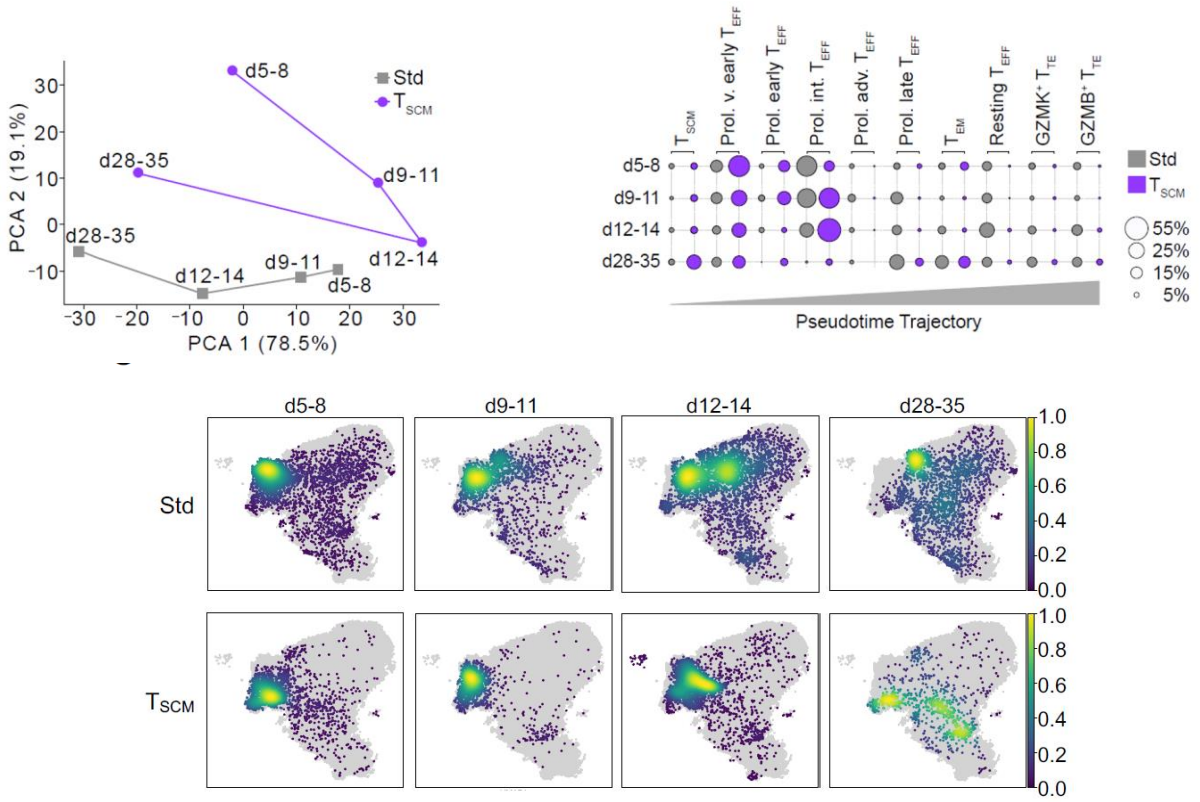

Figure 12. CAR T_{SCM} cells retain the ability to reconstitute the T_{SCM} compartment. (**A**) Principal component analysis (PCA) of CD8$^+$ T cells in standard and T_{SCM} recipients at different time points following CAR T cell infusion. (**B**) Bubble plot showing the frequencies of selected clusters obtained in **Figure 11A** along the pseudotime trajectory shown in **Figure 11B** at indicated time points post-CAR T cell infusion. Bubble size indicates the frequencies of each cluster over the pseudotime trajectory. T_{SCM} (C_8), Prol. v. early T_{EFF} (C_6), Prol. early T_{EFF} (C_{14}), Prol. int. T_{EFF} (C_5), Prol. adv. T_{EFF} (C_{11}), Prol. late T_{EFF} (C_{10}), T_{EM} (C_3), resting T_{EFF} (C_2), GZMK$^+$ T_{TE} (C_7), GZMB$^+$ T_{TE} (C_1). (**C**) Density plot representing the cluster dynamics of CD8$^+$CAR$^+$ T cells over time along the pseudotime trajectory shown in **Figure 11B**. The grey background represents total CD8$^+$ cells. *The experimental design, technical execution, and sample analysis related to **Figures 12A-C** were performed primarily by me with the assistance of Alberto Susana, co-author of the manuscript accepted in CELL. The bioinformatic analysis used to generate **Figures 12A-C** was performed by Simone Puccio, co-author of the manuscript accepted in CELL, under my guidance and the guidance of Prof. Luca Gattinoni and Dr. Enrico Lugli, co-author of the manuscript accepted in CELL.*

Clonal succession sustains long-term CAR T_{SCM} engraftment

To further investigate the *in vivo* clonal dynamics of CAR T cells, we conducted longitudinal tracking of retroviral integration sites (ISs) of each flow cytometry–sorted memory subsets, from the infusion product through day 90 post-infusion (**Figure S3A**). To reduce confounding from disease type and clinical outcome, we selected four ALL patients who achieved negative minimal residual disease (MRD$^-$) complete remission after receiving either standard or T_{SCM}-

enriched CAR T cells, allowing clearer interpretation of clonal behavior. We first evaluated the extent of shared integration sites (ISs) among memory subsets within the infused CAR T cell products. Notably, the T_{SCM} product displayed minimal IS overlap across memory T cell populations, whereas the standard product exhibited a high degree of IS sharing (**Figure 13A**, **B**). A plausible explanation for the low number of shared ISs in the T_{SCM} product may be that the manufacturing conditions have restricted extensive proliferation while preserving stemness. Conversely, the high proportion of shared ISs in the standard CAR T cell product suggests that differentiation occurred already during the *in vitro* expansion. At the late time points (day 90), CAR T cell clonal diversity was lower in T_{SCM} recipients than in standard CAR T cell recipients, with no evidence of clonal dominance or aberrant clonal selection, supporting the safety of T_{SCM} cells (**Figure 13C**, **D**).

To reconstitute the *in vivo* dynamics of standard and T_{SCM} products, individual clones were longitudinally tracked, and their contributions to distinct T cell subsets were analysed. Standard CAR T cell clonotypes underwent rapid expansion post-infusion, followed by a contraction and/or stabilization over time (**Figure 13E**). Accordingly, the top-10 most abundant persisting clones in the standard patients at day 90 derived from attrition or maintenance of early-expanded clones from day 14 (**Figure 13F**, **G**). In sharp contrast, CAR T_{SCM} cells expanded and repopulated through sequential waves of clonal succession (**Figure 13E**). Notably, the top-10 most abundant persisting clones in T_{SCM}-treated patients, emerged from newly expanded clones that were not involved in the initial expansion phase even at a higher level (**Figure 13F**, **G**). Together with flow cytometry data, these findings highlight lasting divergence in the differentiation programs of standard versus CAR T_{SCM} cells.

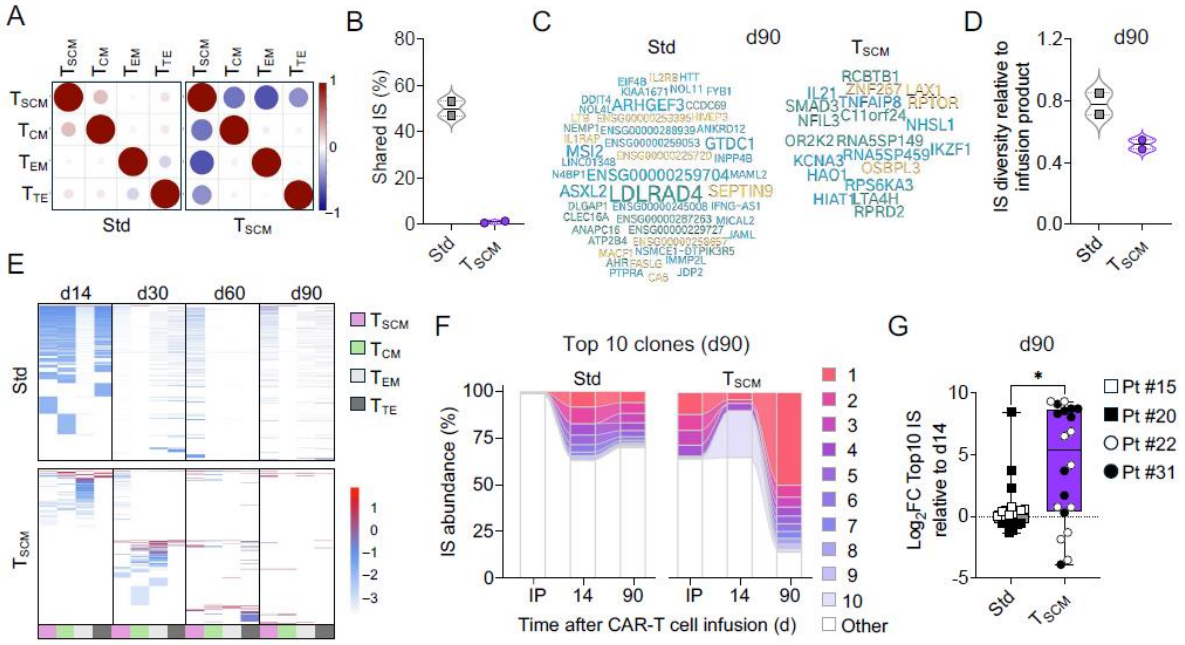

Figure 13. Long-term persistence of CAR T_{SCM} cells is sustained by clonal succession. (**A**) Correlation plots showing degree of sharing of identical integration sites (IS) across each T cell subset in the standard (left) and T_{SCM} (right) CAR products from Pt #15 and #22, respectively. Positive and negative correlations are shown in red and in blue, respectively. The size of circles is proportional to the correlation value (Pearson Correlation coefficient calculated between all pairs of variables). (**B**) Violin plot showing the percentage of shared ISs found among the diverse T cell subsets within standard (n = 2) and T_{SCM} (n = 2) CAR products. (**C**) Word clouds displaying the top 50 represented ISs loci at day 90 following CAR T cell infusion in Pt #15 (standard, left) and #22 (T_{SCM}, right). Each locus is labeled with the name of the closest gene to the relative insertion site. The size of each gene name is proportional to the number of integrations found at that locus, with larger fonts indicating higher integration frequencies. (**D**) Shannon diversity index calculated on total ISs collected at day 90 post-CAR T cell infusion. A higher index indicates greater clonal diversity. Data are shown relative to the diversity index of the infusion products. (**E**) Heatmap showing the longitudinal tracking of individual ISs within each T cell subset for Pt #15 (standard, top) and #22 (T_{SCM}, bottom). Each row represents an individual IS and each column the T cell subset analyzed. The intensity of blue and red is proportional to the relative IS abundance, expressed as log10 percent sequencing reads count belonging to each IS for each sample/timepoint. (**F**) Alluvial plots showing the abundance of top 10 clones persisting at day 90 in Pt #15 (standard, left) and #22 (T_{SCM}, right) backtracked to day 14 and the infusion products (IP). Ribbons connect identical ISs tracked over different time points (bars). The size of each ribbon/bar section is proportional to the relative IS abundance. The abundance of the rest of the ISs (Other) is reported in the white section of each bar. (**G**) Scatter plot showing the Log_2 fold change (FC) of the abundance top 10 ISs retrieved at day 90 relative to day 14 following CAR T cell infusion in standard (n = 2) and T_{SCM} (n = 2) recipients. The top 10 clones per patient are shown as individual values in box-and-whisker plots. Box plot shows the median, interquartile range, and whiskers extending up to 1.5 times the interquartile range (*$p < 0.05$, two-tailed Mann-Whitney test). *Project planning and all the technical experiments necessary to generate* ***Figures 13A-G*** *were entirely conceived and performed by me. Protocol for Integration Site Analysis assay was developed and optimized at Leibniz Institute for Immunotherapy by me. Sequencing was performed by me*

and Johanna Raithel under the guidance of Michael Rheli, co-author of the manuscript accepted in CELL. Bioinformatic analyses were performed by Luca Biasco and Nicholas Strieder, both co-authors of the manuscript accepted in CELL. ***Figures 13A****,* ***13C****,* ***13E****, and* ***13F*** *were generated by Luca Biasco under my guidance.* ***Figures 13B****,* ***13D****, and* ***13G*** *were generated by me under my guidance and the guidance of Prof. Luca Gattinoni, co-first author of the manuscript accepted in CELL.*

CAR T_{SCM} treatment failure depends on tumor and host-related factors

It is well established that CAR T cell expansion in peripheral blood correlates with clinical outcome[90-92]. Consistently, responders in the standard cohort exhibited significantly higher CAR T cell expansion peak compared to non-responders (**Figure 14**, left). In contrast, no significant differences in CAR T cell expansion were observed between responding and non-responding patients receiving CAR T_{SCM} cells. (**Figure 14**, right). These findings emphasize the variability in T cell fitness among standard products, a critical weakness that CAR T_{SCM} cells overcome, ensuring more robust and consistent engraftment.

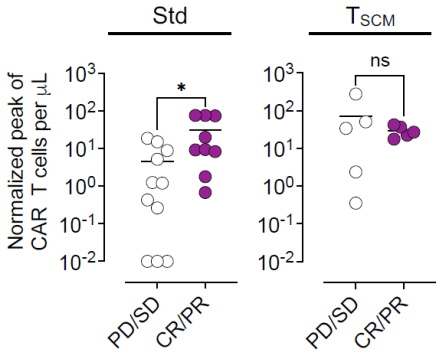

Figure 14. Absence of correlation between CAR T_{SCM} expansion and clinical outcome. Correlation between best response and CAR T cell peak levels (assessed by qPCR) normalized to total infused dose (per 10^8 cells). Zero values plotted as 0.01 for log-scale visualization (*$p < 0.05$; ns, not significant, two-tailed Mann-Whitney test). PD, progressive disease; SD, stable disease; CR, complete response; PR, partial response. *The clinical correlation between treatment response and CAR T cell expansion shown in* ***Figure 14*** *was performed by me, while the graphical design was developed by me under the guidance of Prof. Luca Gattinoni, co–first author of the manuscript accepted in CELL.*

To investigate the mechanisms behind CAR T_{SCM} failure, we initially focused on the only patient (patient #23) experiencing progressive disease (PD). Despite robust CAR T cell proliferation (**Figure 15A**, **B**) and preserved functionality, as evidenced by the induction of B-cell aplasia, leukemia progressed in both peripheral blood and BM (clinical data derived

from NIH datasets are presented in **Figure 35A** in the *Discussion* section). Flow cytometry analysis of CD19 expression in pre- and post-CAR T BM biopsies revealed dim CD19 expression on pre-treatment leukemic blasts, which were enriched in the CD19-negative fraction following CAR T_{SCM} treatment (clinical data derived from NIH datasets are presented in **Figure 35B** in the *Discussion* section). These results indicate that leukemia progression was driven by insufficient CAR T cell reactivity against the low-density antigen on leukemic cells.

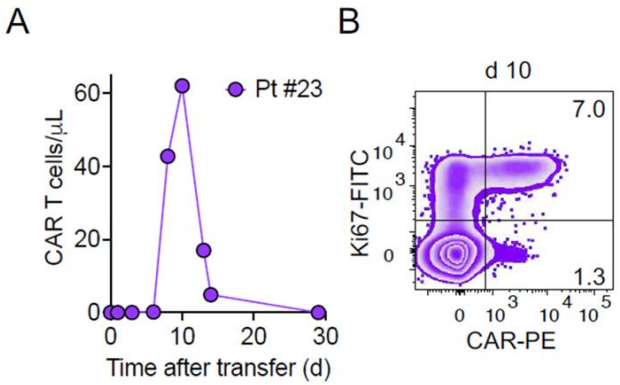

Figure 15. Leukemia progression in patient #23 despite CAR T_{SCM} cell expansion and preserved functionality. (**A**) Absolute CAR^+ T cell numbers per microliter of blood assessed by qPCR in the progressive disease patient #23. Cells are normalized to the total infused dose (per 108 cells). (**B**) Flow cytometry plot showing the frequency of proliferating CAR T cells at the peak of expansion as assessed by Ki67 staining. Numbers indicate the percentage of cells in each quadrant at the day of the peak. *The experimental design, coordination, execution, data analysis, and graphical design related to **Figures 15A, B** were performed entirely by me. The graphical design for **Figures 15A** and **B** was made by me under the guidance of Prof. Luca Gattinoni, the co-first author of the manuscript accepted in CELL.*

We further investigated a stable disease (SD) patient (patient #30), who was the sole T_{SCM} recipient where CAR T_{SCM} cells failed to expand despite the infusion product being highly enriched (> 80%) in T_{SCM} cells (**Figure 16A**). Therefore, we screened the patient's serum for the presence of multiple inhibitory cytokines. While most of the tested cytokines remained within physiological levels in all T_{SCM}-treated patients (**Figure S2**), patient #30 displayed strikingly elevated levels of IL-10 (1.879 ng/ml), a well-characterized immunosuppressive cytokine[93] (**Figure 16B**). To determine whether IL-10 could directly impair CAR T cell expansion, we evaluated its effects on both conventional CAR T cells and CAR T_{SCM} cells. Original CAR T cell products were pre-exposed to IL-10 at concentrations matching those detected in the serum of patient #30 and subsequently co-cultured with $CD19^+$ K562 target

cells in presence of the same IL-10 levels (**Figure 16C**). Unstimulated (UT) CAR T cells not exposed to IL-10 were used as controls. Remarkably, IL-10 pre-exposure did not affect the expansion of conventional CAR T cells, as assessed by Ki67 expression, whereas CAR T_{SCM} expansion was dramatically impaired, revealing a selective sensitivity of the T_{SCM} cells to IL-10–mediated suppression (**Figure 16D**).

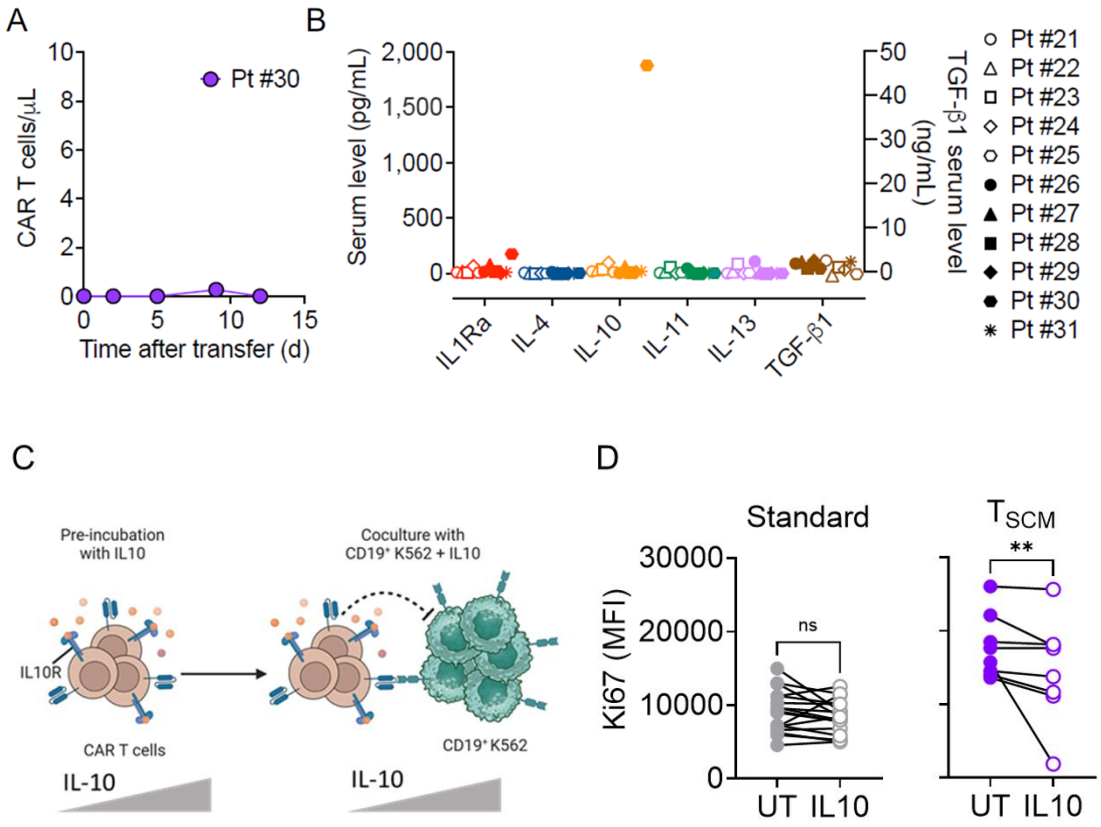

Figure 16. IL-10–mediated immunosuppression as a potential barrier to CAR T_{SCM} expansion. (**A**) Absolute CAR T cell counts in patient #30 from the T_{SCM} cohort. CAR levels were assessed by qPCR. (**B**) Serum levels of immunosuppressive cytokines detected in T_{SCM} recipients (n = 11) pre-CAR T cell infusion. (**C**) Schematic overview of the experimental design. Standard and T_{SCM}-enriched CAR T cell products were pre-incubated for 48 hours with supraphysiological concentrations of IL-10 (1 ng/mL). Following cytokine pre-exposure, CAR T cells were co-cultured for 72 hours with $CD19^+$ K562 target cells, and proliferative capacity was assessed by flow cytometry using Ki67 expression as a surrogate marker of cellular expansion. (D) CAR T cell expansion assessed by flow cytometry as Ki67 mean fluorescence intensity (MFI) in standard and T_{SCM}-enriched products following IL-10 pre-exposure and subsequent co-culture with $CD19^+$ K562 cells. UT denotes CAR T cells not pre-exposed to IL-10, used as controls and co-cultured with $CD19^+$ K562 cells in absence of IL-10. *The experimental design, coordination, execution, data analysis, and graphical design related to* ***Figure 16A-D*** *were performed entirely by me.*

Humoral responses to the mouse-derived single-chain variable fragments (FMC63-28ζ) included in the CD19-CAR construct have been previously reported[94]. Since CAR T cell infusion in our study was administered without lymphodepletion preconditioning, we hypothesized that the induction of anti-CAR antibodies (Abs) could impair CAR T cell performance and influence clinical outcomes. We detected anti-CAR Abs in 35% of patients across the entire treatment cohorts (**Figure 17A**, left). Notably, anti-CAR antibody levels correlated with the presence of B cells at the time of infusion (**Figure 17A**, right). However, the potential inhibitory activity of anti-CAR Abs on CAR T cell function remains a subject of debate. To investigate this, we assessed B cell aplasia as a surrogate marker of CAR T cell functionality in parallel with anti-CAR antibody detection in patients who received a second CAR T cell infusion. Of note, all four patients who underwent multiple CAR T cell treatments exhibited heightened humoral responses upon CAR re-exposure, underscoring a prime-boost effect (**Figure S4**). To assess the impact of anti-CAR antibody on CAR T cell functionality, we then focused on two of these patients, who had detectable circulating B cells at the time of CAR T cell infusions (**Figure 17B**, left). Strikingly, while CAR T cells efficiently eliminated B cells following the first infusion, the second administration—even at higher doses—failed to reduce B cell numbers, coinciding with the induction of an anti-CAR response (**Figure 17B**, right). Together, these findings suggest that CAR T_{SCM} treatment failure is primarily driven by tumor- and host-related factors—including low antigen density, immunosuppressive cytokines, and anti-CAR humoral responses—rather than intrinsic defects in T cell functionality and fitness.

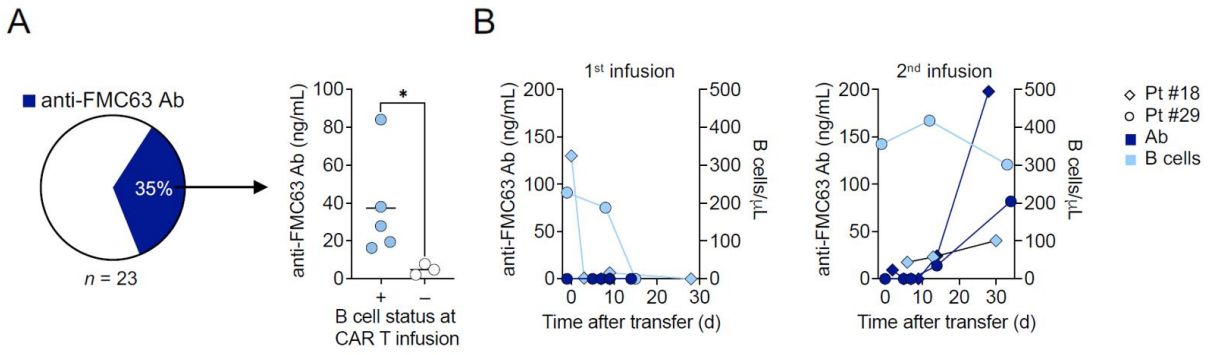

Figure 17. Humoral anti-CAR immunity contributes to CAR T_{SCM} treatment failure. (**A**) Pie chart (left) showing the percentage of anti-FMC63 antibodies detected in the serum of standard and TSCM recipients ($n = 23$) within the 30–90 days following the first CAR T cell infusion. Serum levels of anti-FMC63 antibodies vs. detectable circulating B cells at the time of CAR T cell infusion (*$p < 0.05$; two-tailed Mann-Whitney test). (**B**) Serum levels of anti-FMC63 antibodies and B cell count in two SD patients after the first and second CAR T cell infusion (standard, patient #18; and TSCM-enriched, patient #29). *The experimental design, coordination,*

*execution, and analysis related to **Figure 17A** and **17B** were performed entirely by me. The graphical design for **Figure 17A** was made by me, while the graphical design for **Figure 17B** was made by me under the guidance of Prof. Luca Gattinoni, the co-first author of the manuscript accepted in CELL.*

Absence of GvHD following allogeneic CAR T cell therapy

Despite prior GvHD history post-allogeneic HSCT, no cases of acute GvHD (aGvHD) were observed in either cohort after CAR T cell infusion. However, while all patients in the T_{SCM} cohort had previously undergone 10/10 HLA-matched alloHSCT, only the standard arm included two patients who had received 9/10 HLA-matched alloHSCT. Therefore, these two patients were used as a case study to assess GvHD risk following allogeneic CAR T cell therapy and to define biological mechanisms limiting alloreactivity. Patient #11 underwent alloHSCT for CLL from an unrelated donor (URD) mismatching at the HLA-DR allele. Post-alloHSCT course was complicated by acute skin GvHD, culture-negative neutropenic fevers, recurrent sinopulmonary infections, and hypogammaglobulinemia. Following CAR T cell therapy (3.1×10^6 cells kg^{-1}), the patient achieved a partial response (PR) lasting more than 71 months. CAR T cell administration resulted in grade 2 CRS, but no signs of aGvHD were reported (**Table S2**).

Patient #20 was diagnosed with ALL and received multiple alloHSCTs, before and after allogeneic CAR T cell therapy, from an URD mismatching at the HLA-DQ allele. The first alloHSCT transplant was complicated by aGvHD of skin and some liver involvement. The aGvHD of the skin was biopsy-proven on day 28 after the first alloHSCT. The rash involved the face only and less than 25% body surface area. Liver GvHD was not biopsy-proven, and the total bilirubin was never elevated above the cut-off of 2.0 in the relevant time frame. The overall grade of aGvHD for the first transplant was Grade I. After the first alloHSCT, the patient received an allogeneic CAR T cell infusion (4.2×10^6 cells kg^{-1}), achieving a MRD-negative CR lasting 4 months. Grade 3 CRS occurred but no aGvHD was observed (**Table S2**). A second alloHSCT from the same donor was performed 4 months later and was complicated by chronic GvHD of the eyes, mouth, skin and liver, as well as cryptogenic organizing pneumonia. No aGvHD was evidenced. These clinical findings demonstrate that allogeneic CAR T cell administration was not associated with new aGvHD onset, even in those patients who previously experienced GvHD after alloHSCT from the same HLA-mismatched donor used to manufacture the CAR T cell product.

A cell-based platform for selective expansion of alloreactive T cell clones

To understand the mechanisms underlying the absence of GvHD in these two patients, we developed a cell-based platform capable of selectively expanding rare alloreactive T (alloT) cells from the original donor apheresis PBMCs used to manufacture CAR T cells for both patients #11 and #20. As additional controls, we included two healthy donors mismatched at the relevant HLA-DR and HLA-DQ alleles, recapitulating the same donor–recipient immunologic disparities. The erythromyeloid K562 cell line was selected as a scaffold for generating artificial antigen-presenting cells due to the low HLA class I expression and complete absence of HLA class II (**Figure 18A**)[95]. However, since IFNγ exposure strongly upregulated HLA class I (**Figure 18A**), we knocked out the β2-microglobulin (β2M) gene to prevent nonspecific class I–mediated alloreactivity (**Figure 18B**). β2M-deficient K562 cells were sequentially transduced with HLA-DM and CD74 to support class II expression and peptide loading (**Figure 18B**). Finally, the engineered K562 (*e*K562) cells were transduced with the mismatched recipient HLA (rHLA) α- and β-chains from each patient (**Figure 18B**).

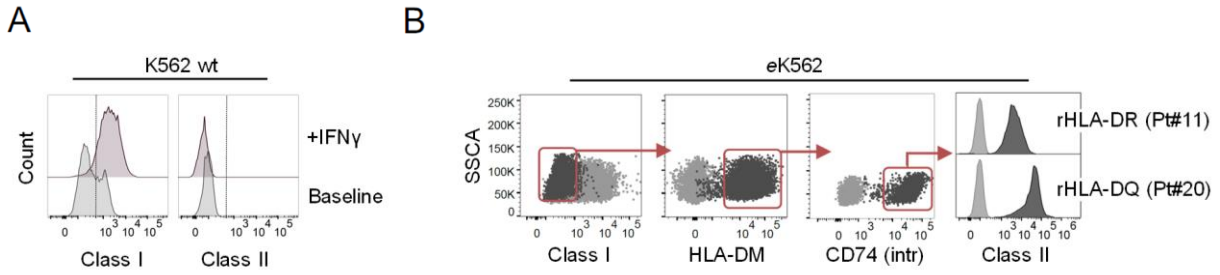

Figure 18. A K562-based artificial antigen presenting cell platform to recapitulate HLA mismatch. (**A**) Class I and Class II HLA expression on wild type (wt) K562 cells at baseline or post-stimulation with IFNγ. (**B**) Flow cytometry plots of the sequential engineering steps to generate rHLA-expressing *e*K562 cells. *Experimental design, technical execution, data processing, and figure graphical design were conceived and performed exclusively by me.*

Given the low precursor frequency of alloT cells (<0.001–5% of total T cells)[96], we hypothesized that rHLA-derived signal 1 alone would be insufficient to drive their robust expansion. We therefore introduced the co-stimulatory molecules CD80 and 41BBL on eK562 cell surface, either alone or in combination, to provide the critical signal 2. CFSE-labelled donor PBMCs were stimulated with irradiated rHLA *e*K562 or control *e*K562 cells lacking rHLA, with or without the costimulatory molecules (**Figures 19A**, **B**). No proliferation occurred with control *e*K562 cells, even when expressing both co-stimulatory

molecules, indicating that rHLA recognition was required to initiate T cell expansion. Minimal proliferation was observed with rHLA *e*K562 cells lacking co-stimulation or expressing only 41BBL. In contrast, while rHLA *e*K562 cells expressing CD80 promoted higher T cell proliferation, the most robust and significant proliferation was observed only when both costimulatory molecules were co-expressed (**Figures 19A**, **B**). Consistent with a class II–restricted mismatch, CD80/41BBL (80/BBL) rHLA *e*K562 preferentially expanded $CD4^+$ T cells (**Figure 19C**). Thus, we selected 80/BBL rHLA *e*K562 as the final platform configuration for selective alloT cell expansion.

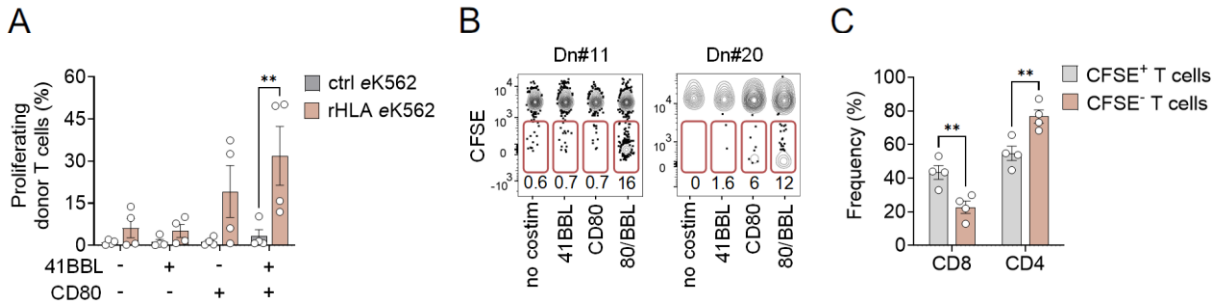

Figure 19. CD80/41BBL co-stimulation is required for efficient rHLA-dependent T cell proliferation. (**A**) Frequency of proliferating T cells (identified as CFSE-negative) post-stimulation with control (ctrl) or rHLA eK562 cells (*p <0.05; **p <0.01, two-way ANOVA, Šídák test). (**B**) Representative flow cytometry plots of PBMCs from unmanipulated donor apheresis used to manufacture CAR T cells for patients #11 and #20. Numbers indicate the percentage of proliferating cells in each quadrant following mixed lymphocyte reaction with rHLA *e*K562 cells expressing a specific combination of costimulatory molecules. (**C**) Percentage of CD8 and CD4 T cells within the CFSE-positive and CFSE-negative subsets post-stimulation with 80/BBL rHLA *e*K562 cells (*p <0.05; **p <0.01, two-way ANOVA, Šídák test). *Experimental design, technical execution, data processing, and figure graphical design were conceived and performed exclusively by me.*

Because CFSE dilution alone cannot distinguish rHLA-specific proliferation from bystander proliferation[97], we examined activation-marker profiles to define the most functional alloT cell subset. Following stimulation with 80/BBL rHLA *e*K562 cells, proliferating T cells predominantly expressed high levels of CD71, CD25, and HLA-DR (**Figure 20A**). Within the CFSE-negative population the $HLA\text{-}DR^-$, $HLA\text{-}DR^+CD25^-CD71^-$, and the triple positive $HLA\text{-}DR^+CD25^+CD71^+$ subsets were sorted. The CFSE-positive subset was further included as baseline control (**Figure 20B**). Interestingly, the triple positive subset was the most abundant among proliferating T cells and was the only group significantly enriched for $CD4^+$ T cells (**Figures 20C**, and **S5**).

A B C

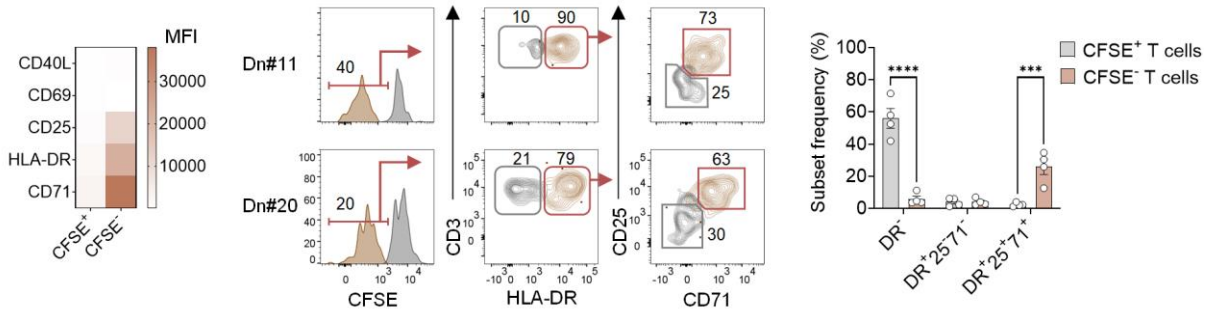

Figure 20. Activation marker profiling identifies functional rHLA-responsive T cells. (**A**) Heatmap showing mean fluorescence intensity (MFI) of early, intermediate, and late activation markers in proliferating and not proliferating T cells post-stimulation with rHLA eK562 cells. (**B**) Representative flow cytometry gating strategy used to isolate the specific T cell subsets from PBMCs obtained from unmanipulated donor apheresis post-stimulation with 80/BBL rHLA *e*K562 cells. Gated populations include CFSE-positive T cells and, within the CFSE-negative compartment, HLA-DR$^-$ cells, HLA-DR$^+$CD25$^-$CD71$^-$ cells, and HLA-DR$^+$CD25$^+$CD71$^+$ T cells. Numbers in the quadrant indicate the percentage of each subset. (**C**) Frequency of each subset within the total CD3$^+$ T cells post-stimulation with 80/BBL rHLA *e*K562 cells. (*p <0.05; **p <0.01, two-way ANOVA, Šídák test). (**I**) Bar plot showing CD4 and CD8 T cell frequencies within each subset post-stimulation with 80/BBL rHLA eK562 cells. (*p <0.05; **p <0.01, two-way ANOVA, Šídák test). *Experimental design, technical execution, data processing, and figure graphical design were conceived and performed exclusively by me.*

While CFSE-positive, HLA-DR$^-$, and HLA-DR$^+$CD25$^-$CD71$^-$ subsets showed background IFNγ responses comparable to the control condition, only the triple positive population exhibited a robust antigen-specific IFNγ response, establishing it as the dominant alloreactive population (**Figure 21**). Together, these results demonstrate that our 80/BBL rHLA *e*K562-based platform enables the selective expansion of rare, functional rHLA-specific alloT cells.

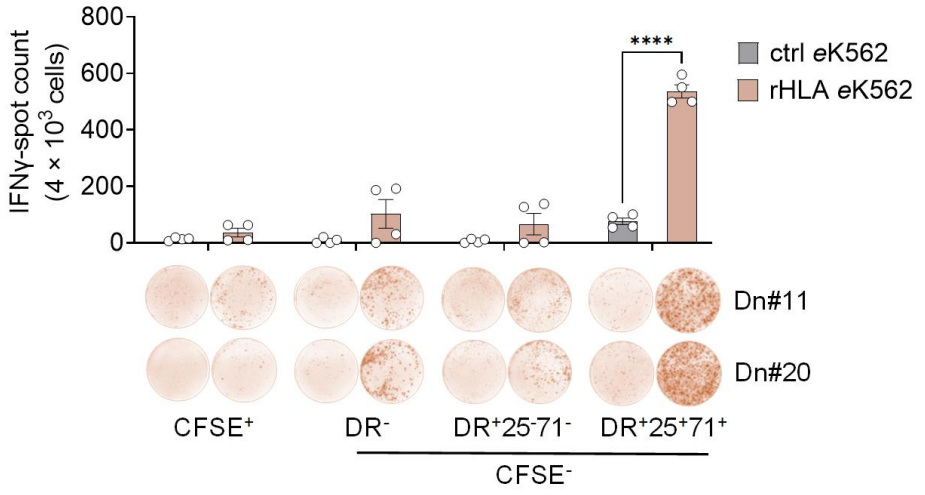

Figure 21. HLA-DR$^+$CD25$^+$CD71$^+$ cells define the most functional rHLA-responsive alloreactive population. (Top) IFNγ ELISpot quantification of each subset following stimulation with control or rHLA

*e*K562 cells. Graph indicates the number of spot-forming units per 4×103 cells. (Bottom) Representative IFNγ ELISpot wells showing alloT cells generated from unmanipulated donors PBMCs used to manufacture CAR T cells for patients #11 (Dn#11) and #20 (Dn#20) (*p <0.05; **p <0.01, two-way ANOVA, Šídák test). *Experimental design, technical execution, data processing, and figure graphical design were conceived and performed exclusively by me.*

Functional assessment of CAR-modified alloT cells in an allogeneic setting

Alloreactive CAR (alloCAR) T cells retain the potential to recognize the tumor through the CAR and host tissues via their endogenous TCR repertoire. To determine whether simultaneous CAR and TCR engagements on alloCAR T cells can interfere with target interaction, we leveraged our 80/BBL rHLA *e*K562-based platform to selectively expand alloT cells from donor PBMCs followed by the transduction with a 28z CD19 CAR construct (**Figure 22A**). In the absence of antigen stimulation, no significant differences were observed between alloCAR T cells and their non-CAR counterparts (**Figure 22B**).

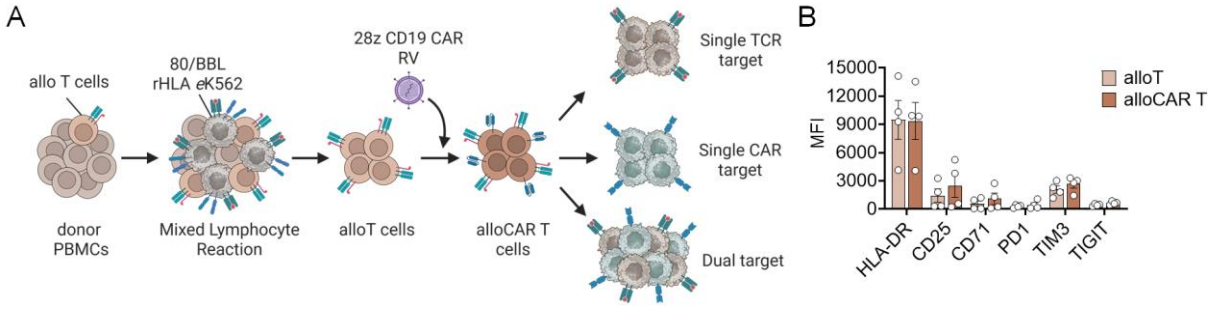

Figure 22. Generation of alloreactive alloCAR T cells using the 80/BBL rHLA *e*K562 platform. (**A**) Schematic of alloCAR T cell generation from donor PBMCs following stimulation with 80/BBL rHLA *e*K562 cells. (**B**) Expression of activation and exhaustion markers on isolated alloT and alloCAR T cells in absence antigen stimulation after 6-day culture. *Experimental design, technical execution, data processing, and graphical designs for **Figure 22A** and **B** were conceived and performed exclusively by me. **Figure 22A** was designed on BioRender.com by me.*

Therefore, we evaluated the effector functions of alloCAR T cells following antigen-specific stimulation with TCR targets alone, CAR targets alone, or a combination of both. When co-cultured with CAR targets, either alone or in presence of TCR targets, alloCAR T cells produced higher levels of IFNγ compared to the single TCR target co-culture (**Figure 23A**). Next, we assessed the ability of alloCAR T cells to mediate tumor-specific cytotoxicity. CAR

targets were efficiently eliminated at comparable levels in the single or dual target conditions, indicating that CAR-mediated recognition was unaffected by the presence of TCR targets (**Figure 23B**, right). In contrast, while alloCAR T cells exhibited robust killing efficiency of TCR targets in the single condition, their elimination dramatically declined when CAR targets were simultaneously included in the co-culture (**Figure 23B**, left). Collectively, these findings demonstrate that when both targets can be simultaneously engaged, alloCAR T cells maintain CAR-cytotoxicity, whereas TCR-mediated recognition is markedly compromised.

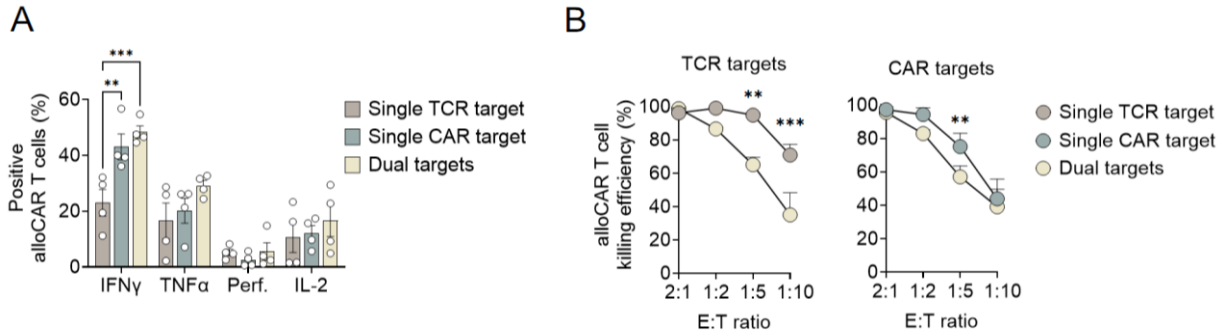

Figure 23. Dual target exposure impairs TCR-mediated recognition in alloCAR T cells. (**A**) Intracellular cytokine detection on alloCAR T cells stimulated with TCR target, CAR target, or a combination of both (*p <0.05; **p <0.01, two-way ANOVA, Šídák test). (**B**, left) Killing efficiency of TCR targets alone (grey) or in presence of CAR targets (yellow) at different E:T ratios. (**B**, right) Killing efficiency of CAR targets alone (green) or in presence of TCR targets (yellow) at different E:T ratios (*p <0.05; **p <0.01, two-way ANOVA, Šídák test). *Experimental design, technical execution, data processing, and figure graphical design were conceived and performed exclusively by me.*

Differential antigen exposure drives distinct alloCAR T cell states

To understand the cause of the reduced TCR-target killing efficiency, we profiled alloCAR T cells across the three conditions. In the single TCR target setting, alloCAR T cells expanded proportionally with the antigen load (**Figure 24A**, **B**). In contrast, stimulation with either CAR targets alone or both led to significantly reduced proliferation (**Figure 24A**, **B**). Therefore, we reasoned that the impaired alloCAR T cell recovery might further reflect a dysfunctional state. Stimulation with CAR targets alone or both resulted in robust PD1 upregulation (**Figure 24C**). Single TCR target exposure induced the highest expression of the anti-apoptotic molecule Bcl-2 and the lowest expression of the pro-apoptotic Bax molecule (**Figure 24D**). Conversely, both single CAR target and dual target conditions showed marked

downregulation of Bcl-2 and increased expression of Bax, with the dual target exposure exhibiting the most pronounced reduction of Bcl-2 and the strongest induction of Bax (**Figure 24D**). In line with the limited expansion potential, single CAR and dual target conditions were associated with the highest frequencies of the effector memory subset (**Figure 24E**). Finally, to explore the impact of differential antigen exposures, we further assessed the downstream events (**Figure 24F**). The lowest STAT5 phosphorylation (pSTAT5), associated with impaired survival, memory development, and effector functions[98,99], was detected only in the dual-target stimulation. In contrast, while no significant changes were observed in pSTAT3 and pERK1/2, high pAKT levels, a signaling state linked to reduced anti-tumor activity and poor long-term persistence[100], were exhibited in both single CAR- and dual target-conditions. Collectively, our results show that, although CAR-antigen exposure was sufficient to impair alloCAR T cell fitness, dual antigen stimulation further constrain their survival, indicating an amplified detrimental signaling.

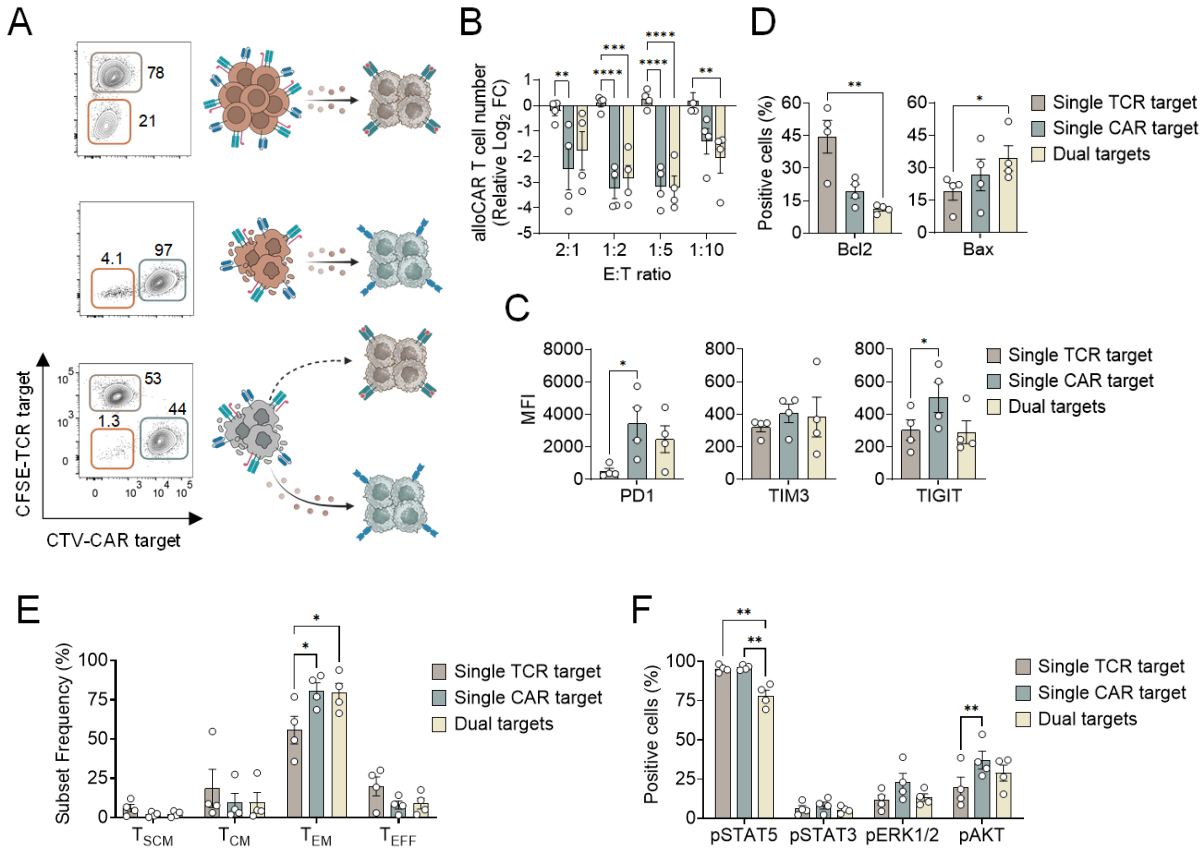

Figure 24. Cumulative dual antigen stimulation impairs alloCAR T cell fitness. (**A**) Representative flow cytometry plots showing alloCAR T cells (brown box) from donor #20 in presence of TCR targets, CAR targets, or both. Numbers indicate the percentage of alloCAR T or target cells in each quadrant. (**B**) Log2 fold change (FC) of alloCAR T cell counts normalized to unstimulated cells across the three different conditions (*p <0.05;

p <0.01, two-way ANOVA, Šídák test). (C**) Mean Fluorescence Intensity (MFI) of exhaustion markers on alloCAR T cells measured by flow cytometry post-coculture with the respective target at 1:5 E:T ratio (Friedman test with Dunn's correction). (**D**) Flow cytometric quantification of anti- and pro-apoptotic marker–positive cells after coculture at a 1:5 E:T ratio (Friedman test with Dunn's correction) (**E**) Percentage of each T cell memory subset post-coculture with the respective target at 1:5 E:T ratio (*p <0.05; **p <0.01, two-way ANOVA, Šídák test). (**F**) Quantification of phosphorylated protein levels in alloCAR T cells after a 10-minute stimulation with the appropriate target cells at an E:T ratio of 1:3 (*p <0.05; **p <0.01, two-way ANOVA, Šídák test). *Experimental design, technical execution, data processing, and figure graphical design were conceived and performed exclusively by me.* ***Figure 24A*** *was designed on BioRender.com by me.*

Modulation of 28z CAR intracellular signaling in alloCAR T cells

Most studies indicate that 28z-based CARs signal more rapidly and intensely than those incorporating a BBz costimulatory domain at early time points, ultimately resulting in impaired CAR T cell persistence and fitness[101]. Reversible inhibition of the phosphatidylinositol 3-kinase (PI3K)–AKT pathway—the principal 28z-downstream signaling—has been shown to enhance CAR T cell expansion and functionality in multiple trials[102]. Therefore, we compared 28z alloCAR T cell performance to either 28z alloCAR T cells pretreated with an AKT inhibitor (iAKT-28z) or alloCAR T cells engineered with a BBz-containing anti-CD19 CAR across the three different culture settings (**Figure 25A**). In line with our prior observations, 28z alloCAR T cells displayed the highest pAKT levels following single or dual target stimulation (**Figure 25B**). All alloCAR T cell groups exhibited comparable CAR and TCR target cytotoxicity in individual coculture conditions, with BBz alloCAR T cells demonstrating superior cytolytic activity against single TCR targets. However, similarly to our previous finding, 28z CAR T cells showed impaired target recognition under dual antigen setting, while iAKT-28z or BBz alloCAR T cells maintained the ability to efficiently eliminate both TCR and CAR targets at a similar rate (**Figure 25C**).

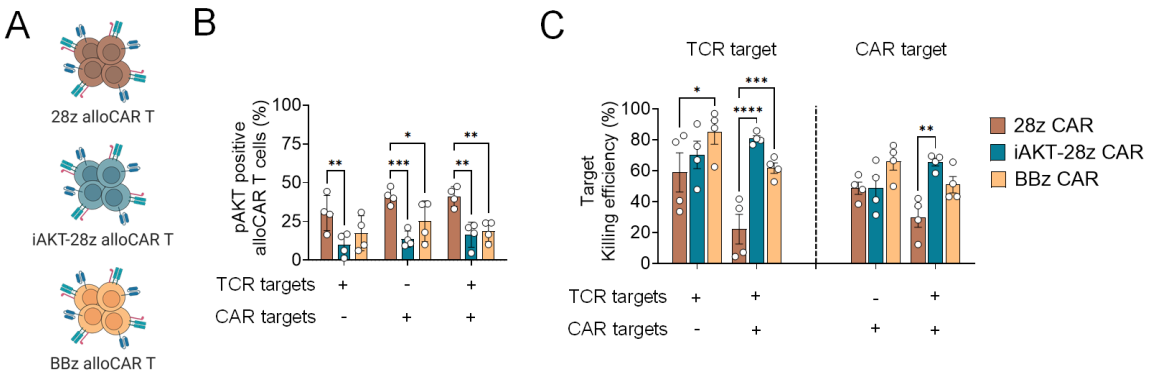

Figure 25. AKT inhibition or BBz CAR integration enhance alloCAR T cell functionality. (**A**) Cartoon showing the three different alloCAR T cell populations: alloCAR T cells expressing a CD28 costimulatory domain (28z alloCAR T), alloCAR T cells expressing a CD28 costimulatory domain pre-treated with the AKT inhibitor (iAKT-28z alloCAR T), and alloCAR T cells expressing a 41BB costimulatory domain (BBz alloCAR T). (**B**) Levels of AKT phosphorylation across the three alloCAR T cell groups after stimulation with target cells at a 1:3 E:T ratio under each condition (*p <0.05; **p <0.01, two-way ANOVA, Šídák test). (**C**) Killing efficiency of TCR targets (left) and CAR targets (right) in the presence or absence of the respective target cells (as indicated by the plus/minus symbol), at a 1:5 E:T ratio (*p <0.05; **p <0.01, two-way ANOVA, Šídák test). *Experimental design, technical execution, data processing, and figure graphical design were conceived and performed exclusively by me.* ***Figure 25A*** *was designed on BioRender.com by me.*

Strikingly, while 28z CAR T cells consistently decreased after either single CAR or dual target exposure, iAKT-28z and BBz alloCAR T cells persisted at greater levels, with BBz alloCAR T cells showing the highest frequency (**Figure 26A**, **B**). Interestingly, BBz and iAKT-28z alloCAR T cells exhibited the least dysfunctional phenotypes, with BBz showing the lowest PD1 and iAKT-28z the lowest TIM3 levels compared with their 28z-counterparts (**Figure 26C**). Together, these findings demonstrate that the selective targeting of 28z-associated downstream signaling molecules or the incorporation of a less potent costimulatory domain in the CAR module restore alloCAR T cell ability to recognize and eliminate TCR targets under dual antigen exposure, while reducing their exhaustion and enhancing persistence.

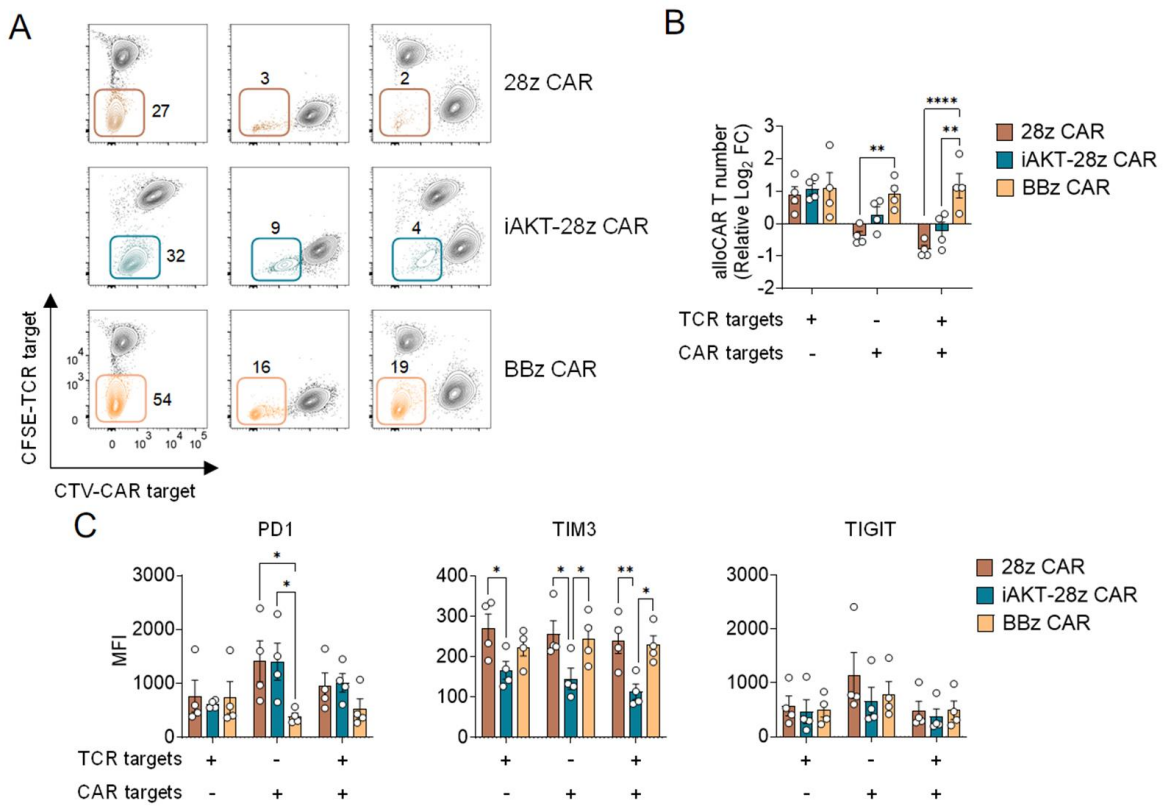

Figure 26. CAR signaling modulation improves alloCAR T cell persistence. (**A**) Representative flow cytometry plots showing alloCAR T cells generated from the unmanipulated donor apheresis PBMCs of dn#20 in presence of TCR targets (top), CAR targets (middle), or both (bottom). Numbers in the quadrant indicate the percentage of cells in each condition. (**B**) Log2 fold change (FC) of alloCAR T cell counts normalized to unstimulated cells across the three different conditions (*p <0.05; **p <0.01, two-way ANOVA, Šídák test). (**C**) Mean Fluorescence Intensity (MFI) of exhaustion markers on alloCAR T cells post-coculture with the respective target at 1:5 E:T ratio (*p <0.05; **p <0.01, two-way ANOVA, Šídák test). *Experimental design, technical execution, data processing, and figure graphical design were conceived and performed exclusively by me.*

Characterization of donor-derived alloCAR T cells in patients at the expansion phase

Having established the detrimental impact of a CAR including a 28z costimulatory moiety, we reasoned that the exhausted phenotype and the limited proliferation of alloCAR T cells observed in our *in vitro* model might also reflect a dysfunctional state of these cells in the two patients following CAR T cell infusion. To investigate this, we first defined the expansion window of CAR T cells in patients #11 and #20 to ensure that both interactions with tumor cells and host tissues could occur. Both qPCR and flow cytometry analyses revealed a peak of CAR T cells at day 8 and day 6 for patients #11 and #20, respectively, followed by a rapid decline (**Figure 27A**, **B**).

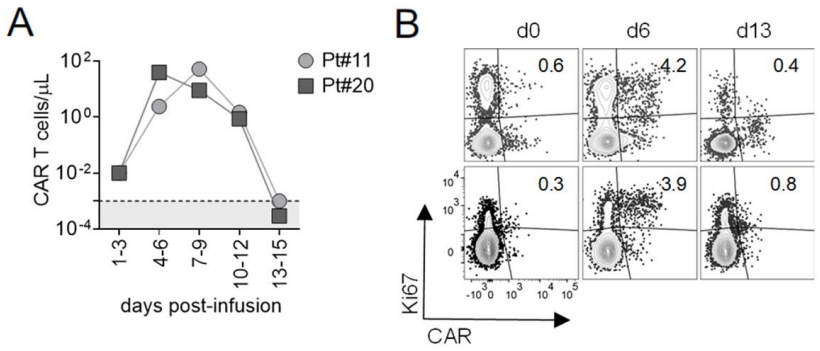

Figure 27. Defining the *in vivo* expansion window of allogeneic CAR T cells. (**A**) Circulating CAR T cell counts measured by qPCR in patients #11 and #20 following allogeneic CAR T cell therapy (**B**) CAR T cell expansion in the peripheral blood of patients #11 and #20 assessed by Ki67 staining via flow cytometry. *The experimental design, coordination, execution, and analysis related to **Figure 27A**, and **B** were performed entirely by me. Figure graphical design was performed exclusively by me.*

We leveraged our cell-based platform to generate and characterize alloCAR T cells from these time points (**Figure 28**). To precisely isolate the effects of the CAR integration, alloT cells generated from unmanipulated apheresis PBMCs of the respective donors were used as a baseline control, since these cells had not undergone any previous CAR or tumor exposure (**Figure 28**). Interestingly, while we expanded alloCAR T cells from post-infusion patient PBMCs, we also observed elevated levels of alloT cells. Given that nearly all the infused donor T cells expressed the CAR (**Figure S6**), we hypothesize that these alloT cells originated from previously tolerized cells post-alloHSCT that were reactivated upon re-encounter with the mismatched-rHLA molecule. Therefore, these cells were used as an additional control to account for the effects of prior treatment and tumor exposure.

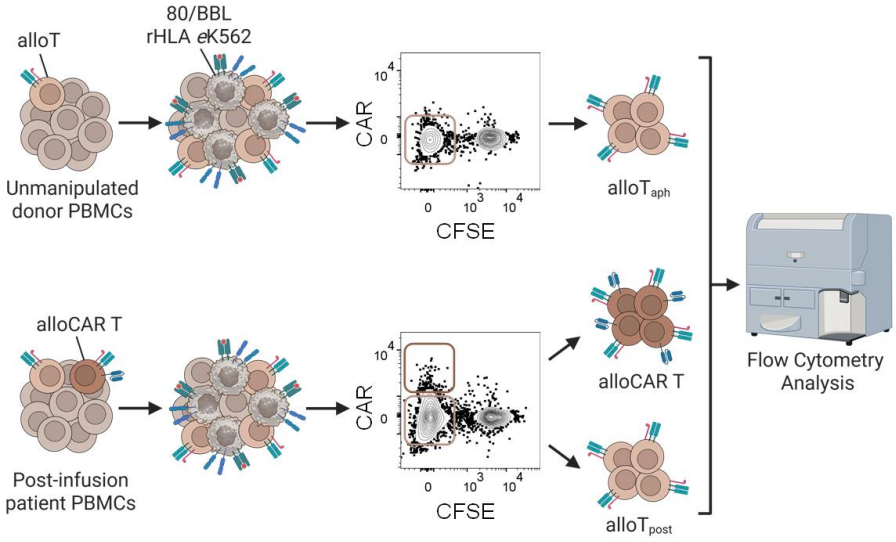

Figure 28. *Ex vivo* profiling of patient-derived alloCAR T at the time of the CAR T cell peak. Workflow schematic illustrating the generation of both alloreactive CAR T cells (alloCAR T) and alloreactive T cells ($alloT_{post}$) from patient PBMCs (patients #11 and #20) at the time of the CAR T cell expansion peak (day 6 and day 8 for patients #20 and #11, respectively), alongside the generation of alloreactive T cells from unmanipulated donor apheresis PBMCs ($alloT_{aph}$). For flow cytometry analysis, the alloreactive population was identified within the $CFSE^{-}$ fraction as $CD25^{+}CD71^{+}HLA\text{-}DR^{+}$ cells, as shown in **Figure 20B**. *The experimental design, coordination, execution, and analysis related to flow cytometry plot in the Figure were performed entirely by me.* ***Figure 28*** *was designed on BioRender.com by me.*

By combining high-dimensional flow cytometry with unsupervised Uniform Manifold Approximation and Projection (UMAP) analysis, we identified nine distinct clusters (C1–C9) defined by a unique pattern of activation and exhaustion markers (**Figure 29A**, **B**). As expected, the three alloreactive populations were characterized by a predominantly CD4-driven signature. Both $alloT_{aph}$ and $alloT_{post}$ exhibited a progressive activation pattern with a differential enrichment of early, intermediate, and late activated states (**Figure 29C**). Specifically, $alloT_{aph}$ cells were mainly enriched in early activated CD4 clusters (C4), with a minor contribution from late activated (C3), hyperactivated (C5) and hyperactivated/exhausted (C1) CD4 clusters. CD8 alloT cells were preferentially enriched in the less dysfunctional cluster (C7). Similarly, $alloT_{post}$ cells showed a comparable transitioning profile, centered on the late activated CD4 cluster (C3), with CD8 cells remaining a minor component. In stark contrast, alloCAR T cells exhibited more pronounced hyperactivated and exhaustion-skewed states for both CD4 and CD8 compartments with a strong enrichment of the most dysfunctional CD4 clusters (C1, C2, and C5) and CD8 cells representing a dominant population of a highly activated and late exhausted population (C6 and C9) (**Figure 29C**). Strikingly, while alloT cells from both apheresis and post-infusion clustered closely in the UMAP, underscoring a more overlapping profile, alloCAR T cells mapped into a completely diverse area, suggesting that these cells had undergone a distinct *in vivo* program (**Figure 29D**). In line with our *in vitro* model, alloCAR T cells exhibited the highest levels of pAKT compared to alloT cells expanded from donor apheresis or post-infusion (**Figure 29E**). Collectively, we confirmed alloCAR T cells at the early expansion phase undergo a divergent trajectory, characterized by sustained hyperactivation, pronounced exhaustion, and strong 28z-mediated signaling, and completely distinct from their non-CAR counterpart.

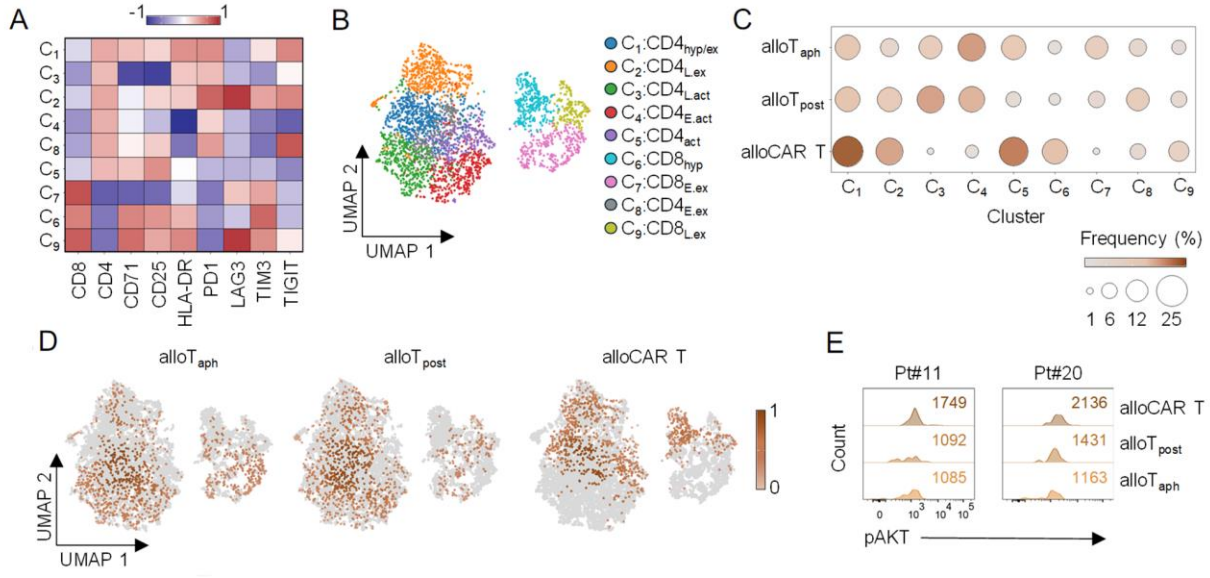

Figure 29. Donor-derived alloCAR T cells at the expansion phase exhibit a dysfunctional signature. (**D**) Heatmap showing relative frequencies (z-score) of activation and exhaustion markers in alloCAR and alloT cells at days 8 and 6 post-infusion in Pts #11 and #20, respectively, and in alloT cells from donor apheresis. Clusters were identified using the VIA algorithm; Color gradient indicates marker expression intensity. (**E**) UMAP plots of concatenated alloCAR and alloT cells from patients #11 and #20 showing spatial cluster distribution. (**F**) Bubble plot graph showing the proportion of each cluster in alloT (from apheresis and post-infusion) and alloCAR T cells at the expansion phase. (**G**) UMAP plots of concatenated data from Pts #11 and #20 showing the localization of donor-apheresis alloT cells, post-infusion alloT, and alloCAR T cells at their expansion peak. (**H**) Mean fluorescence intensity (MFI) of phosphorylated AKT (pAKT) in donor-apheresis alloT cells and in post-infusion alloT and alloCAR T cells at the expansion peak (days 6 and 8). Numbers indicate MFI values. *Experimental design, technical execution, data processing, bioinformatic analysis, and figure graphical design were conceived and performed exclusively by me.*

Longitudinal clonal Tracking of alloCAR T cells

Given the hyperactivated and dysfunctional phenotype observed at peak of CAR T cell expansion, we longitudinally tracked individual TCR clonotypes from the original CAR T cell product and from the pre-infusion (day before CAR T cell infusion) to day 60 post-infusion in both patients to define the *in vivo* dynamics of alloCAR T cells. Infusion CAR T cell products, pre- and post-infusion patient PBMCs collected from the respective time point were stimulated with our cell-based platform, and proliferating T cells, identified as $CAR^{-}CFSE^{-}CD3^{+}$ T cells, and proliferating CAR T cells, identified as $CAR^{+}CFSE^{-}CD3^{+}$ cells, were

isolated. Single cell RNA and TCR sequencing was performed on both populations (**Figure 30**).

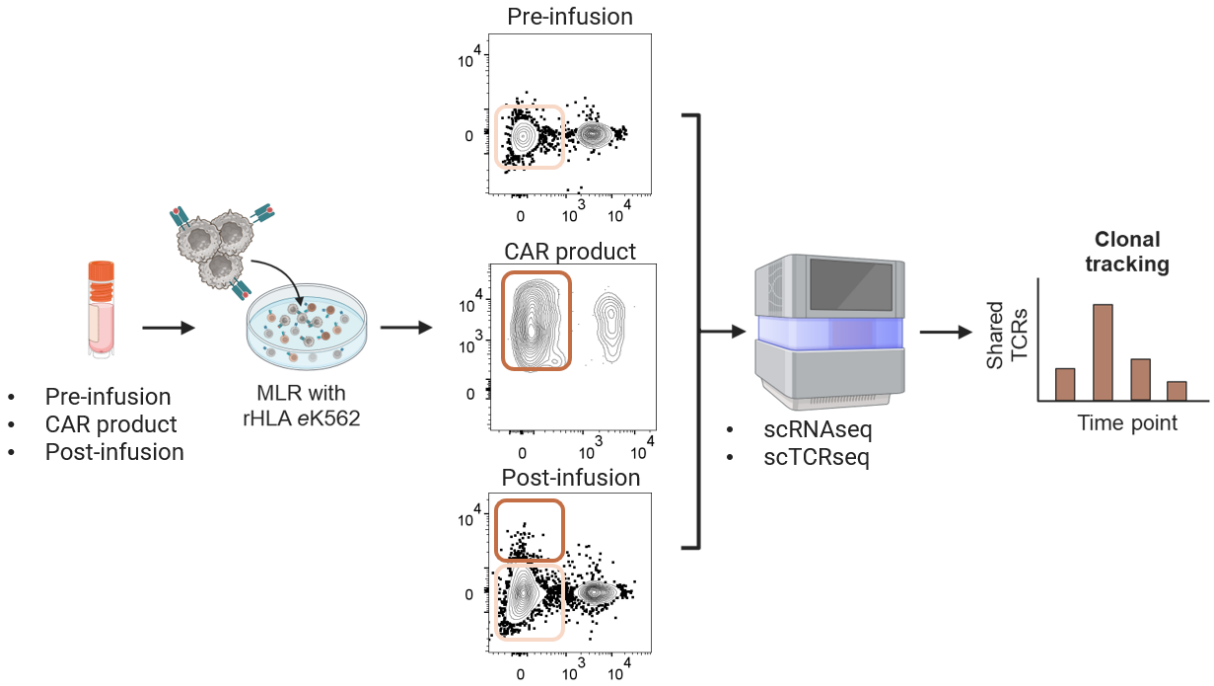

Figure 30. Schematic overview of the workflow used to isolate alloT and alloCAR T from pre- and post-infusion patient PBMCs and CAR T cell products. Pre- (day -1) and post-infusion patient PBMCs (from day 6 to day 60), and the original CAR T cell products of both patients #11 and #20 were co-cultured with irradiated rHLA-*e*K562 cells for 6 days. Proliferating T cells and CAR T cells, defined as $CFSE^{-}CAR^{-}CD3^{+}$ and $CFSE^{-}CAR^{+}CD3^{+}$ cells, respectively, were isolated by fluorescence-activated cell sorting, followed by single-cell RNA and TCR sequencing. Unique paired TCRαβ clonotypes were identified and analyzed. *The experimental design, coordination, execution, and analysis related to flow cytometry plot in the figure were performed entirely by me.* ***Figure 30*** *was designed on BioRender.com by me.*

Within the proliferating cell compartment, alloT and alloCAR T cells were distinguished based on transcriptomic expression of CAR, CD8, CD4, CD71, CD25, and HLA-DR (**Figure 31**). Importantly, within the alloT cell population, any cells expressing the CAR transgene were excluded to ensure the analysis was restricted to a pure population of truly CAR-negative T cells.

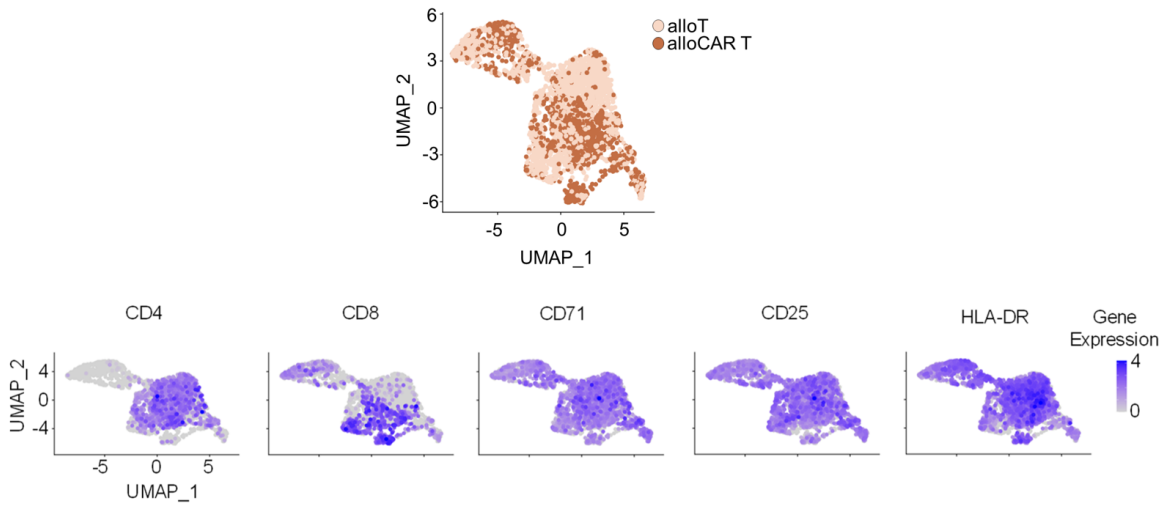

Figure 31. Transcriptomic identification of proliferating alloCAR T and alloT cells. (Top) UMAP plot showing the distribution of alloT cells and alloCAR T cells from the infusion products, pre- and post-infusion samples. (Bottom) UMAP feature plots showing transcriptomic expression of the marker genes used to define alloT and CAR T cells. *All the technical experiments were performed by me. The graphical design and bioinformatic analysis were conceived by me and Nisha Rana, bioinformatician in Prof. Luca Gattinoni's lab.*

Notably, differential gene expression analysis revealed that alloT cells from post-infusion samples were significantly enriched for genes associated with an early/memory or resting state, including *TCF7*, *LEF1*, and *G0S2* (**Figure 32A**). Consistent with this profile, gene set enrichment analysis demonstrated a strong enrichment of pathways related to memory formation, persistence, and cellular survival (**Figure 32B**). In contrast, alloCAR T cells exhibited a pronounced activation signature, characterized by elevated expression of effector-associated genes such as *GZMA*, *CD70*, and *PRF1*, alongside markers of T cell exhaustion, including *LAG3*, *CD244*, and *LGALS3* (**Figure 32A**). Notably, key negative regulators of T cell activation and TCR signaling, including *UBASH3B*, *PTPN22*, and *CBLB*, were also highly expressed. In line with a more divergent differentiation trajectory, these cells showed significant enrichment of cytotoxicity-associated pathways and heightened activation states (**Figure 32B**).

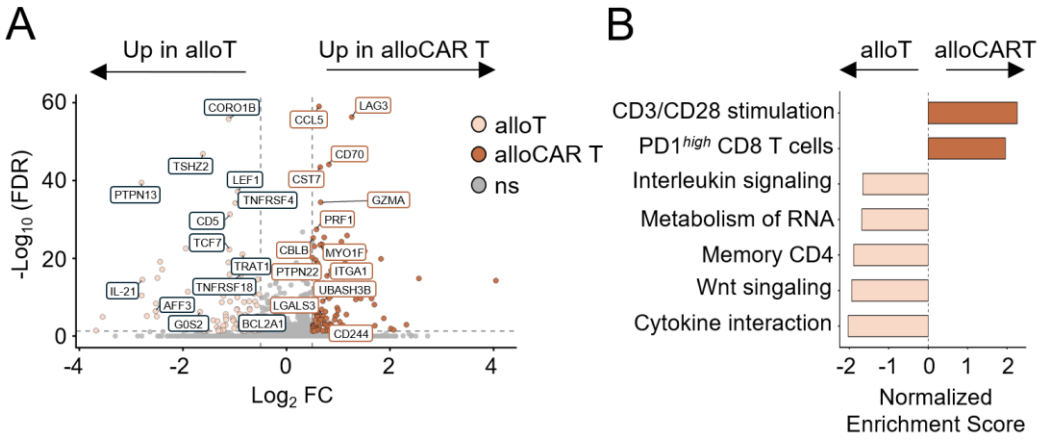

Figure 32. Divergent *in vivo* transcriptional profiles of alloT and alloCAR T cells. (**A**) Volcano plot depicting the top 50 differentially expressed genes between alloT and alloCAR T cells. (**B**) Gene set enrichment analysis (GSEA) highlighting significantly enriched pathways based on the MSigDB C2 (curated gene sets) and C7 (immunologic signatures) collections. *All the technical experiments were performed by me. The FASTA data processing was performed by Nisha Rana, while bioinformatic analyses and graphical design were performed entirely by me.*

Longitudinal tracking of shared TCR sequences revealed that alloT cells predominantly underwent transient clonal expansion; however, a subset of clones (n = 29) persisted across at least two time points (**Figure 33**, left). Notably, the majority of these shared TCR clones were already present in the pre-infusion samples, suggesting that the clones expanding post-infusion were primarily alloreactive populations established after alloHSCT. These clones appear to have subsequently undergone functional attenuation and entered a latent or quiescent state. This observation is further supported by their resting or memory/early-differentiated transcriptional program, as no significant activation or cytotoxic gene signatures were detected (**Figure 32**). Conversely, alloCAR T cells exhibited a pronounced clonal expansion at day 6 post-infusion (**Figure 33**, right). This peak occurred in parallel with the previously described expansion of the total CAR T cells (**Figure 27**), suggesting a CAR-driven activation. Notably, no shared TCR sequences were identified among alloCAR T cells at any of the analyzed time points, except for 1 low expanding clone at day 30 and day 60 (**Figure 33**, right).

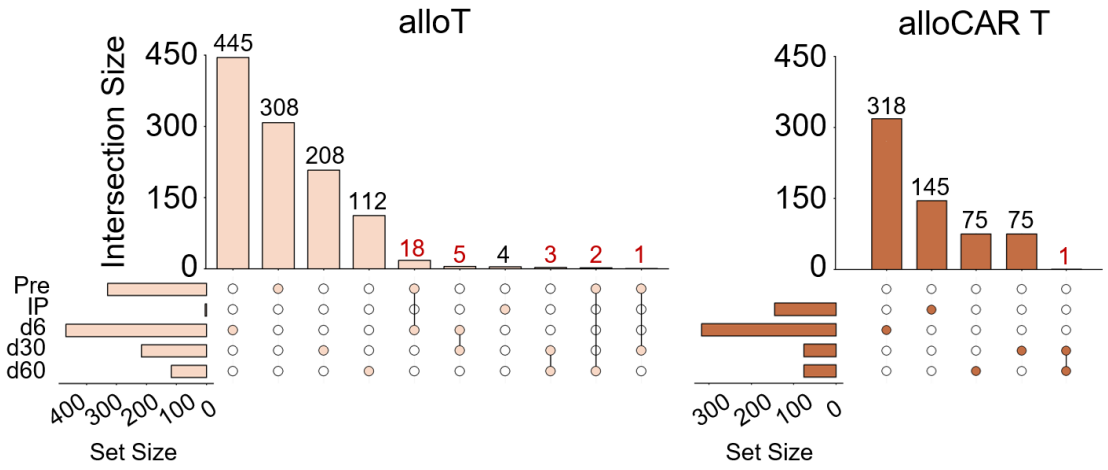

Figure 33. Longitudinal clonal tracking of alloCAR T cells shows transient expansion and limited persistence. Upset plot summarizing shared TCR clonotypes within alloT (left) and alloCAR T cells (right) across time points. Filled circles indicate the presence of a clonotype at a given time point, and bar heights denote the number of clonotypes within each intersection. Connecting lines between circles indicate clonotypes shared across the corresponding time points. *All the technical experiments were performed by me. The FASTA data processing was performed by Nisha Rana, while bioinformatic analyses and graphical design were performed entirely by me.*

Together, these data delineate two fundamentally distinct *in vivo* behaviors where alloT cells displayed features of transient clonal expansion followed by stabilization into a quiescent, memory-like state, consistent with functional immune tolerance of pre-existing alloreactive clones derived from prior alloHSCT. In contrast, alloCAR T cells were characterized by a highly divergent transcriptional program marked by concurrent activation and exhaustion, coupled with altered TCR signaling and a lack of clonal persistence. Collectively, these findings support a model in which alloCAR T cells undergo a rapid, time point–restricted expansion without establishing durable clonal maintenance.

Discussion

CD19-targeted CAR T cell therapies have revolutionized the treatment of refractory and/or relapsing B-cell malignancies post-alloHSCT, achieving unprecedented rates of complete remission[50,103,104]. Nevertheless, long-term follow-up of patients has revealed that only 20–50% of patients experience durable responses following CAR T cell therapy[105]. Poor engraftment, limited expansion, and short persistence of infused CAR T cells have been identified as a major contributor to early relapse and treatment failure[106]. Over the past years, strategies to enhance these T cell–intrinsic properties have primarily focused on structural modifications of the CAR, particularly through the incorporation of alternative intracellular costimulatory domains[107]. However, while CAR architecture undoubtedly plays a critical role, accumulating evidence indicates that CAR T cell products enriched for early-differentiated T cell populations can substantially enhance therapeutic efficacy[108-110].

T_{SCM} cells represent the least differentiated antigen-experienced memory T cell subset, as they combine phenotypic and functional attributes traditionally ascribed to both naïve and memory T cells, including robust proliferative capacity, long-term persistence, multipotency, self-renewal, and the ability to rapidly acquire effector functions upon antigen re-exposure[76]. Despite their compelling biological properties, T_{SCM} cells have remained largely underrepresented in current FDA-approved CAR T cell products, primarily due to their relative paucity in unfractionated PBMCs collected from the apheresis and the lack of scalable manufacturing methods[111]. Early attempts to generate clinically relevant numbers of T_{SCM} cells for adoptive cell therapy, including cytokine-driven approaches using IL-7 and IL-15, yielded T_{SCM}-like populations with more advanced differentiation phenotypes, thereby raising concerns regarding their real stem-like properties[112,113].

In 2016, Gattinoni and colleagues established a clinical-grade platform to generate and expand CD19 CAR–redirected T_{SCM} cells, demonstrating superior and long-lasting anti-leukemic activity compared with conventional CD19 CAR T cell products in systemic acute lymphoblastic leukemia xenografts[78]. Based on these preclinical results, 11 patients with relapsed and/or refractory B-cell malignancies after alloHSCT were treated with donor-derived CD19 CAR T_{SCM} cells. These patients were included in the immunomonitoring study described in the present thesis, which was specifically designed to longitudinally assess the *in vivo* kinetics, expansion, and persistence of CAR-modified T_{SCM} cells and to determine

whether these characteristics differ from those of standard CAR T cells. Importantly, the unique design of the trial examined here provides a stringent opportunity to directly compare both CAR T cell products under conditions that most closely reflect their standalone therapeutic potential, as the CAR construct was identical, the patient cohorts were comparable, and—critically—no lymphodepleting chemotherapy was administered prior to infusion.

Lymphodepletion is widely regarded as a prerequisite for effective CAR T cell therapy, as it promotes homeostatic cytokine release, reduces immunoregulatory cell populations, and contributes to creating a favorable immune environment, facilitating *in vivo* CAR T cell expansion and persistence[114,115]. Our results challenge this paradigm by demonstrating that CAR T_{SCM} cells achieve robust expansion, sustained persistence, and clinically meaningful activity at doses comparable to conventional CAR T cells, without relying on preconditioning-mediated amplification effect. Importantly, this observation does not argue against the clinical utility of lymphodepletion per se but rather demonstrates that it is not strictly required for a robust and durable *in vivo* activity when the infused product is highly enriched for T_{SCM} cells. This distinction has relevant and direct clinical implications, particularly in post-alloHSCT settings, where additional cytotoxic conditioning carries substantial risk in already immunocompromised patients. Notably, although patients were not stratified by disease subtype, the consistent *in vivo* behavior of CAR T_{SCM} cells observed across heterogeneous malignancies suggests that the differences between the two cohorts are more likely driven by intrinsic properties of the CAR T cell products rather than by disease-specific factors, supporting the biological relevance of this therapeutic platform.

However, although *in vivo* expansion is a prerequisite for CAR T cell–mediated antitumor activity[89-91], it is also closely associated with treatment-related toxicity, particularly CRS[116]. Meta-analyses of real-world studies indicate that CRS occurs in approximately 50–80% of treated patients, with an incidence of grade ≥3 CRS of about 15–20%[117]. Consistent with these reports, CRS occurred in the majority of patients (>70%) treated with the standard CAR T cells, with severe CRS observed in 28.6% of patients. Notably, despite demonstrating robust and sustained expansion, patients receiving CAR T_{SCM} cells exhibited a markedly improved safety profile, with no cases of severe CRS, except in a single patient with a higher disease burden. Strikingly, a patient achieving a complete response after receiving a total dose of 216×10^6 CAR T_{SCM} cells experienced only grade 2 CRS, whereas a total dose of 167×10^6

standard CAR T cells was sufficient to induce grade 4 CRS in a patient who achieved only a partial response. This dissociation between greater expansion magnitude and reduced CRS severity indicates that the biological properties associated with CAR T_{SCM} cells may uncouple efficacy from toxicity.

However, the improved safety profile cannot be explained solely by the delayed expansion kinetics and reduced differentiation status of CAR-modified T_{SCM}. Based on preclinical evidence generated exclusively with CD8 T cells[78], and early clinical observations correlating *in vivo* CD8 T cell expansion to clinical responses[79], CAR T_{SCM} product was intentionally enriched for $CD8^+$ T cells. In contrast, the standard CAR T cell products consisted of a mixed CD4/CD8 population. Despite CD4 T cells are indispensable for effective CAR T therapy, as they support the generation of functional CD8 T cells during manufacturing[118,119] and contribute to antitumor activity *in vivo*[120], accumulating clinical and preclinical evidence highlights the role of CD4 CAR T cells as major contributors to CRS. Boulch et al. reported that in a cohort of 76 patients with DLBCL, those experiencing CRS had higher frequencies of CD4 than CD8 CAR T cells in circulation compared with patients without CRS[121]. Preclinical studies in humanized mice further underscore a predominant role for CD4 CAR T cells in triggering CRS and neurotoxicity[122]. Mechanistically, CD4 CAR T cells are likely to license monocytes/macrophages, the primary producers of IL-6, a hallmark of CRS-associated inflammation[123,124]. Consistent with this framework, elevated serum IL-6 levels were observed in patients receiving standard CAR T cells, whereas IL-6 remained comparatively restrained in CAR T_{SCM}–treated patients. In line with these findings, single-cell secretome analysis of the original CAR T cell products revealed that, while CAR T_{SCM} cells exhibited a highly polyfunctional profile, generally attributed to improved T cell fitness[125], standard CAR T cells were characterized by a predominantly CD4-skewed cytokine signature associated with elevated IL-6 production. Collectively, our findings support a model in which the inflammatory toxicity of CAR T cell therapy is shaped not only by the extent of expansion but also by the functional and lineage composition of the infused cells.

Previous longitudinal clonal tracking studies aimed to characterize T_{SCM} cell dynamics over time and to link their differentiation and persistence to the magnitude and durability of responses. Bonini and colleagues, by tracking gene-modified memory T cells infused after T-repleted haploidentical HSCT, showed that the majority of long-term persistent clones originated from T_{SCM} cells[126]. Marraco et al. demonstrated that, following yellow fever

vaccination, effector and conventional memory T cell populations expanded transiently and progressively declined, whereas T_{SCM} cells accumulated over time and were stably maintained for decades[127]. Biasco and colleagues extended these observations to the CAR T cell field, showing that CAR T cell clones derived from T_{SCM} cells differentiated into downstream memory subsets after infusion and supported both early expansion and long-term persistence[128]. However, while informative, these studies are difficult to interpret due to reliance on indirect readouts, variability in infused products, and confounding contributions from conditioning regimens. Consequently, the *in vivo* trajectory of CAR T_{SCM} cells remains unresolved.

By applying high-resolution longitudinal tracking, we addressed this limitation and enabled a precise reconstruction of T_{SCM} post-infusion dynamics. Here, we propose a model of linear differentiation whereby T_{SCM} cells retain the dual capacity to generate downstream effector progeny while preserving the T_{SCM} reservoir, consistent with their stem-like transcriptional and functional program. In contrast, standard CAR T cells follow a unidirectional pathway toward more terminal differentiation states without reconstitution of early memory compartments. Furthermore, integration site analysis allowed us to define the architecture underlying CAR T cell persistence of both products at clonal level. In standard patients, early-expanded CAR T cell clones progressively decline over time. Conversely, CAR T_{SCM} cells show sequential waves of clonal expansion, with distinct clonotypes emerging at successive time points and overall sustaining long-term CAR T_{SCM} cell maintenance (**Figure 34**). This finding indicates that durable persistence of CAR T_{SCM} cells is not driven by the long-term survival of a limited number of dominant clones but rather by continuous recruitment of newly differentiated progeny from a stem-like reservoir. This behaviour closely mirrors the clonal dynamics observed in hematopoietic stem cell–driven reconstitution, where long-term maintenance is achieved through serial contribution of multiple clones rather than permanent dominance of a single progenitor[129].

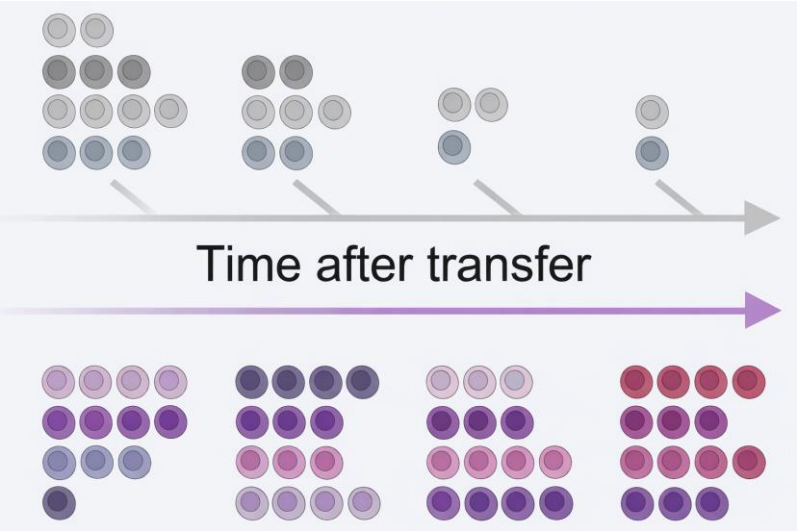

Figure 34. Distinct clonal dynamics of standard and CAR T_{SCM} products after transfer. Schematic representation of longitudinal clonal behavior of standard CAR T cells (top) and CAR T_{SCM} cells (bottom). Each individual clone or group of clones is denoted by a specific color code. Standard CAR T cells are characterized by early clonal dominance followed by progressive contraction, resulting in long-term persistence driven by a limited set of initially expanded clones. In contrast, CAR T_{SCM} cells sustain long-term engraftment through sequential waves of clonal succession, with newly emerging clones progressively contributing to the persisting pool. This model illustrates population-level maintenance of stemness through clonal replacement. *This figure was designed by me on BioRender.com.*

After excluding intrinsic defects of the CAR T_{SCM} product, the present study sought to understand why a subset of patients failed to respond or eventually relapsed. While we observed that in the standard CAR T cell cohort clinical responses were associated with *in vivo* expansion, no such correlation was observed in CAR T_{SCM}–treated patients, where robust expansion occurred irrespective of clinical outcome. This discrepancy indicates that proliferative fitness alone is insufficient to account for therapeutic success of CAR T cell-based therapies and implicates additional extrinsic mechanisms in driving treatment failure. To explore potential contributors to the lack of response after CAR T_{SCM} administration, two informative case studies were in-depth examined.

In the only patient with progressive disease following CAR T_{SCM} infusion, CAR T_{SCM} cells expanded efficiently and mediated rapid depletion of circulating B cells, demonstrating preserved *in vivo* activity (**Figure 35A**). However, leukemic cells in the bone marrow displayed dim CD19 expression (**Figure 35B**), a condition known to impair productive CAR engagement[130]. Our results corroborate with previous studies identifying insufficient antigen density as a plausible mechanism limiting efficacy despite intact CAR T cell functionality[131].

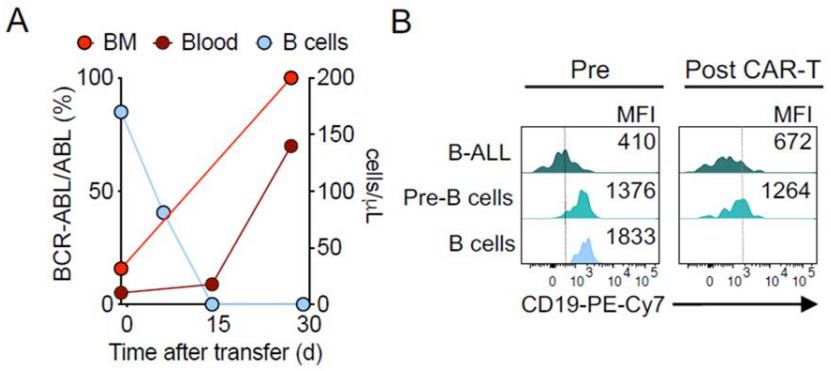

Figure 35. Leukemia progression in a T_{SCM} patient (Patient #23) was attributed to loss of CD19 antigen expression. (**A**) B cell count and % BCR-ABL transcript levels relative to ABL in bone marrow and blood in patient #23 post-CAR T cell infusion. (**B**) Flow cytometry plots showing CD19 expression levels on B-ALL, pre-B, and mature B cells in patient #23 before and 1 month after CAR T cell infusion. Numbers in each plot represent CD19 mean fluorescence intensity (MFI). Dashed vertical line indicates the background levels of CD19 staining in CD19- cells. *Figures were generated using data from experiments conducted at the National Institutes of Health, with the permission of Dr. Jennifer Brudno and Dr. James Kochenderfer, the last authors of the manuscript accepted in CELL. The graphical design for **Figures 35A** and **B** was made by me under the guidance of Prof. Luca Gattinoni, the co-first author on the manuscript accepted in CELL.*

A second non-responder case involved a patient with CLL in whom CAR T_{SCM} cells failed to expand. CLL is characterized by a profoundly immunosuppressive microenvironment, and elevated IL-10 levels have been implicated in CAR T cell inhibition[132]. Consistently, multiplex cytokine profiling revealed supraphysiologic systemic IL-10 concentrations in this patient, suggesting that an inhibitory cytokine milieu may have impaired CAR T_{SCM} expansion or early functional priming. Elucidating how IL-10 signaling shapes T_{SCM} biology and developing strategies to overcome cytokine-mediated immunosuppression—including dominant-negative receptors[133] or synthetic intramembrane proteolysis receptors (SNIPRs)[134]—may represent a promising avenue to enhance CAR T_{SCM} efficacy in hostile tumor microenvironments.

Beyond antigen-related and immunosuppressive cytokine-mediated mechanisms, immunogenicity against the CAR itself represents an additional barrier to durable activity, particularly in the absence of lymphodepletion[94]. Mouse-derived scFv domains in the CAR construct can trigger both cellular and humoral immune responses, leading to anti-CAR antibodies that can further limit persistence and function of the infused cells. Post-infusion anti-CAR antibodies have been reported in 36.7% of ALL patients and 5% of r/r DLBCL patients treated with tisagenlecleucel, supporting the clinical relevance of this

phenomenon[135,136]. Consistently, in our study, anti-CAR antibodies were detected in the 35% of the patients, suggesting that humoral immunity directed against the FMC63 scFv as an additional mechanism capable of limiting both CAR T_{SCM} and conventional CAR T cells. Notably, while initial CAR T cell infusions mediated effective B cell depletion, subsequent infusions failed to do so in the presence of rising anti-CAR antibody titers, suggesting functional neutralization of the infused cells.

The present study also provides a unique opportunity to critically evaluate the safety of donor-derived CAR T cell therapy in the context of major HLA mismatches and, specifically, the associated risk of graft-versus-host disease (GvHD).

Although allogeneic CAR T cells offer clear practical and biological advantages over autologous products—including improved T cell fitness, immediate availability, and reduced manufacturing constraints[137]—the risk of GvHD has long been regarded as the principal obstacle to their broader clinical application[137]. As a result, autologous CAR T cell products remain the only approved therapies[54,105] and most published studies employing allogeneic CAR T cells remain small-scale[139-142].
In our study, no cases of *de novo* acute GvHD were observed following donor-derived CAR T cell therapy, despite a history of GvHD after alloHSCT in a substantial proportion of patients. This observation is particularly notable given that CAR T cells were manufactured from both related and unrelated donors, including donors mismatched at major HLA alleles. Similarly, numerous early-phase trials have consistently reported minimal or no GvHD following donor-derived CAR T cell therapy[139-142], with rates lower than those observed after donor lymphocyte infusion[143] or second alloHSCT[144], thereby suggesting that the actual GvHD risk may be less substantial in the current clinical experience[145].

A preclinical study in an HLA-mismatched lymphoma model has provided a mechanistic rationale for this apparent paradox, demonstrating that cumulative signaling from simultaneous CAR and TCR engagement induces aberrant hyperactivation of alloreactive CAR T cells, leading to rapid exhaustion and premature *in vivo* deletion, thereby limiting GvHD onset[145]. However, whether this mechanism operates in humans has yet to be established, and real-world evidence remains limited.

To address this gap, we employed an artificial antigen-presenting cell platform to selectively expand rare, naturally occurring alloreactive T cells from the original donor apheresis and to interrogate their functional behavior following CD28-based CAR engineering. Importantly, rather than relying on unfractionated allogeneic lymphocytes[146] or on T cells engineered to express an antigen-specific exogenous TCR[147], the present study employs a defined population of polyclonal naturally occurring alloreactive T cells preserving their endogenous TCR repertoire. Our findings not only corroborate with prior preclinical observations[146] but also extend them to a more mechanistical level, demonstrating that CD28-based CAR-signaling alone is sufficient to drive functional burnout of alloreactive CAR T cells, limiting their persistence and effectively acting as an intrinsic safety switch. However, concurrent TCR engagement further amplifies apoptotic signaling, promoting their rapid contraction (**Figure 36**). Importantly, modulation of CD28-associated downstream signaling—either through transient AKT inhibition or substitution of CD28 with a weaker costimulatory domain such as 41BB—partially restored alloreactive T cell proliferation and function. This observation provides a mechanistic explanation for the higher incidence of GvHD reported in allogeneic CAR T cell trials employing 41BB–based CAR constructs[148] and underscores how CAR signaling architecture directly shapes alloreactive potential.

To extend these *in vitro* findings to our clinical observations, the *in vivo* dynamics of alloreactive CAR T cells was defined in the two selected major HLA-mismatched patients from the standard arm. During the expansion phase—when interactions with both tumor and host tissues were simultaneously possible—donor-derived alloreactive CAR T cells displayed a divergent phenotype compared to their non-CAR counterparts, intrinsically biased toward a hyperactivated and dysfunctional state. Longitudinal tracking revealed a transient expansion followed by rapid functional attrition, indicating that alloreactive CAR T cells fail to establish long-lived clonal dominance after infusion.

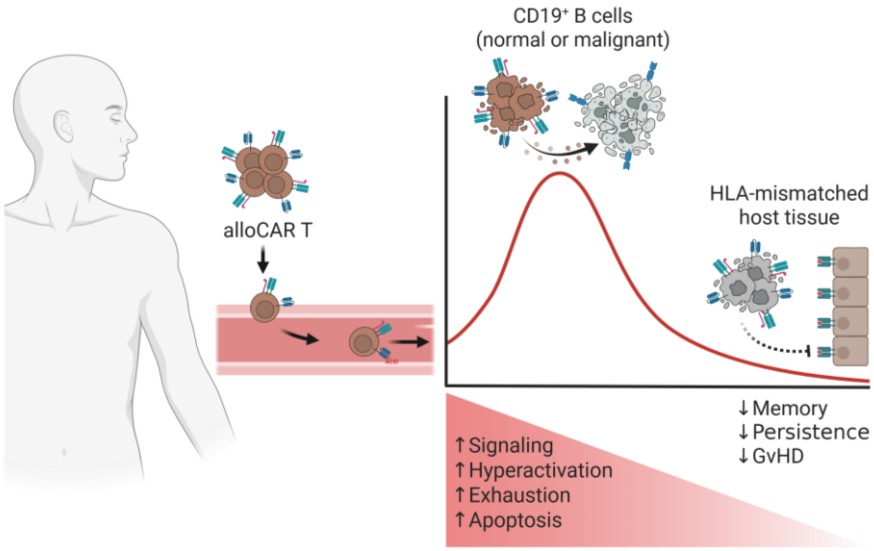

Figure 36. Cumulative signaling–driven dysfunction model in alloreactive CAR T cells. Following infusion, alloreactive CAR T cells (alloCAR T) traffic through the circulation (or bone marrow) and engage CD19⁺ B cells (normal or malignant), triggering a rapid and strong CD28-mediated CAR signaling. CAR-mediated signaling is sufficient to induce robust activation, exhaustion, and increased apoptosis, thereby acting as an intrinsic safety molecular switch that limits alloCAR T cell fitness. Upon subsequent exposure to HLA-mismatched host tissues, TCR stimulation further augments the overall signaling burden, exacerbating dysfunction and accelerating loss of effector competence, resulting in a lower risk of graft-versus-host disease (GvHD). *This figure was designed by me on BioRender.com.*

Notably, although our analysis focused exclusively on a major HLA Class II mismatch setting, both CD8⁺ and CD4⁺ alloreactive CAR T cells displayed similar dysfunctional phenotypes. This observation parallels findings from another preclinical model showing that concurrent CAR and TCR engagement in dual-specific CAR CD8⁺ T cells induced rapid loss of functionality, accelerated exhaustion, and apoptosis[149].

Because lymphodepletion was not administered prior to CAR T cell infusion, endogenous T cells and NK cells were likely retained at the time of donor-derived CAR T cell transfer. Consequently, host-mediated immune rejection may have contributed, at least in part, to the limited persistence of alloreactive CAR T cells[150]. Analysis of the patient's PBMCs performed immediately prior to CAR T cell infusion (data not shown), revealed complete donor chimerism, indicating that host-mediated rejection alone cannot fully account for the selective loss of dominant alloreactive CAR T cell clones

Current strategies aimed at advancing allogeneic CAR T cell therapy increasingly rely on extensive genome editing to eliminate endogenous TCR expression[151], modulate HLA

expression[152], or introduce immune-evasive viral molecules[153]. While these approaches may significantly reduce potential alloimmune recognition and reduce the GvHD risk, accumulating clinical evidence suggests that genetic manipulation, such as endogenous TCR knockout, can also compromise CAR T cell *in vivo* persistence[154]. For instance, the first in-human study evaluating the safety and antileukemic activity of UCART19, an allogeneic double TCR/CD52-knockout CAR T cell product, showed a much shorter duration than autologous CAR T cell products, with only 4 out of 25 patients having CAR T cell persistence beyond 42 days[154].

Collectively, despite the limited cohort size requiring validation in larger prospective and randomized studies, the findings from the immunomonitoring study provide the first in-patient characterization of CAR T_{SCM} cells, supporting their intrinsic therapeutic potential compared to conventional CAR T cells. These data also identify key tumor- and host-related mechanisms that may constrain treatment efficacy, thereby offering a biological framework to guide the optimization of next-generation CAR T cell strategies. The results described here further elucidate the mechanistic factors contributing to the low incidence of GvHD observed with allogeneic CD28-based CAR T cell products and provide the first comprehensive in-human characterization of alloreactive CAR T cells in the setting of strong immunological pressure imposed by major HLA mismatches. Together, this study informs the rational design of safer and more effective allogeneic CAR T cell therapies and support their continued clinical development.

Supplementary Tables and Figures

Table S1. Patients treated with CAR T_{SCM} cells

Patient Number	Malignancy	Donor Type	Treatment number	CAR+ T-cell dose (per kg body weight)	CRS Grade*	Highest grade of neurologic adverse event in first 30 days after CAR T-cell infusion (CTCAE v4.03)	Duration of response in months**	Event-free survival in months***
21	LBCL	sibling	1	0.25×10^6	No CRS	0	SD (2)^	3
			2	0.5×10^6	No CRS	0	SD (2)	3
22	Ph+ ALL	sibling		0.25×10^6	No CRS	0	MRD negative CR (24)	25
23	Ph+ ALL	sibling		0.25×10^6	1	0	PD	1
24	CLL transformed to LBCL	sibling		0.5×10^6	No CRS	0	SD (1)	1
25	LBCL	sibling		1×10^6	2	0	PR (25)	27
26	Ph- ALL	unrelated		1×10^6	3	0	CR with incomplete blood count recovery (1)	2
27	CLL	unrelated		1×10^6	1	0	CR with incomplete blood count recovery, MRD negative (46)	48
28	Ph- ALL	unrelated		1×10^6	2	$2^{\%}$	MRD negative CR (24)	26
29	Ph- ALL	unrelated	1	1×10^6	No CRS	0	SD (5)^	6
			2	2×10^6	No CRS	0	SD (4)	5
30	CLL	sibling		1×10^6	2	0	SD (1)	1
31	Ph- ALL	sibling		2×10^6	2	0	MRD negative CR (4)	5

ALL: acute lymphoblastic leukemia. CLL: chronic lymphocytic leukemia. LBCL: large B-cell lymphoma. MCL: mantle cell lymphoma. Ph+: Philadelphia chromosome positive. Ph- Philadelphia chromosome negative. MRD: minimal residual disease. CR: complete remission. PR: partial remission. PD: progressive disease. SD: stable disease. *CRS toxicity grading is per Lee et al. "ASTCT Consensus Grading for Cytokine Release Syndrome and Neurologic Toxicity Associated with Immune Effector Cells." Biology of Blood and Marrow Transplantation 2019; 25(4):625-638. **Duration of response is time between first response of PR or better, or SD if SD is best response, and last malignancy assessment, progressive malignancy, initiation of new anti-malignancy treatment, or death from any cause. ***Event-free survival is time between cell infusion and last malignancy assessment, progressive malignancy, initiation of new anti-malignancy treatment, or death from any cause. (+) Indicates an ongoing response at last assessment. (^) Patient with stable disease until they received a second CAR T-cell infusion. ($^{\%}$) Neurologic adverse event was a headache.

Table S2. Patients treated with standard CAR T cells

Patient Number	Malignancy	Donor Type	Treatment number	Anti-CD19 CAR exressing T cell infused/kg	CRS grade*	Highest grade of neurologic adverse event in first 30 days after CAR T-cell infusion (CTCAE v4.03)	Duration of response in months**	Event-free survival in months***
1	CLL	unrelated		0.4×10^6	3	0	SD (2)	3
2	LBCL	sibling		0.7×10^6	1	0	SD (1)	2
3	CLL	sibling		2.4×10^6	4	0	PD	1
4	LBCL	sibling		2.2×10^6	0	0	SD (42+)^	43+
5	CLL	unrelated		1.0×10^6	2	0	CR (96+)^^	98+
6	MCL	sibling		4.6×10^6	0	0	SD (2)	3
7	CLL	unrelated		0.7×10^6	1	0	PD	1
8	MCL	sibling		3.9×10^6	0	0	CR (59+)^^	90+
9	MCL	unrelated	1	2.2×10^6	1	0	PR (2)	3
			2	2.5×10^6	0	0	PD	2
10	MCL	sibling		7.8×10^6	2	3%	SD (1)	2
11	CLL	unrelated		3.1×10^6	2	0	PR (70+)^^	71+
12	Ph+ ALL	sibling		5.2×10^6	1	3% (also grade 2 dysphasia and floaters)	MRD-negative CR (59+)^^	60+
13	MCL	sibling		7.1×10^6	0	0	SD (8)	9
14	Ph- ALL	sibling		7.0×10^6	3	0	MRD-negative CR (4)	5
15	Ph- ALL	sibling		6.9×10^6	4	2	MRD-negative CR (3)	4
16	Ph- ALL	sibling		5.6×10^6	3	3%	PD	1
17	LBCL	sibling		8.2×10^6	2	0	CR (3)#	5
18	LBCL	sibling	1	3.1×10^6	1	2%	SD (1)	2
			2	9×10^6	0	0	SD (1)	2
19	FL transformed to LBCL	unrelated		4.3×10^6	4	2	PD	1
20	Ph- ALL	unrelated		4.2×10^6	3	0	MRD-negative CR (2)##	4

ALL: acute lymphoblastic leukemia. CLL: chronic lymphocytic leukemia. LBCL: large B-cell lymphoma. FL: follicular lymphoma. MCL: mantle cell lymphoma. Ph+: Philadelphia chromosome positive. Ph-: Philadelphia chromosome negative. MRD: minimal residual disease. sibling: fully HLA matched sibling donor. unrelated: fully HLA matched unrelated donor. CR: complete remission. PR: partial remission. PD: progressive disease. SD: stable disease. *CRS toxicity grading is per Lee et al. "ASTCT Consensus Grading for Cytokine Release Syndrome and Neurologic Toxicity Associated with Immune Effector Cells." Biology of Blood and Marrow Transplantation 2019; 25(4):625-638. **Duration of response is time between first response of PR or better, or SD if SD is best response, and last malignancy assessment, progressive malignancy, initiation of new anti-malignancy treatment, or death from any cause. ***Event-free survival is time between cell infusion and last malignancy assessment, progressive malignancy, initiation of new anti-malignancy treatment, or death from any cause. (+) Indicates an ongoing response at last assessment. ^Patient off study due to noncompliance. ^^Patients came off study in remission to continue care with outside oncology teams. #Patient off study to receive systemic therapy for control of chronic graft versus host disease, which could have provided anti-malignancy effect. ##Patient off study to receive a second allogeneic stem cell transplant. %Neurologic adverse event was a headache.

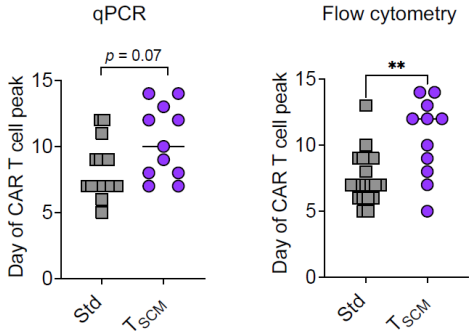

Figure S1. CAR T_{SCM} cells exhibit a delayed peak expansion relative to standard CAR T cells, related to Figure 4. Day of peak of CAR T cell expansion measured by qPCR (left) and flow cytometry (right). Lines represent median values (**p < 0.01, two-tailed Mann-Whitney test). *The technical experiments used to generate **Figure S1 (left)** were performed by me and Danielle A. Natrakul (National Cancer Institute), the co-author of the manuscript accepted in CELL. The technical experiments used to generate **Figure S1 (right)** were conceived and performed by me. The graphical design for **Figure S1** was made by me under the guidance of Prof. Luca Gattinoni.*

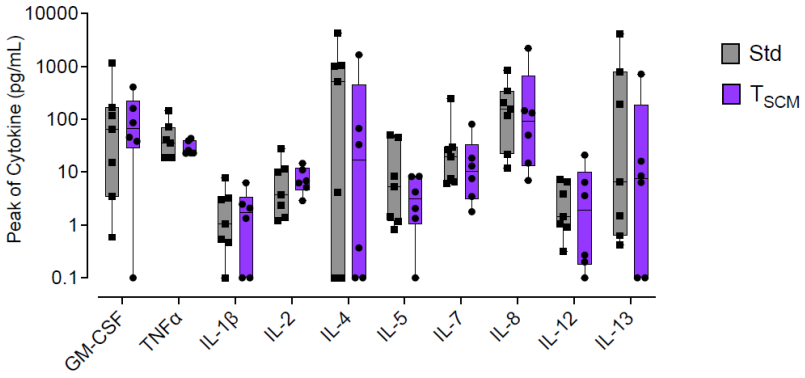

Figure S2. Serum cytokine profiling following CAR T cell infusion, related to Figures 8 and 15. Peak serum levels of key cytokines involved in CRS onset in responder patients within two weeks following infusion of standard or CAR T_{SCM} cells (standard n = 7; T_{SCM} n = 6). No significant differences were observed (multiple t-test, Holm-Šídák correction for multiple comparisons). *The technical experiments used to generate* ***Figure S2*** *were conceived and performed entirely by me. The graphical design for* ***Figure S2*** *was made by me.*

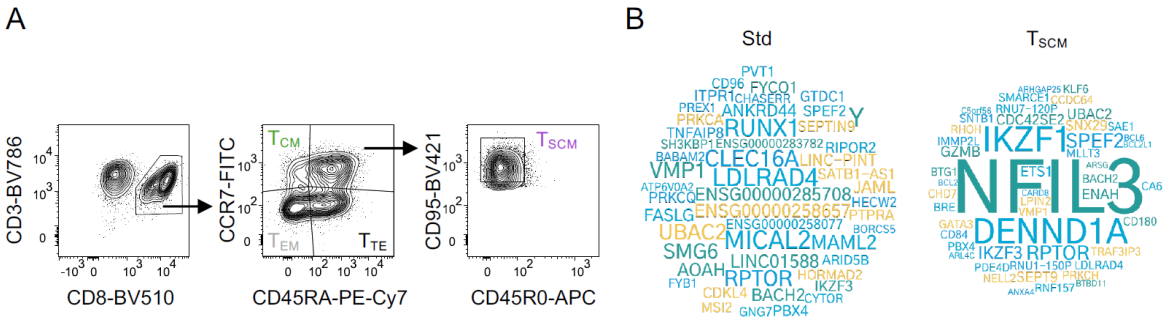

Figure S3. Diversity of CAR T cell infusion products, related to Figure 13. (**A**) Gating strategy for a representative patient (patient #15) employed to isolate each T cell subset for integration site analysis. (**B**) Word clouds displaying the top 50 represented ISs loci in the CAR T cell infusion products in patient #15 (standard, left) and #22 (T_{SCM}, right). Each locus is labeled with the name of the closest gene to the relative insertion site. The size of each gene name is proportional to the number of integrations found at that locus, with larger fonts indicating higher integration frequencies. *Project planning and all the technical experiments necessary to generate* ***Figure S3*** *were entirely conceived and performed by me. Protocol for Integration Site Analysis assay was developed and optimized at Leibniz Institute for Immunotherapy by me. Sequencing was performed by me and Johanna Raithel under the guidance of Michael Rheli, co-author of the manuscript accepted in CELL. Bioinformatic analyses were performed by Luca Biasco and Nicholas Strieder, both co-authors of the manuscript accepted in CELL. The bioinformatic analysis used for* ***Figure S3*** *was performed by Luca Biasco. The graphical design for* ***Figure S3*** *was made through my guidance and that of Luca Biasco and Prof. Luca Gattinoni, the co-first author of the manuscript accepted in CELL.*

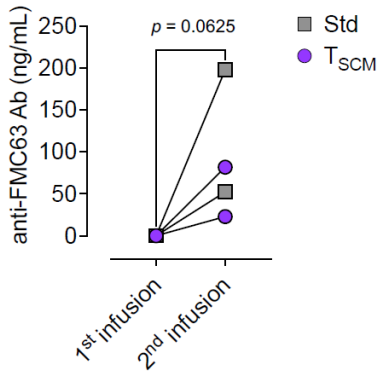

Figure S4. Enhanced humoral immunity against CARs following second CAR T cell infusion, related to Figure 17. Patient serum levels of anti-FMC63 antibodies measured after the first and second CAR T cell infusions (standard, Pt#9 and 18; and T_{SCM}-enriched, Patients #21 and 29). one-tailed Wilcoxon test). *All the technical experiments used to generate **Figure S4** were conceived and performed by me. The graphical design for **Figure S4** was made by me under the guidance of Prof. Luca Gattinoni.*

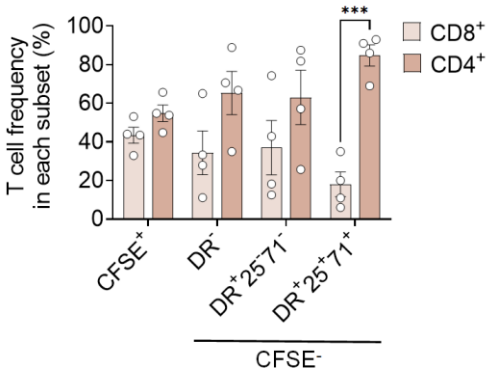

Figure S5. Original CAR T cell products expressed high levels of CAR related to Figure 20. Bar plot showing CD4 and CD8 T cell frequencies within each subset post-stimulation with 80/BBL rHLA eK562 cells. (*p <0.05; **p <0.01, two-way ANOVA, Šídák test). *All the technical experiments used to generate **Figure S5** were conceived and performed by me. The graphical design for **Figure S5** was made by me.*

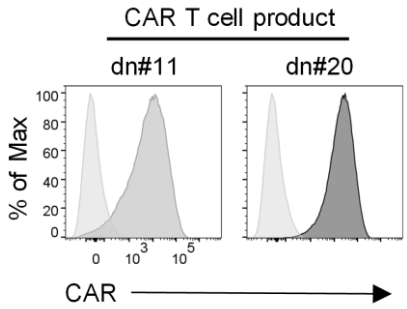

Figure S6. Original CAR T cell products expressed high levels of CAR. CAR percentage measured by Flow Cytometry from both original CAR T cell products administered to patients #11 and #20. *All the technical*

*experiments used to generate **Figure S6** were conceived and performed by me. The graphical design for **Figure S6** was made by me.*

References

1. Fehleisen, F. Über die Züchtung der Erysipel-Kokken auf künstlichen Nährböden und die Übertragbarkeit auf den Menschen. *Dtsch. Med. Wochenschr.* **8**, 533–554 (1882).
2. Bruns P. [Die Heilwirkung des Erysipels auf Geschwülste]. Beitr Klin Chir 1888;3:443–66.
3. Coley, W. B. II. Contribution to the knowledge of sarcoma. *Ann. Surg.* **14**, 199–220 (1891). https://doi.org/10.1097/00000658-189112000-00015.
4. Coley, W. B. The treatment of malignant tumors by repeated inoculations of erysipelas with a report of ten original cases. *Am. J. Med. Sci.* **105**, 487–511 (1893).
5. Smyth, M. J., Dunn, G. P. & Schreiber, R. D. Cancer immunosurveillance and immunoediting: the roles of immunity in suppressing tumor development and shaping

tumor immunogenicity. *Adv. Immunol.* **90**, 1–50 (2006). https://doi.org/10.1016/S0065-2776(06)90001-7.

6. Galluzzi, L. *et al.* Classification of current anticancer immunotherapies. *Oncotarget* **5**, 12472–12508 (2014). https://doi.org/10.18632/oncotarget.2998.
7. Waldman, A. D., Fritz, J. M. & Lenardo, M. J. A guide to cancer immunotherapy: from T cell basic science to clinical practice. *Nat. Rev. Immunol.* **20**, 651–668 (2020). https://doi.org/10.1038/s41577-020-0306-5.
8. Rosenberg, S. A. & Restifo, N. P. Adoptive cell transfer as personalized immunotherapy for human cancer. *Science* **348**, 62–68 (2015). https://doi.org/10.1126/science.aaa4967.
9. Jenq RR, van den Brink MR. Allogeneic haematopoietic stem cell transplantation: individualized stem cell and immune therapy of cancer. Nat Rev Cancer. 2010 Mar;10(3):213-21. doi: 10.1038/nrc2804. Epub 2010 Feb 19. Erratum in: Nat Rev Cancer. 2010 Mar;10(3). doi: 10.1038/nrc2825. PMID: 20168320.
10. Lee SJ, Klein J, Haagenson M, et al. High-resolution donor-recipient HLA matching contributes to the success of unrelated donor marrow transplantation. Blood. 2007; 110:4576–4583. doi: 10.1182/blood-2007-06-097386.
11. Reddy P, Arora M, Guimond M, Mackall CL. GVHD: a continuing barrier to the safety of allogeneic transplantation. Biol Blood Marrow Transplant. 2009 Jan;15(1 Suppl):162-8. doi: 10.1016/j.bbmt.2008.10.014.
12. Weiden, P. L. et al. Antileukemic effect of graft-versus-host disease in human recipients of allogeneic-marrow grafts. N. Engl. J. Med. 300, 1068–1073 (1979). doi: 10.1056/NEJM197905103001902.
13. Srinivasan, R. et al. Allogeneic stem cell transplantation as immunotherapy for nonhematological cancers. Semin. Oncol. 31, 47–55 (2004). https://doi.org/10.1053/j.seminoncol.2003.10.008.
14. D'Souza, A. et al. Current Use of and Trends in Hematopoietic Cell Transplantation in the United States. Biol Blood Marrow Transplant 26, e177-e182 (2020). https://doi.org:10.1016/j.bbmt.2020.04.013.
15. Pagliuca S. *et al*. Donor lymphocyte infusion after allogeneic haematopoietic cell transplantation for haematological malignancies: basic considerations and best practice recommendations from the EBMT. Lancet Haematol. 2024 Jun;11(6):e448-e458. doi: 10.1016/S2352-3026(24)00098-X. PMID: 38796194.

16. Collins RH, Shpilberg O, Drobyski WR, et al. Donor leukocyte infusions in 140 patients with relapsed malignancy after allogeneic bone marrow transplantation. J Clin Oncol 1997;15:433-44. doi: 10.1200/JCO.1997.15.2.433.

17. Schmid C. *et al*. Donor lymphocyte infusion in the treatment of first hematological relapse after allogeneic stem-cell transplantation in adults with acute myeloid leukemia: a retrospective risk factors analysis and comparison with other strategies by the EBMT Acute Leukemia Working Party. J Clin Oncol. 2007 Nov 1;25(31):4938-45. doi: 10.1200/JCO.2007.11.6053.

18. Marks DI, Lush R, Cavenagh J, et al: The toxicity and efficacy of donor lymphocyte infusions given after reduced-intensity conditioning allogeneic stem cell transplantation. Blood 100:3108-14, 2002. doi: 10.1182/blood-2002-02-0506.

19. Grimm EA, Mazumder A, Zhang HZ, Rosenberg SA. Lymphokine-activated killer cell phenomenon. Lysis of natural killer-resistant fresh solid tumor cells by interleukin 2-activated autologous human peripheral blood lymphocytes. J Exp Med. 1982 Jun 1;155(6):1823-41. doi: 10.1084/jem.155.6.1823.

20. Lindemann A, Herrmann F, Oster W, Mertelsmann R. Lymphokine activated killer cells. Blut. 1989 Oct;59(4):375-84. doi: 10.1007/BF00321208.

21. Rosenberg SA, Spiess P, Lafreniere R. A new approach to the adoptive immunotherapy of cancer with tumor-infiltrating lymphocytes. Science. 1986 Sep 19;233(4770):1318-21. doi: 10.1126/science.3489291.

22. Rosenberg SA. *et al*. Treatment of patients with metastatic melanoma with autologous tumor-infiltrating lymphocytes and interleukin 2. J Natl Cancer Inst. 1994 Aug 3;86(15):1159-66. doi: 10.1093/jnci/86.15.1159.

23. Dudley ME. *et al*. Adoptive cell therapy for patients with metastatic melanoma: evaluation of intensive myeloablative chemoradiation preparative regimens. J Clin Oncol. 2008 Nov 10;26(32):5233-9. doi: 10.1200/JCO.2008.16.5449.

24. Rosenberg SA. *et al*. Durable complete responses in heavily pretreated patients with metastatic melanoma using T-cell transfer immunotherapy. Clin Cancer Res. 2011 Jul 1;17(13):4550-7. doi: 10.1158/1078-0432.CCR-11-0116.

25. Rohaan, M.W. et al. Tumor-infiltrating lymphocyte therapy or ipilimumab in advanced melanoma. N. Engl. J. Med. 387, 2113–2125 (2022). https://doi.org/10.1056/NEJMoa2210233

26. Rodrigo, B. N. et al. Immune correlates and mechanisms of TIL therapy efficacy: current insights and knowledge gaps. *Trends Cancer* 11, 993–1004 (2025). doi:10.1016/j.trecan.2025.08.002.

27. Amer MH. Gene therapy for cancer: present status and future perspective. Mol Cell Ther. 2014 Sep 10;2:27. doi: 10.1186/2052-8426-2-27.

28. Schumacher TN. T-cell-receptor gene therapy. Nat Rev Immunol. 2002 Jul;2(7):512-9. doi: 10.1038/nri841.

29. Clay TM. *et al*. Efficient transfer of a tumor antigen-reactive TCR to human peripheral blood lymphocytes confers anti-tumor reactivity. J Immunol. 1999 Jul 1;163(1):507-13. doi: 10.4049/jimmunol.163.1.507.

30. Morgan RA. *et al*. Cancer regression in patients after transfer of genetically engineered lymphocytes. Science. 2006 Oct 6;314(5796):126-9. doi: 10.1126/science.1129003.

31. Johnson LA. *et al*. Gene therapy with human and mouse T-cell receptors mediates cancer regression and targets normal tissues expressing cognate antigen. Blood. 2009 Jul 16;114(3):535-46. doi: 10.1182/blood-2009-03-211714.

32. Robbins PF. *et al*. A pilot trial using lymphocytes genetically engineered with an NY-ESO-1-reactive T-cell receptor: long-term follow-up and correlates with response. Clin Cancer Res. 2015 Mar 1;21(5):1019-27. doi: 10.1158/1078-0432.CCR-14-2708.

33. Rapoport AP. *et al*. NY-ESO-1-specific TCR-engineered T cells mediate sustained antigen-specific antitumor effects in myeloma. Nat Med. 2015 Aug;21(8):914-921. doi: 10.1038/nm.3910.

34. Manfredi F. *et al*. TCR Redirected T Cells for Cancer Treatment: Achievements, Hurdles, and Goals. Front Immunol. 2020 Sep 3;11:1689. doi: 10.3389/fimmu.2020.01689.

35. Bendle, G. M. *et al.* Lethal graft-versus-host disease in mouse models of T cell receptor gene therapy. Nat. Med. 16, 565–570 (2010). https://doi.org/10.1038/nm.2128.

36. McGranahan, N. et al. Allele-specific HLA loss and immune escape in lung cancer evolution. Cell 171, 1259–1271.e11 (2017). https://doi.org/10.1016/j.cell.2017.10.001.

37. Chmielewski, M. & Abken, H. Antigen-specific T-cell activation independently of the MHC: chimeric antigen receptor-redirected T cells. *Front. Immunol.* **4**, 371 (2013). https://doi.org/10.3389/fimmu.2013.00371.

38. June, C. H., O'Connor, R. S., Kawalekar, O. U., Ghassemi, S. & Milone, M. C. CAR T cell immunotherapy for human cancer. *Science* 359, 1361–1365 (2018). https://doi.org/10.1126/science.aar6711.

39. Gross, G., Waks, T. & Eshhar, Z. Expression of immunoglobulin–T-cell receptor chimeric molecules as functional receptors with antibody-type specificity. *Proc. Natl Acad. Sci. USA* 86, 10024–10028 (1989). https://doi.org/10.1073/pnas.86.24.10024.

40. Rafiq S, Hackett CS, Brentjens RJ. Engineering strategies to overcome the current roadblocks in CAR T cell therapy. *Nat Rev Clin Oncol.* 2020 Mar;17(3):147-167. doi: 10.1038/s41571-019-0297-y.

41. Eshhar Z, Waks T, Gross G, Schindler DG. Specific activation and targeting of cytotoxic lymphocytes through chimeric single chains consisting of antibody-binding domains and the gamma or zeta subunits of the immunoglobulin and T-cell receptors. Proc Natl Acad Sci U S A. 1993 Jan 15;90(2):720-4. doi: 10.1073/pnas.90.2.720. PMID: 8421711.

42. Brocker T, Karjalainen K. Signals through T cell receptor-zeta chain alone are insufficient to prime resting T lymphocytes. J Exp Med. 1995 May 1;181(5):1653-9. doi: 10.1084/jem.181.5.1653.

43. Milone et al. Incorporation of a CD28 costimulatory domain enhances expansion and persistence of CAR-modified T cells in vivo. *Mol. Ther.* 17, 1453–1464 (2009). https://doi.org/10.1038/mt.2009.83.

44. Song, D. G., Ye, Q., Carpenito, C., et al. 4-1BB costimulation enhances CAR T cell persistence, tumor localization and antitumor activity in vivo. *J. Immunother.* 34, 1-10 (2011). https://doi.org/10.1097/CJI.0b013e318205b68e.

45. Till, B. G. et al. CD20-specific adoptive immunotherapy for lymphoma using a chimeric antigen receptor with both CD28 and 4-1BB domains: pilot clinical trial results. Blood 119, 3940–3950 (2012). https://doi.org/10.1182/blood-2011-10-387969.

46. Chmielewski, M. & Abken, H. TRUCKs: the fourth generation of CARs. Expert Opin. Biol. Ther. 15, 1145–1154 (2015). https://doi.org/10.1517/14712598.2015.1046430.

47. Kagoya, Y. et al. A novel chimeric antigen receptor containing a JAK–STAT signaling domain mediates superior antitumor effects. Nat. Med. 24, 352–359 (2018). https://doi.org/10.1038/nm.4478.

48. Uckun FM. *et al*. Detailed studies on expression and function of CD19 surface determinant by using B43 monoclonal antibody and the clinical potential of anti-CD19 immunotoxins. Blood. 1988 Jan;71(1):13-29. doi: 10.1182/blood.v71.1.13.13.

49. Kochenderfer JN. *et al*. Eradication of B-lineage cells and regression of lymphoma in a patient treated with autologous T cells genetically engineered to recognize CD19. Blood. 2010 Nov 18;116(20):4099-102. doi: 10.1182/blood-2010-04-281931.

50. Porter DL, Levine BL, Kalos M, Bagg A, June CH. Chimeric antigen receptor-modified T cells in chronic lymphoid leukemia. N Engl J Med. 2011 Aug 25;365(8):725-33. doi: 10.1056/NEJMoa1103849.

51. Davila ML. *et al*. Efficacy and toxicity management of 19-28z CAR T cell therapy in B cell acute lymphoblastic leukemia. Sci Transl Med. 2014 Feb 19;6(224):224ra25. doi: 10.1126/scitranslmed.3008226.

52. Schuster SJ. *et al*. Chimeric Antigen Receptor T Cells in Refractory B-Cell Lymphomas. N Engl J Med. 2017 Dec 28;377(26):2545-2554. doi: 10.1056/NEJMoa1708566.

53. Maude SL. *et al*. Tisagenlecleucel in Children and Young Adults with B-Cell Lymphoblastic Leukemia. N Engl J Med. 2018 Feb 1;378(5):439-448. doi: 10.1056/NEJMoa1709866.

54. Arunachalam, A. K., Grégoire, C., Coutinho de Oliveira, B. & Melenhorst, J. J. Advancing CAR T-cell therapies: Preclinical insights and clinical translation for hematological malignancies. Blood Rev. 68, 101241 (2024). https://doi.org/10.1016/j.blre.2024.101241

55. Morris EC, Neelapu SS, Giavridis T, Sadelain M. Cytokine release syndrome and associated neurotoxicity in cancer immunotherapy. Nat Rev Immunol. 2022 Feb;22(2):85-96. doi: 10.1038/s41577-021-00547-6.

56. Wudhikarn K. *et al*. Infection during the first year in patients treated with CD19 CAR T cells for diffuse large B cell lymphoma. Blood Cancer J. 2020 Aug 5;10(8):79. doi: 10.1038/s41408-020-00346-7.

57. Wat J, Barmettler S. Hypogammaglobulinemia After Chimeric Antigen Receptor (CAR) T-Cell Therapy: Characteristics, Management, and Future Directions. J Allergy Clin Immunol Pract. 2022 Feb;10(2):460-466. doi: 10.1016/j.jaip.2021.10.037.

58. Lee, D. W. et al. T cells expressing CD19 CAR in adult ALL patients: long-term follow-up of toxicity and efficacy. Blood 126, 681–689 (2015). https://doi.org/10.1182/blood-2015-03-635354.

59. Farber DL, Yudanin NA, Restifo NP. Human memory T cells: generation, compartmentalization and homeostasis. Nat Rev Immunol. 2014 Jan;14(1):24-35. doi: 10.1038/nri3567.

60. Restifo NP, Gattinoni L. Lineage relationship of effector and memory T cells. Curr Opin Immunol. 2013 Oct;25(5):556-63. doi: 10.1016/j.coi.2013.09.003.

61. Mackay CR, Kimpton WG, Brandon MR, Cahill RN. Lymphocyte subsets show marked differences in their distribution between blood and the afferent and efferent lymph of peripheral lymph nodes. J Exp Med. 1988 Jun 1;167(6):1755-65. doi: 10.1084/jem.167.6.1755.

62. Mackay CR. Homing of naive, memory and effector lymphocytes. Curr Opin Immunol. 1993 Jun;5(3):423-7. doi: 10.1016/0952-7915(93)90063-x.

63. Sanders ME. *et al*. Human memory T lymphocytes express increased levels of three cell adhesion molecules (LFA-3, CD2, and LFA-1) and three other molecules (UCHL1, CDw29, and Pgp-1) and have enhanced IFN-gamma production. J Immunol. 1988 Mar 1;140(5):1401-7. doi: 10.4049/jimmunol.140.5.1401.

64. Lugli E, Zanon V, Mavilio D, Roberto A. FACS Analysis of Memory T Lymphocytes. Methods Mol Biol. 2017;1514:31-47. doi: 10.1007/978-1-4939-6548-9_3.

65. Sallusto F, Lenig D, Förster R, Lipp M, Lanzavecchia A. Two subsets of memory T lymphocytes with distinct homing potentials and effector functions. Nature. 1999 Oct 14;401(6754):708-12. doi: 10.1038/44385.

66. Manjunath N. *et al*. Effector differentiation is not prerequisite for generation of memory cytotoxic T lymphocytes. J Clin Invest. 2001 Sep;108(6):871-8. doi: 10.1172/JCI13296.

67. Hamann D, Baars PA, Rep MH, Hooibrink B, Kerkhof-Garde SR, Klein MR, van Lier RA. Phenotypic and functional separation of memory and effector human CD8+ T cells. J Exp Med. 1997 Nov 3;186(9):1407-18. doi: 10.1084/jem.186.9.1407.

68. Valmori D. *et al*. Circulating Tumor-reactive $CD8^+$ T cells in melanoma patients contain a $CD45RA^+CCR7^-$ effector subset exerting ex vivo tumor-specific cytolytic activity. Cancer Res. 2002 Mar 15;62(6):1743-50. PMID: 11912149. doi: 10.1158/0008-5472.CAN-01-3680.

69. Sallusto F, Geginat J, Lanzavecchia A. Central memory and effector memory T cell subsets: function, generation, and maintenance. Annu Rev Immunol. 2004;22:745-63. doi: 10.1146/annurev.immunol.22.012703.104702.

70. Klebanoff CA. *et al*. Central memory self/tumor-reactive CD8+ T cells confer superior antitumor immunity compared with effector memory T cells. Proc Natl Acad Sci U S A. 2005 Jul 5;102(27):9571-6. doi: 10.1073/pnas.0503726102.

71. Champagne P. *et al*. Skewed maturation of memory HIV-specific CD8 T lymphocytes. Nature. 2001 Mar 1;410(6824):106-11. doi: 10.1038/35065118.

72. Zhang Y, Joe G, Hexner E, Zhu J, Emerson SG. Host-reactive $CD8^+$ memory stem cells in graft-versus-host disease. Nat Med. 2005 Dec;11(12):1299-305. doi: 10.1038/nm1326.

73. Gattinoni L. *et al.* Acquisition of full effector function in vitro paradoxically impairs the in vivo antitumor efficacy of adoptively transferred $CD8^+$ T cells. J Clin Invest. 2005 Jun;115(6):1616-26. doi: 10.1172/JCI24480.

74. Gattinoni L. *et al*. Wnt signaling arrests effector T cell differentiation and generates $CD8^+$ memory stem cells. Nat Med. 2009 Jul;15(7):808-13. doi: 10.1038/nm.1982.

75. Gattinoni L. *et al*. A human memory T cell subset with stem cell-like properties. Nat Med. 2011 Sep 18;17(10):1290-7. doi: 10.1038/nm.2446.

76. Gattinoni L, Speiser DE, Lichterfeld M, Bonini C. T memory stem cells in health and disease. Nat Med. 2017 Jan 6;23(1):18-27. doi: 10.1038/nm.4241.

77. Gattinoni L, Powell DJ Jr, Rosenberg SA, Restifo NP. Adoptive immunotherapy for cancer: building on success. Nat Rev Immunol. 2006 May;6(5):383-93. doi: 10.1038/nri1842.

78. Sabatino M. *et al*. Generation of clinical-grade CD19-specific CAR-modified CD8+ memory stem cells for the treatment of human B-cell malignancies. Blood. 2016 Jul 28;128(4):519-28. doi: 10.1182/blood-2015-11-683847.

79. Brudno, J. N. et al. Allogeneic T cells that express an anti-CD19 chimeric antigen receptor induce remissions of B-cell malignancies that progress after allogeneic hematopoietic stem-cell transplantation without causing graft-versus-host disease. Journal of Clinical Oncology 34, 1112–1121 (2016). doi: 10.1200/JCO.2015.64.5929.

80. D. Przepiorka *et al*. 1994 Consensus Conference on Acute GVHD Grading. Bone Marrow Transplant 15, 825-828 (1995).

81. A. H. Filipovich *et al.* National Institutes of Health Consensus Development Project on Criteria for Clinical Trials in Chronic Graft-versus-Host Disease: I. Diagnosis and Staging Working Group Report. Biology of Blood and Marrow Transplantation 11, 945-956 (2005). doi: 10.1016/j.bbmt.2005.09.004.

82. B. D. Cheson *et al.* Revised response criteria for malignant lymphoma. J Clin Oncol 25, 579-586 (2007). doi: 10.1200/JCO.2006.09.2403.

83. B. D. Cheson et al., Recommendations for initial evaluation, staging, and response assessment of Hodgkin and non-Hodgkin lymphoma: the Lugano classification. J Clin Oncol 32, 3059-3068 (2014). doi: 10.1200/JCO.2013.54.8800.

84. M. Hallek et al., iwCLL guidelines for diagnosis, indications for treatment, response assessment, and supportive management of CLL. Blood 131, 2745-2760 (2018). doi: 10.1182/blood-2017-09-806398.

85. D. W. Lee et al., ASTCT Consensus Grading for Cytokine Release Syndrome and Neurologic Toxicity Associated with Immune Effector Cells. Biology of Blood and Marrow Transplantation 25, 625-638 (2019). https://doi.org/10.1016/j.bbmt.2018.12.758

86. S. Puccio et al., CRUSTY: a versatile web platform for the rapid analysis and visualization of high-dimensional flow cytometry data. Nature Communications 14, 5102 (2023). https://doi.org/10.1038/s41467-023-40790-0

87. M. Setty et al., Wishbone identifies bifurcating developmental trajectories from single-cell data. Nature Biotechnology 34, 637-645 (2016). https://doi.org/10.1038/nbt.3569

88. A. Yan et al., IS-Seq: a bioinformatics pipeline for integration sites analysis with comprehensive abundance quantification methods. BMC Bioinformatics 24, 286 (2023). doi: 10.1186/s12859-023-05390-1.

89. D. W. Lee et al., T cells expressing CD19 chimeric antigen receptors for acute lymphoblastic leukaemia in children and young adults: a phase 1 dose-escalation trial. Lancet 385, 517-528 552 (2015). https://doi.org/10.1186/s12859-023-05390-1

90. K. T. Mueller et al., Cellular kinetics of CTL019 in relapsed/refractory B-cell acute lymphoblastic leukemia and chronic lymphocytic leukemia. Blood 130, 2317-2325 (2017). doi: 10.1182/blood-2017-06-786129.

91. V. Blumenberg et al., Early quantification of anti-CD19 CAR T cells by flow cytometry 558 predicts response in R/R DLBCL. Blood Adv 7, 6844-6849 (2023). doi: 10.1182/bloodadvances.2023010364.

92. C. J. Turtle et al., CD19 CAR-T cells of defined $CD4^+$:$CD8^+$ composition in adult B cell ALL patients. J Clin Invest 126, 2123-2138 (2016). doi: 10.1172/JCI85309.

93. R. de Waal Malefyt, *et al*. Interleukin 10 (IL-10) inhibits cytokine synthesis by human monocytes: an autoregulatory role of IL-10 produced by 576 monocytes. J Exp Med 174, 1209-1220 (1991). doi: 10.1084/jem.174.5.1209.

94. Wagner DL. *et al*. Immunogenicity of CAR T cells in cancer therapy. Nat Rev Clin Oncol. 2021 Jun;18(6):379-393. doi: 10.1038/s41571-021-00476-2.

95. Turtle CJ, Riddell SR. Artificial antigen-presenting cells for use in adoptive immunotherapy. Cancer J. 2010 Jul-Aug;16(4):374-81. doi: 10.1097/PPO.0b013e3181eb33a6.

96. Cavazzana-Calvo M. *et al*. Improving immune reconstitution while preventing graft-versus-host disease in allogeneic stem cell transplantation. Semin Hematol. 2002 Jan;39(1):32-40. doi: 10.1053/shem.2002.29251.

97. Godfrey WR. *et al*. Ex vivo depletion of alloreactive cells based on CFSE dye dilution, activation antigen selection, and dendritic cell stimulation. Blood. 2004 Feb 1;103(3):1158-65. doi: 10.1182/blood-2003-04-1098.

98. Tripathi, P., Kurtulus, S., Wojciechowski, S., Sholl, A., Hoebe, K. & Morris, S. C. STAT5 is critical to maintain effector CD8+ T cell responses. J. Immunol. 185, 2116–2124 (2010). doi:10.4049/jimmunol.1000842.

99. Ding, Z.-C., Shi, H., Aboelella, N. S., Fesenkova, K., Park, E. J., Liu, Z., Pei, L., Li, J., McIndoe, R. A., Xu, H., Piazza, G. A., Blazar, B. R., Munn, D. H. & Zhou, G. Persistent STAT5 activation reprograms the epigenetic landscape in $CD4^+$ T cells to drive polyfunctionality and antitumor immunity. Sci. Immunol. 5, eaba5962 (2020). **doi:**10.1126/sciimmunol.aba5962. https://doi.org/10.1126/sciimmunol.aba5962

100. Klebanoff CA. *et al*. Inhibition of AKT signaling uncouples T cell differentiation from expansion for receptor-engineered adoptive immunotherapy. JCI Insight. 2017 Dec 7;2(23):e95103. doi: 10.1172/jci.insight.95103.

101. Selli ME. *et al*. Costimulatory domains direct distinct fates of CAR-driven T-cell dysfunction. Blood. 2023 Jun 29;141(26):3153-3165. doi: 10.1182/blood.2023020100.

102. Urak R. *et al*. Ex vivo Akt inhibition promotes the generation of potent CD19CAR T cells for adoptive immunotherapy. J Immunother Cancer. 2017 Mar 21;5:26. doi: 10.1186/s40425-017-0227-4.

103. Grupp SA. *et al*. Chimeric antigen receptor-modified T cells for acute lymphoid leukemia. N Engl J Med. 2013 Apr 18;368(16):1509-1518. doi: 10.1056/NEJMoa1215134.

104. Westin, J.R. *et al*. Survival with Axicabtagene Ciloleucel in Large B-Cell Lymphoma. N Engl J Med. 2023; 389, 148-157. doi: 10.1056/NEJMoa2301665.

105. Cappell, K. M. & Kochenderfer, J. N. Long-term outcomes following CAR T cell therapy: what we know so far. Nature Reviews Clinical Oncology vol. 20 359–371 https://doi.org/10.1038/s41571-023-00754-1 (2023).

106. Ruella, M., Korell, F., Porazzi, P. & Maus, M. V. Mechanisms of resistance to chimeric antigen receptor-T cells in haematological malignancies. Nat. Rev. Drug Discov. 22, 976–995 (2023). https://doi.org/10.1038/s41573-023-00807-1

107. Zugasti, I., Espinosa-Aroca, L., Fidyt, K., Mulens-Arias, V., Diaz-Beya, M., Juan, M. *et al.* CAR-T cell therapy for cancer: current challenges and future directions. *Signal Transduction and Targeted Therapy* 10, 210 (2025). https://doi.org/10.1038/s41392-025-02269-w.

108. Leslie Popplewell. *et al.* CD19-CAR Therapy Using Naive/Memory or Central Memory T Cells Integrated into the Autologous Stem Cell Transplant Regimen for Patients with B-NHL, Blood, Volume 132, Supplement 1, 2018, Page 610, ISSN 0006-4971, doi: 10.1182/blood-2018-99-119650.

109. Aldoss I. *et al*. Favorable Activity and Safety Profile of Memory-Enriched CD19-Targeted Chimeric Antigen Receptor T-Cell Therapy in Adults with High-Risk Relapsed/Refractory ALL. Clin Cancer Res. 2023 Feb 16;29(4):742-753. doi: 10.1158/1078-0432.CCR-22-2038.

110. Crompton JG, Sukumar M, Restifo NP. Uncoupling T-cell expansion from effector differentiation in cell-based immunotherapy. Immunol Rev. 2014 Jan;257(1):264-276. doi: 10.1111/imr.12135.

111. Lugli E. *et al*. Superior T memory stem cell persistence supports long-lived T cell memory. J Clin Invest. 2013 Feb;123(2):594-9. doi: 10.1172/JCI66327.

112. Cieri N. *et al*. IL-7 and IL-15 instruct the generation of human memory stem T cells from naive precursors. Blood. 2013 Jan 24;121(4):573-84. doi: 10.1182/blood-2012-05-431718.

113. Gattinoni L, Restifo NP. Moving T memory stem cells to the clinic. Blood. 2013 Jan 24;121(4):567-8. doi: 10.1182/blood-2012-11-468660.

114. Canelo-Vilaseca, M., Sabbah, M., Di Blasi, R., Cristinelli, C., Sureda, A., Caillat-Zucman, S. & Thieblemont, C. Lymphodepletion chemotherapy in chimeric antigen receptor-engineered T (CAR-T) cell therapy in lymphoma. Bone Marrow Transplant. 60, 559–567 (2025). https://doi.org/10.1038/s41409-025-02539-9.

115. Gattinoni L. *et al*. Removal of homeostatic cytokine sinks by lymphodepletion enhances the efficacy of adoptively transferred tumor-specific CD8+ T cells. J Exp Med. 2005 Oct 3;202(7):907-12. doi: 10.1084/jem.20050732.

116. Hamilton, M. P. et al. CAR19 monitoring by peripheral blood immunophenotyping reveals histology-specific expansion and toxicity. Blood Advances 8, 3314–3326 (2024). https://doi.org/10.1182/bloodadvances.2024012637.

117. Cao, J.-X., Wang, H., Gao, W.-J., You, J., Wu, L.-H. & Wang, Z.-X. The incidence of cytokine release syndrome and neurotoxicity of CD19 chimeric antigen receptor–T cell therapy in patients with acute lymphoblastic leukemia and lymphoma. Cytotherapy 22, 214–226 (2020). https://doi.org/10.1016/j.jcyt.2020.01.015.

118. Lee, S.Y. *et al*. $CD8^+$ chimeric antigen receptor T cells manufactured in absence of $CD4^+$ cells exhibit hypofunctional phenotype. J Immunother Cancer, 2023. 11. doi: 10.1136/jitc-2023-007803.

119. Sommermeyer, D. *et al*. Chimeric antigen receptor-modified T cells derived from defined $CD8^+$ and $CD4^+$ subsets confer superior antitumor reactivity in vivo. Leukemia, 2016. 30, 492-500. doi: 10.1038/leu.2015.247.

120. Melenhorst, J.J. *et al*. Decade-long leukaemia remissions with persistence of $CD4^+$ CAR T cells. Nature, 2022. 602, 503-509. doi: 10.1038/s41586-021-04390-6.

121. Boulch, M. *et al*. A major role for $CD4^+$ T cells in driving cytokine release syndrome during CAR T cell therapy. Cell Rep, 2023. Med 4, https://101161. 10.1016/j.xcrm.2023.101161.

122. Bove, C. et al. CD4 CAR-T cells targeting CD19 play a key role in exacerbating cytokine release syndrome, while maintaining long-term responses. J. Immunother. Cancer 11, e005878 (2023). https://doi.org/10.1136/jitc-2022-005878.

123. Norelli, M. et al. Monocyte-derived IL-1 and IL-6 are differentially required for cytokine-release syndrome and neurotoxicity due to CAR T cells. Nat. Med. 24, 739–748 (2018). https://doi.org/10.1038/s41591-018-0036-4.

124. Giavridis, T., van der Stegen, S. J. C., Eyquem, J., Hamieh, M., Piersigilli, A. & Sadelain, M. CAR T cell-induced cytokine release syndrome is mediated by macrophages and abated by IL-1 blockade. Nat. Med. 24, 731–738 (2018). https://doi.org/10.1038/s41591-018-0041-7.

125. Rossi J. *et al*. Preinfusion polyfunctional anti-CD19 chimeric antigen receptor T cells are associated with clinical outcomes in NHL. Blood. 2018 Aug 23;132(8):804-814. doi: 10.1182/blood-2018-01-828343.

126. Oliveira G. *et al*. Tracking genetically engineered lymphocytes long-term reveals the dynamics of T cell immunological memory. Sci Transl Med. 2015 Dec 9;7(317):317ra198. doi: 10.1126/scitranslmed.aac8265.

127. Fuertes Marraco SA. *et al*. Long-lasting stem cell-like memory CD8+ T cells with a naïve-like profile upon yellow fever vaccination. Sci Transl Med. 2015 Apr 8;7(282):282ra48. doi: 10.1126/scitranslmed.aaa3700.

128. Biasco L. *et al*. Clonal expansion of T memory stem cells determines early anti-leukemic responses and long-term CAR T cell persistence in patients. Nat Cancer. 2021 Jun;2(6):629-642. doi: 10.1038/s43018-021-00207-7.

129. Kim, S. *et al*. Dynamics of HSPC repopulation in nonhuman primates revealed by a decade-long clonal-tracking study. Cell Stem Cell, 2014. 14, 473-485. 10.1016/j.stem.2013.12.012.

130. Majzner, R. G., Rietberg, S. P., Sotillo, E., Dong, R., Vachharajani, V. T., Labanieh, L., Myklebust, J. H., Kadapakkam, M., Weber, E. W., Tousley, A. M., et al. Tuning the antigen density requirement for CAR T-cell activity. Cancer Discov. 10, 702–723 (2020). https://doi.org/10.1158/2159-8290.CD-19-0945

131. Spiegel, J. Y. *et al*. B. CAR T cells with dual targeting of CD19 and CD22 in adult patients with recurrent or refractory B cell malignancies: a phase 1 trial. Nat. Med. 27, 1419–1431 (2021). https://doi.org/10.1038/s41591-021-01436-0

132. Dingfelder, J. et al. Functional differences between CLL- and ALL-derived CAR T cells in a 3D tumor microenvironment highlight CXCR4 and IL-10 as potential modulatory targets. HemaSphere 9, e70279 (2025). https://doi.org/10.1002/hem3.70279.

133. Kloss, C. C., Lee, J., Zhang, A., Chen, F., Melenhorst, J. J., Lacey, S. F., Maus, M. V., Fraietta, J. A., Zhao, Y., & June, C. H. (2018). Dominant-negative TGF-β receptor enhances PSMA-targeted human CAR T cell proliferation and augments prostate cancer eradication. *Molecular Therapy*, 26(7), 1855–1866. https://doi.org/10.1016/j.ymthe.2018.05.003.

134. Piraner, D. I., Abedi, M. H., Duran Gonzalez, M. J., Chazin-Gray, A., Lin, A., Zhu, I., Ravindran, P. T., Schlichthaerle, T., Huang, B., Bearchild, T. H., Lee, D., Wyman, S., Jun, Y.-w., Baker, D., & Roybal, K. T. (2025). Engineered receptors for soluble cellular communication and disease sensing. *Nature*, 638, 805–813. https://doi.org/10.1038/s41586-024-08366-0.

135. Mueller KT. *et al*. Clinical Pharmacology of Tisagenlecleucel in B-cell Acute Lymphoblastic Leukemia. Clin Cancer Res. 2018 Dec 15;24(24):6175-6184. doi: 10.1158/1078-0432.CCR-18-0758.

136. Awasthi R. *et al*. Tisagenlecleucel cellular kinetics, dose, and immunogenicity in relation to clinical factors in relapsed/refractory DLBCL. Blood Adv. 2020 Feb 11;4(3):560-572. doi: 10.1182/bloodadvances.2019000525.

137. Locatelli, F., del Bufalo, F. & Quintarelli, C. Allogeneic chimeric antigen receptor T cells for children with relapsed/refractory B-cell precursor acute lymphoblastic leukemia. Haematologica vol. 109 1689–1690 https://doi.org/10.3324/haematol.2023.284604 (2024).

138. Depil, S., Duchateau, P., Grupp, S. A., Mufti, G. & Poirot, L. 'Off-the-shelf' allogeneic CAR T cells: development and challenges. Nature Reviews Drug Discovery vol. 19 185–199. https://doi.org/10.1038/s41573-019-0051-2 (2020).

139. Cruz, C. R. Y. et al. Infusion of donor-derived CD19-redirected virus-specific T cells for B-cell malignancies relapsed after allogeneic stem cell transplant: a phase 1 study. Blood (2013). https://doi.org/10.1182/blood-2013-06-507607.

140. Shahid, S. et al. Allogeneic off-the-shelf CAR T-cell therapy for relapsed or refractory B-cell malignancies. Blood Adv. 9, 1644–1657 (2025). https://doi.org/10.1182/bloodadvances.2024001234.

141. Kebriaei, P. et al. Phase I trials using Sleeping Beauty to generate CD19-specific CAR T cells. J. Clin. Invest. 126, 3363–3376 (2016). https://doi.org/10.1172/JCI85315.

142. Zhang, C., et al. Long-term survival with donor-derived CD19 CAR-T cell treatment for relapsed patients after allogeneic hematopoietic stem cell transplantation. J. Hematol. Oncol. 17, 150 (2024). https://doi.org/10.1186/s13045-024-01626-6.

143. Frey, N. V. & Porter, D. L. Graft-versus-host disease after donor leukocyte infusions: presentation and management. Best Pract. Res. Clin. Haematol. 21, 205–222 (2008). https://doi.org/10.1016/j.beha.2008.02.007.

144. Rodríguez-Arbolí, E., et al. Second allogeneic hematopoietic cell transplantation for relapsed adult acute myeloid leukemia: outcomes and prognostic factors. *Transplant. Cell. Ther.* **30**, 905.e1–905.e14 (2024). https://doi.org/10.1016/j.jtct.2024.06.019.

145. Orti, G. et al. Graft-versus-host disease after anti-CD19 chimeric antigen receptor T-cell therapy following allogeneic hematopoietic cell transplantation: a transplant complications and paediatric diseases working parties joint EBMT study. Leukemia 39, 431–437 (2025). https://doi.org/10.1038/s41375-024-02467-5.

146. Ghosh, A. et al. Donor CD19 CAR T cells exert potent graft-versus-lymphoma activity with diminished graft-versus-host activity. Nat. Med. 23, 242–249 (2017). https://doi.org/10.1038/nm.4258.

147. Wachsmann, T.L.A., et al. (2025). CAR-mediated target recognition limits TCR-mediated target recognition of TCR- and CAR-dual-receptor-edited T cells. *Molecular Therapy*, 33(4), 1642–1658. https://doi.org/10.1016/j.ymthe.2025.02.035.

148. Smith, M., Zakrzewski, J., James, S. & Sadelain, M. Posttransplant chimeric antigen receptor therapy. Blood 131, 1045–1052 (2018). https://doi.org/10.1182/blood-2017-08-752121.

149. Yang, Y. et al. TCR engagement negatively affects CD8 but not CD4 CAR T cell expansion and leukemic clearance. Sci. Transl. Med. 9, eaag1209 (2017). https://doi.org/10.1126/scitranslmed.aag1209.

150. Diorio, C., Teachey, D. T. & Grupp, S. A. Allogeneic chimeric antigen receptor cell therapies for cancer: progress made and remaining roadblocks. Nat. Rev. Clin. Oncol. 22, 10–27 (2025). https://doi.org/10.1038/s41571-024-00959-y.

151. Torikai, H. et al. A foundation for universal T-cell based immunotherapy: T cells engineered to express a CD19-specific chimeric-antigen-receptor and eliminate expression of endogenous TCR. Blood 119, 5697–5705 (2012). https://doi.org/10.1182/blood-2012-01-405365.

152. Kagoya, Y. et al. Genetic ablation of HLA class I, class II, and the T-cell receptor enables allogeneic T cells to be used for adoptive T-cell therapy. Cancer Immunol. Res. 8, 926–936 (2020). https://doi.org/10.1158/2326-6066.CIR-19-0691.

153. Perica, K. et al. HIV immune evasin Nef enhances allogeneic CAR T cell potency. Nature 640, 793–801 (2025). https://doi.org/10.1038/s41586-025-08657-0.

154. Stenger, D. et al. Endogenous TCR promotes in vivo persistence of CD19-CAR-T cells compared to a CRISPR/Cas9-mediated TCR knockout CAR. Blood 136, 1407–1418 (2020). https://doi.org/10.1182/blood.2020005185

155. Benjamin, R. et al. UCART19, a first-in-class allogeneic anti-CD19 chimeric antigen receptor T-cell therapy for adults with relapsed or refractory B-cell acute lymphoblastic leukaemia (CALM): a phase 1, dose-escalation trial. Lancet Haematol. 9, e833–e843 (2022). https://doi.org/10.1016/S2352-3026(22)00245-9.

I, Gabriele Inchingolo, born on 7 November 1992 in Andria, hereby declare that I have written this thesis without unauthorized aid and without using sources other than those listed.

Data and concepts that have been taken directly or indirectly from other sources have been marked as such, citing the source. In particular, I have not used paid agency or advisory services (commercial advisers for doctoral degrees or others).

This thesis has so far never been submitted to another examination authority in Germany or abroad, neither in this form nor in a similar form.

Regensburg, 1 April 2026